

DIGITAL ACCESS TO SCHOLARSHIP AT HARVARD
DASH.HARVARD.EDU



HARVARD LIBRARY
Office for Scholarly Communication

Air Quality in Southeast Asia: The Growing Threat of Coal Emissions and Land Use Change Fires to Human Health in a Rapidly Evolving Region

The Harvard community has made this article openly available. Please share how this access benefits you. Your story matters

Citation	Koplitz, Shannon N. 2017. Air Quality in Southeast Asia: The Growing Threat of Coal Emissions and Land Use Change Fires to Human Health in a Rapidly Evolving Region. Doctoral dissertation, Harvard University, Graduate School of Arts & Sciences.
Citable link	https://nrs.harvard.edu/URN-3:HUL.INSTREPOS:37365505
Terms of Use	This article was downloaded from Harvard University's DASH repository, and is made available under the terms and conditions applicable to Other Posted Material, as set forth at http://nrs.harvard.edu/urn-3:HUL.InstRepos:dash.current.terms-of-use#LAA

Air Quality in Southeast Asia: The growing threat of coal emissions and land use change fires to human health in a rapidly evolving region

A DISSERTATION PRESENTED
BY
SHANNON KOPLITZ
TO
THE DEPARTMENT OF EARTH AND PLANETARY SCIENCES

IN PARTIAL FULFILLMENT OF THE REQUIREMENTS
FOR THE DEGREE OF
DOCTOR OF PHILOSOPHY
IN THE SUBJECT OF
EARTH AND PLANETARY SCIENCES

HARVARD UNIVERSITY
CAMBRIDGE, MASSACHUSETTS

SEPTEMBER 2016

©2016 – Shannon Koplitz
all rights reserved.

Thesis Advisors: Loretta Mickley and Daniel Jacob Shannon Koplitz

Air Quality in Southeast Asia: The growing threat of coal emissions and land use change fires to human health in a rapidly evolving region

Abstract

Southeast Asia is one of the most densely populated, rapidly developing regions in the world. Despite the extreme rate of economic and population growth, the implications for air quality and human health from the consequent rise in particulate matter (PM) and ozone pollution remain largely unquantified. In this thesis I investigate how anthropogenic activity associated with rapid economic growth in Southeast Asia influences regional air quality and human health, and how these processes are projected to change in the future. In particular, I use the GEOS-Chem chemical transport model (CTM) along with surface and satellite observations to assess 1) the human health implications of projected coal plant expansion across Southeast Asia, and 2) the meteorological and anthropogenic factors contributing to severe haze events stemming from agricultural fires in Indonesia.

I first quantify the burden of disease from rapidly expanding coal fired power plant emissions, both in the present day and for projected 2030 levels. Southeast Asia has a very high population density and is on a fast track to economic development, with most of the growth in electricity demand currently projected to be met by coal. From a detailed analysis of coal-fired power plants presently planned or under construction in Southeast Asia, we project in a business-as-usual scenario that emissions from coal in the region will triple to 2.6 Tg a^{-1} SO_2 and 2.6 Tg a^{-1} NO_x by 2030, with the largest increases occurring in Indonesia and Vietnam. Simulations with the GEOS-

Chem chemical transport model show large resulting increases in surface air pollution, up to 11 μg m^{-3} for annual mean fine particulate matter ($PM_{2.5}$) in northern Vietnam and up to 15 ppb for seasonal maximum 1-h ozone in Indonesia. We estimate 20,000 excess deaths per year from Southeast Asian coal emissions at present, increasing to 70,000 by 2030. 9,000 of these excess deaths in 2030 are in China. As Chinese emissions from coal decline in coming decades, transboundary pollution influence from rising coal emissions in Southeast Asia may become an increasing issue.

Next, I assess the contributions of fires in different geographic areas to deteoriated air quality across Equatorial Asia during an extreme haze event in September-October 2015, demonstrating for the first time the utility of a new rapid assessment framework. In September-October 2015, El Nino and positive Indian Ocean Dipole conditions set the stage for massive fires in Sumatra and Kalimantan (Indonesian Borneo), leading to persistently hazardous levels of smoke pollution across much of Equatorial Asia. Here we quantify the emission sources and health impacts of this haze episode and compare the sources and impacts to an event of similar magnitude occurring under similar meteorological conditions in September-October 2006. Using the adjoint of the GEOS-Chem chemical transport model, we first calculate the influence of potential fire emissions across the domain on smoke concentrations in three receptor areas downwind Indonesia, Malaysia, and Singapore during the 2006 event. This step maps the sensitivity of each receptor to fire emissions in each grid cell upwind. We then combine these sensitivities with 2006 and 2015 fire emission inventories from the Global Fire Assimilation System (GFAS) to estimate the resulting population-weighted smoke exposure. This method, which assumes similar smoke transport pathways in 2006 and 2015, allows near real-time assessment of smoke pollution exposure, and therefore the consequent morbidity and premature mortality, due to severe haze.

Our approach also provides rapid assessment of the relative contribution of fire emissions generated in a specific province to smoke-related health impacts in the receptor areas. We estimate that haze in 2015 resulted in 100,300 excess deaths across Indonesia, Malaysia and Singapore, more than double those of the 2006 event, with much of the increase due to fires in Indonesias South Sumatra Province. The model framework we introduce in this study can rapidly identify those areas where land use management to reduce and/or avoid fires would yield the greatest benefit to human health, both nationally and regionally.

In the final section of this thesis, I diagnose the meteorological drivers of an unexpected haze event in Singapore during June 2013, and I demonstrate that the conditions responsible for June 2013 are in fact a recurring mechanism for smoke exposure in the Malay Peninsula that has never been identified before. In June 2013, Singapore experienced severe smoke levels, with surface particulate matter concentrations reaching above 300 $\mu g\ m^{-3}$. Unlike other intense haze events in Singapore and Equatorial Asia (e.g., September 1997, October 2006, September 2015), the June 2013 episode occurred in the absence of El Nino-positive Indian Ocean Dipole (pIOD) conditions generally associated with drought. The smoke originated from fires in the Riau province of central Sumatra and was carried to the Malay Peninsula by westerly winds, unlike typical conditions in September-October events when Singapore is affected by smoke from fires in southern Sumatra and Kalimantan transported by southerly winds. We show that June 2013 was not an exceptional event; inspection of the 2005-2015 record identifies two other severe haze events in the Malay Peninsula (August 2005 and October 2010) occurring under the same conditions. Common to all three events was a combination of late-phase Madden-Julian Oscillation (MJO) and negative phase of the IOD. Our work suggests that the MJO-IOD combination

in medium-range weather forecasts could help predict severe haze events in Singapore and the Malay Peninsula.

Contents

Abstract **vii**

Acknowledgements **x**

1 Introduction **1**
- 1.1 Economic development in Southeast Asia . . . 1
- 1.2 Air pollution and human health . . . 3
- 1.3 Research objectives and approach . . . 4
- 1.4 Summary of results . . . 5

2 Burden of disease from rising coal emissions in Southeast Asia **7**
- 2.1 Introduction . . . 7
- 2.2 Methods . . . 9
  - 2.2.1 GEOS-Chem simulations . . . 9
  - 2.2.2 National coal emission inventories . . . 11
  - 2.2.3 Emissions from future plants . . . 15
  - 2.2.4 Health impact assessment . . . 17
  - 2.2.5 Future health impact projections . . . 20
- 2.3 Results and Discussion . . . 22

3 Public health impacts of the severe haze in Equatorial Asia in September-October 2015: Demonstration of a new framework for informing fire management strategies to reduce downwind smoke exposure **29**
- 3.1 Introduction . . . 30
- 3.2 Methods . . . 32
  - 3.2.1 Fire emissions . . . 32
  - 3.2.2 Surface particulate matter observations . . . 34
  - 3.2.3 Satellite observations . . . 34
- 3.3 Results . . . 35
  - 3.3.1 Fire emissions . . . 35
  - 3.3.2 Smoke exposure during haze events . . . 38
  - 3.3.3 Emission sources . . . 41
  - 3.3.4 Health impact estimates . . . 43
- 3.4 Discussion and Conclusions . . . 44

4 Madden-Julian Oscillation during negative Indian Ocean Dipole conditions as a driver of severe haze events in the Malay Peninsula **48**
4.1 Introduction . . . 48
4.2 Data and Methods . . . 54
4.3 Results . . . 55
4.3.1 Extreme haze in the Malay Peninsula during 2005-2015 . . . 55
4.3.2 Fire activity in Riau . . . 58
4.3.3 Wind anomalies and smoke plumes during August 2005, October 2010, and June 2013 . . . 60
4.3.4 The role of the Madden-Julian Oscillation . . . 64
4.4 Discussion and Conclusions . . . 67

Appendix A **70**
A.1 Concentration response factors . . . 71
A.2 Coal plant locations . . . 72
A.3 National simulations . . . 73
A.4 Contributions to mortality from population projections . . . 75
A.5 Domestic and transboundary contributions to mortality in 2011 . . . 77

Appendix B **78**
B.1 The GEOS-Chem adjoint . . . 79
B.2 Health impact calculations . . . 80
B.3 High resolution FRP observations in concessions . . . 83
B.4 Province masks . . . 86
B.5 Adjoint sensitivities . . . 87
B.6 Fire management strategies in Indonesia . . . 89
B.6.1 Regulating fires in smallholder farms vs. industrial plantations . 89
B.6.2 Extinguishing fires in peatlands . . . 90
B.6.3 Enforcing existing policies . . . 91

Appendix C **93**
C.1 Satellite aerosol observations during June 2004 . . . 94
C.2 Climatological winds . . . 96
C.3 Daily satellite observations of haze events . . . 97
C.4 BSISO timeseries . . . 100

References **117**

To my family and the great city of New Orleans.

Acknowledgments

I would like to start by thanking my advisors Loretta Mickley and Daniel Jacob for the years of patient support and guidance. I am doubly fortunate to have had the opportunity to work with and learn from two impressive scientists so completely committed to the success of their students. I am so grateful to you both. I would like to thank my other committee members, Zhiming Kuang and Dave Johnston, for their continued support and for being easy to find for scheduling. I would also like to acknowledge my former mentors Joelle Underwood and Noah Diffenbaugh for opening my mind to new ideas, and for the many rounds of fellowship application rec letters.

The chapters in this thesis were produced through a significant investment of energy and care by many individuals. I would like to say a big thank you to my collaborators, all of whom have dedicated so much of their own time and efforts to the content of this dissertation: Jonathan Buonocore, Ruth DeFries, David Gaveau, Tina Liu, Bruno Locatelli, Sam Myers, Lauri Myllyvirta, Montira Pongsiri, Colleen Reid, and Joel Schwartz. I would like to especially thank Miriam Marlier and Melissa Sulprizio for being so generous and kind to me throughout our multiple collaborations.

The degree of camaraderie present amongst the Jacob-Mickley students is, I firmly believe, exceptional. In particular, I would like to thank my office mates Bram Maasakkers, Ploy Achakulwisut, and Peter Zoogman, and my mentors Patrick Kim, Helen Amos, Eloise Marais and Mike Long. Thank you all for everything you have taught me. I

would also like to thank Bob Yantosca and the other members of the GEOS-Chem Support Team for keeping us all afloat and for doing it so graciously, and to our group administrator Brenda Mathieu, who somehow manages to keep multiple groups of scientists organized at once. The EPS department is a wonderful place to be a grad student. A special thank you to Sarah Colgan, Maryorie Grande, Chenoweth Moffatt, and the rest of the Hoffman 4th floor team for turning what could have been a typical grad school environment into a warm and welcoming place of community.

I have formed some of my greatest friendships in Boston. Because listing everyone by name would require another hundred pages, I will just say - to my EPS crew, the ladies of wine time, Foul Play and affiliates, and the lawyers (and friends): I love you all. Thank you for everything.

Finally and most importantly, I want to thank my family. My grandparents, aunts, uncles, and cousins for being an exceptionally loving and good natured group of people. My beautiful partner Karen for the endless support and encouragement, especially during the last few months. The rest of the Tarkulich family, Joan, Bill, Michelle, Suzanne and Abby for welcoming me into their home and providing some much needed evenings away from work. My younger brother Trevor, for being an example of empathy and diligence. And of course my parents, for 28 years of unconditional love and respect, and for showing me that being generous and compassionate is always the most important thing.

1

Introduction

1.1 Economic development in Southeast Asia

Southeast Asia is one of the most densely populated and rapidly growing regions in the world. It is also resource rich with abundant fossil fuel reserves, dense forests full of valuable timber, and conditions prime for crop production. Between 2000 and 2013, Southeast Asia as a region experienced the 3rd most gross domestic product (GDP) growth globally, exceeded only by China and India (HV et al., 2014). Electricity demand in 2035 is projected to increase by 83% from 2011 levels, more than twice the global average (IEA, 2013). Most of this growing electricity demand is projected to be met by coal given its local abundance and consequently lower cost (Zhu, 2013). Keeping pace with this econcomic expansion is a growing population; the population of Southeast Asia is currently growing at 1.1% (6 million people) per year projected to

continue growing at this rate for the foreseeable future (Jones, 2013). People are also migrating from rural areas to cities, increasing the population density in urban centers even further (IEA, 2015). Such booming development coupled with an expanding, urbanizing population is compounding the existing, already severe air quality problem plaguing this growing region (Chapter 2).

In addition to domestic economic development, growing global markets have also catalyzed the expansion of anthropogenic activity within the region, particularly in Indonesia. Since the 1970s, Indonesia has become a global leader in the production of timber for pulp and paper, and oil palm fruit for palm oil, whose applications range from cosmetics and food products to biofuels. To accomodate the increasing global demand for these products, extensive swaths of land are cleared every year with slash and burn techniques to make way for large plantations. Unlike other regions that experience significant annual burning such as sub-Saharan Africa or the western U.S., high fire activity is not a natural feature of the Indonesian landscape (Mouillot & Field, 2005; Page et al., 2009). Indonesia's two main islands, Sumatra and Borneo, both contain large mountain ranges through their centers, signficantly limiting the amount of flat land available for crop cultivation. The remaining surface area is dominated by low lying coastal wetlands, which, in their pristine state, are covered in standing water for more than half the year (Turetsky et al., 2015). In order to burn more efficiently, the peatlands are drained via massive canals cut through the swamps. Consequently, the once fire-resistant peatswamps have become increasing vulnerable to burning, and under particular meteorological conditions can create massive haze events blanketing the entire Equatorial Asian region, such as those in 1997 and 2006. Despite growing awareness about the underlying meteorological and anthropogenic drivers of these extreme haze events, regional governmental efforts to reduce the eco-

nomic and air quality damage during these episodes remain ineffective, as was evidenced by the recent haze of 2015 (Chapter 3). In some areas like Riau province, peat degradation may be extensive enough that extreme drought conditions are no longer needed to facilitate haze, for example the unexpected haze in the Malay Peninsula during June 2013 (Chapter 4).

1.2 Air pollution and human health

The primary outdoor air pollutants responsible for degraded human health are fine particulate matter ($PM_{2.5}$) and ozone. Both are respiratory irritants that can lead to a range of respiratory and cardiopulmonary afflictions in humans, as well as reduced visibility and damage to crops and ecosystems (Ainsworth, 2008; Anenberg et al., 2010). Many anthropogenic and natural process release emissions of chemical species that go on to form $PM_{2.5}$ and ozone in the atmosphere. Primary $PM_{2.5}$, i.e. particles directly emitted as $PM_{2.5}$ from the source, is produced mainly by combustion processes, for example fly ash from coal burning or the carbonaceous aerosol present in smoke from fires. Secondary $PM_{2.5}$, or particles that were originally emitted in the gas phase and then became aerosols as a result of chemical proccesing in the atmosphere, is formed from a range of atmospheric emissions but most prevalently from sulfur dioxide (SO_2) and nitrogen oxides (NO_x), both of which are also released from coal combustion. NO_x is also a precursor for ozone formation.

Given knowledge about the atmospheric composition in a particular region, which can be estimated with a well-constrained a chemical transport model, it is possible to estimate the human health impacts of air pollutant concentrations with emperically derived concentration-response functions (CRFs) from the epidemiological literature

(Jerrett et al., 2009; Krewski et al., 2009). CRFs quantitatitvely relate a change in a particular risk factor (e.g. $PM_{2.5}$ or ozone) to a change in a the health endpoint of interest (e.g. premature death). A range of possible CRFs exist in the literature, and so it can be difficult to compare across assessments that make different assumptions. Additionally, many of the CRFs used in the literature are based on data from the U.S. or Europe, potentially confounding efforts to apply such relationships in other parts of the world. Despite these challenges, incorporating assessments of the human health implications of economic and energy-related decisions is increasingly regarded as an important consideration for state, regional, and national governments (Kemm, 2001).

1.3 Research objectives and approach

Despite its large populations and accelerating development, the situation in Southeast Asia has been largely overshadowed by the scale of activity occuring elsewhere in Asia. The goal of this thesis is to understand and quantify the rising risk to human health of the vigorous economic expansion occuring in such a dynamic yet understudied region. Specifically, I address the following objectives:

1. Develop updated inventories of presently operating and planned coal fired power plant emissions across Southeast Asia to estimate the implications of rising coal pollution for regional air quality and human health.

2. Quantify the contributions from fires in specific geographic areas to regional smoke-related $PM_{2.5}$ and the associated premature mortality during the severe El Nino-positive Indian Ocean Dipole haze of September-October 2015, demonstrating for the first time the utility of a new near real-time assessment framework during an

ongoing haze event.

3. Understand the meteorological mechanism driving the unexpected non-El Nino-pIOD haze in the Malay Peninsula during June 2013 (as well as the previously unexplained events of October 2010 and August 2005) in order to better predict and mitigate the damage from similar events in the future.

To achieve these objectives, I use simulations of $PM_{2.5}$ and ozone concentrations from the GEOS-Chem chemical transport model in conjunction with a suite of surface and satellite observations, state-of-the-science emission inventories, and empirically derived concentration-response functions from the epidemiological literature.

1.4 Summary of results

Emissions from coal fired power plants in Southeast Asia could triple by 2030, leading to more than 70,000 premature deaths annually. Southeast Asian coal pollution will be increasingly important for air quality in China as domestic emissions there decrease.

Using the SMOKE rapid assessment framework to characterize an ongoing haze event for the first time, we estimate that fires in Indonesia during September-October 2015 released enough particulate pollution to cause upwards of 100,000 premature deaths across Indonesia, Malaysia, and Singapore. Because of its low computational costs, the SMOKE framework could be easily implemented to help stakeholders allocate fire management resources more effectively in the future, even as a haze event is still unfolding.

The Madden Julian Oscillation (MJO) - negative Indian Ocean Dipole (nIOD) conditions that lead to the severe haze in Singapore during June 2013 represent a previ-

ously unappreciated meteorological pathway by which fires in Riau province are repeatedly degrading air quality and impacting human health across the Malay Peninsula. Our results suggest that the MJO-nIOD pathway may occur more frequently than the El Nino-pIOD mechanism conventionally associated with extreme haze in Equatorial Asia.

2

Burden of disease from rising coal emissions in Southeast Asia

2.1 Introduction

Coal emissions have been decreasing in the U.S. and Europe for the past two decades due to concern over public health and now increasingly over climate change. In contrast, coal emissions in much of Asia have been increasing rapidly (Amann et al., 2013; Klimont et al., 2013). Air quality impacts of coal use in China and India have received considerable attention (Chen & Xu, 2010; Wang et al., 2010; Lu et al., 2013; Guttikunda & Jawahar, 2014). Far less attention has been given to the growing use of coal in Southeast Asia including Indonesia, Vietnam, Thailand, and neighboring coun-

A version of this chapter written with Daniel J. Jacob, Melissa P. Sulprizio, Lauri Myllyvirta, and Colleen Reid is in review with Environmental Science & Technology.

tries. Southeast Asia is one of the fastest developing regions in the world; electricity demand in 2035 is projected to increase by 83% from 2011 levels, more than twice the global average (IEA, 2013). Accompanying this economic development is population growth. Indonesia alone is projected to increase its population by 67 million people (28%) between 2010 and 2035 (McDonald, 2014). Population migration from rural areas to cities, or urbanization, also increases population densities in polluted areas and heightens demand for grid-based electricity produced by power plants; urbanization rates in Southeast Asia are some of the highest globally, and are projected to increase significantly by 2030 (IEA, 2015). This growing demand for energy is presently expected to be met by coal because of its low cost and domestic abundance (Zhu, 2013). We show here that the public health consequences would be severe.

Coal combustion emits sulfur dioxide (SO_2) and nitrogen oxides (NO_x), leading to formation of fine particulate matter ($PM_{2.5}$), particles less than 2.5 μm in diameter) and ozone. $PM_{2.5}$ increases the risk of premature mortality from respiratory and cardiovascular disease. It is the most harmful pollutant to human health worldwide (WHO, 2010). Surface ozone is also a major concern for public health and ecosystems (Ainsworth, 2008; Anenberg et al., 2010). Emissions of SO_2 and NO_x can vary widely by coal plant depending on the grade of coal combusted, the type of boiler used, and the emission controls in place (Miller, 1986; Zhao et al., 2010).

Here we estimate the burden of air pollution disease due to current (2011) and projected (2030) coal use in Southeast Asia and other East Asian countries outside of China and India. Our 2030 projection is for a coal future scenario including all plants currently in construction or in the planning stages. The resulting $PM_{2.5}$ and ozone concentrations are computed with a high-resolution version of the GEOS-Chem global 3-D chemical transport model, and the resulting premature mortalities are estimated

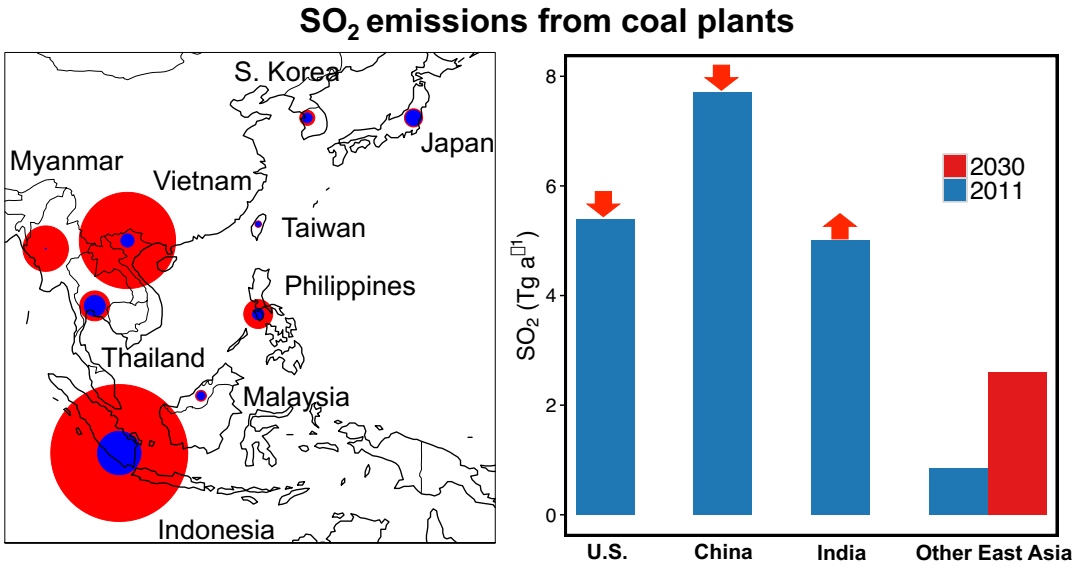


Figure 2.1: Coal SO_2 emissions in 2011 and 2030 for the countries considered in this work (see Table 2.1). The left panel shows national emissions in 2011 and 2030, where the areas of the circles are proportional to emissions (see Figure A.1 for plant locations). The right panel compares 2011 and 2030 total regional emissions from countries in this work (Other East Asia) to 2010 estimates for the U.S.(USEIA, 2011), China (Liu et al., 2015), and India (Lu et al., 2011). The red arrows represent projected future trends for China, India, and the U.S.

using approaches from the epidemiological literature.

2.2 Methods

2.2.1 GEOS-Chem simulations

We use the GEOS-Chem simulation of aerosol-oxidant chemistry (Park, 2004; Kim et al., 2015a) (v9-02; `http://geos-chem.org`) driven by 2011 assimilated meteorological data from the Goddard Earth Observation System (GEOS-5) of the NASA Global Modeling and Assimilation Office (GMAO). The GEOS-5 data have 0.5 x 0.666 native horizontal resolution and 72 vertical levels (14 levels below 2 km). The GEOS-Chem simulation is conducted at the native resolution over East Asia and

adjacent oceans (11S-55 N, 70-150 E) (Chen et al., 2009; Wang et al., 2013) nested within a global simulation at 2 x 2.5 resolution that provides dynamic boundary conditions. This East Asian nested version of GEOS-Chem has been extensively evaluated for China with observations of aerosols (Wang et al., 2013; van Donkelaar et al., 2008; Fairlie et al., 2010; Fu et al., 2012; Xu et al., 2013) and ozone (Zhang et al., 2008; Wang et al., 2009; Worden et al., 2009; Wang et al., 2011). Evaluations have also been performed for Southeast Asia (Trivitayanurak et al., 2012; Kim et al., 2015b), but observations are more limited in that region.

Global anthropogenic emissions of SO_2 and NO_x are from the Emissions Database for Global Atmospheric Research (EDGAR) v4.2 for 2008, the most recently available year (http://edgar.jrc.ec.europa.eu). Coal emissions in East Asian countries outside of China and India are superseded by our own inventories, as described below.

We conduct three 1-year simulations using 2011 meteorology, differing only in their coal emissions for East Asia outside of China and India: (1) 2011 coal emissions, (2) 2030 emissions projected for the coal future scenario, and (3) zero coal emissions. EDGAR provides total emissions from energy generation but does not resolve the contribution of each fuel type. We isolate the coal-related emissions by gridding and subtracting our 2011 emissions from the EDGAR values in each grid square at 1 x 1 horizontal resolution, resulting in scenario (3). If this subtraction results in a negative no-coal value (i.e. our 2011 emissions exceed the EDGAR value for that grid square), the no-coal value for that grid square is set to zero. We then add in either our 2011 emissions or projected 2030 emissions to create scenarios (1) and (2). We simulate scenarios (1) and (2) for all countries included in this work taken together, as well as for each country individually. Our analysis here will mostly focus on totals for all countries taken together, but results for individual countries (called national simu-

lations) will be used to separate domestic and transboundary pollution influences. Results for all the national simulations are in the Supporting Information. Each simulation was initialized for four months prior to January 2011.

2.2.2 National coal emission inventories

We implement into GEOS-Chem a new plant-specific inventory for 2011 coal emissions of SO_2, NO_x, and primary $PM_{2.5}$ in East Asia outside of China and India. Countries included are Cambodia, Indonesia, Japan, Laos, Malaysia, Myanmar, the Philippines, South Korea, Taiwan, Thailand, and Vietnam (Table 2.1). Plant location and capacity information are based on the Platts Utility Data Institute (UDI) World Electric Power Plant Database (WEPP) (Platts, 2014). Plant locations are shown in Figure A.1. Our approach for estimating pollutant emissions at each facility is described below.

Table 2.1: National inventories of emissions from coal-fired power plants.[a]

Country	# of plants 2011	# of plants 2030	SO_2 2011	SO_2 2030	NO_x 2011	NO_x 2030	$PM_{2.5}$ 2011	$PM_{2.5}$ 2030
Cambodia	1	6	< 0.01	< 0.01	< 0.01	< 0.01	< 0.01	< 0.01
Indonesia	147	323	0.29	0.90	0.29	0.88	0.03	0.05
Japan	160	172	0.10	0.12	0.10	0.12	< 0.01	< 0.01
Laos	0	3	< 0.01	< 0.01	< 0.01	< 0.01	< 0.01	< 0.01
Malaysia	18	26	0.05	0.07	0.07	0.11	< 0.01	< 0.01
Myanmar	3	16	0.01	0.30	< 0.01	0.18	< 0.01	0.01
Philippines	30	77	0.07	0.19	0.08	0.25	< 0.01	0.01
South Korea	97	123	0.06	0.10	0.08	0.12	< 0.01	< 0.01
Taiwan	71	81	0.03	0.04	0.05	0.06	< 0.01	< 0.01
Thailand	37	48	0.14	0.20	0.11	0.15	0.01	0.01
Vietnam	38	133	0.09	0.63	0.08	0.69	0.01	0.07
Total	**602**	**1008**	**0.84**	**2.60**	**0.86**	**2.63**	**0.06**	**0.16**

[a]Annual emissions for 2011 and projections for 2030. The 2030 projections are for a business-as-usual, coal future scenario including all plants currently planned or under construction, with emission controls based on current national standards and practices. See text for details.

The magnitude of emissions from coal plants varies widely for individual facilities depending on (1) the grade of coal combusted (lignite, sub-bituminous, bituminous, or anthracite), (2) the sulfur content of the coal, (3) the type of boiler used to combust the coal, (4) emission control technologies, and (5) the operational profile of the facility defined by the electricity generation capacity, load factor (ratio of the average output to the maximum possible output), and thermal efficiency (amount of electrical energy output per unit of coal heat content consumed). Factors (1)-(4) determine the stack gas concentration at a given facility in units of mg Nm^{-3} (the N denotes normalized to dry conditions at 1 atm, 6% excess oxygen, 25° C). Factor (5) determines the fuel consumption H [GJ a^{-1}] at facility i:

$$H_{\mathrm{i}} = \frac{(\lambda_{\mathrm{i}}\gamma_{\mathrm{i}})}{\eta_{\mathrm{i}}} \tag{2.1}$$

where λ [GJ a^{-1}] is the electric capacity, is the fractional load factor, and is the thermal efficiency. Multiplying the fuel consumption by the stack gas concentration of pollutant j (Ω) and specific flue gas volume of the fuel used σ [Nm^3 GJ^{-1}] yields annual emission estimates $E_{i,j}$ [Tg a^{-1}] of pollutant j from facility i:

$$E_{\mathrm{i,j}} = H_{\mathrm{i}}\sigma_{\mathrm{i}}\Omega_{\mathrm{i,j}} \tag{2.2}$$

Operational data for ηand γfor most existing plants were obtained from the Carbon Monitoring for Action Database (CARMA; Wheeler & Ummel, 2008)(http://www.carma.org). For individual plants not covered by CARMA, national average

values were calculated and applied based on information available for plant size and steam condition (Ansolabehere, 2007). Aggregated national fuel consumption totals were scaled to match the 2011 statistics for total coal consumption in the power sector by country from the International Energy Agency (IEA). Fuel consumption values at individual facilities were then adjusted based on these national scale factors derived from the IEA comparison. Specific flue gas volume estimates of 337.1 Nm^3 GJ^{-1} for hard coal (anthracite, bituminous, sub-bituminous) and 360.6 Nm^3 GJ^{-1} for lignite were used based on data from the European Environment Agency (EEA, 2008). If coal type was not reported, we assumed the specific flue gas volume for hard coal.

Stack gas concentrations (Ω) used in equation (2.2) were obtained through three different approaches, in order of preference: a) reported stack gas concentrations for the facility; b) company averages provided by Corporate Social Responsibility (CSR) reports; c) national emission standard based on electric capacity and operational start year of the facility.

In countries that do not regulate stack emission concentrations of pollutants (Myanmar for all pollutants; Taiwan for SO_2 and NO_x), rather than using equations (2.1) and (2.2), a national average emission rate per TJ of power generated by coal was derived from the Regional Emission inventory in Asia (REAS v2.1; Kurokawa et al., 2013). These emission rates were then combined with the 2011 IEA estimates for total power generation from coal for that country to estimate total national emissions in 2011. The derived national emission totals were then spatially allocated to individual facilities based on capacity.

Primary particulate matter (PM) emissions from power plants are often reported in terms of total PM. To obtain estimates of $PM_{2.5}$ specifically, $PM_{2.5}$ fractions were estimated using PM size distributions from the U.S. Environmental Protection Agency

AP-42 database (USEPA, 1995) for different control technologies when plant-specific emission control technology information was available. Otherwise we assumed the use of an electrostatic precipitator (ESP) to remove fine primary particles with a 99% removal efficiency for all plants in countries with any stack emission regulations. If PM emissions were unregulated or above 500 mg Nm^{-3} (implying lack of any emission control), we applied the AP-42 particle size distribution associated with uncontrolled combustion.

2.2.3 Emissions from future plants

Our 2030 inventory includes the 2011 estimates as well as projected emissions from plants currently listed as under construction or planned based on a comprehensive mapping of new power plant projects from the CoalSwarm database (Shearer et al., 2015). We include the presently operating 2011 plants in our future projections because the average lifetime of a coal plant is 30-40 years (Proops et al., 1996) and most current plants were built after 1990.

New power plants are assumed to meet current national emission standards for new plants (when more specific information about emissions is not available), and to operate at a load factor of 80%, in line with available data from CARMA for newly operational units in this region. For countries in which 2011 emission rates from existing plants are below national standards, new power plants are assumed to over-achieve the standards by the same ratio. In addition, when information about the emission control configuration is reported at a facility planned or under construction, standard performance in the control of emissions (emissions per unit of fuel consumption) is assumed based on the US EPA AP-42 database (USEPA, 1995) values for the technologies in that configuration. Such configuration components include low-NO_x boilers,

flue gas desulfurization (FGD), selective catalytic reduction devices, and baghouses. All new power plants for which information on particulate control technology is not available are still assumed to install an ESP (described above).

In countries with lenient emission standards for new power plants such as Indonesia and Myanmar, these minimum emission control performance assumptions likely lead to conservative emission estimates from new plants and therefore a possible underestimate of future coal pollution and health impacts in these countries. On the other hand, our 2030 estimates represent a Business As Usual scenario where we do not account for possible future improvements in the extent or type of emission control technologies.

Coal-fired power plant emissions of SO_2, NO_x, and $PM_{2.5}$ for each country in 2011 and 2030 are listed in Table 2.1. National SO_2 emissions for 2011 and 2030 are shown in Figure 2.1. Total SO_2 emissions from coal in 2011 are 0.84 Tg a^{-1} for the countries in Table 2.1, as compared to 7.7 Tg a^{-1} in China (Liu et al., 2015) and 5 Tg a^{-1} in India (Lu et al., 2011). Total NOx emissions are 0.86 Tg a^{-1} for the countries in Table 2.1, compared to 8.3 Tg a^{-1} in China (Liu et al., 2015) and 2 Tg a^{-1} in India (Lu & Streets, 2012). Indonesia is the largest East Asian source in 2011 outside of China and India.

By 2030, our projections indicate that total SO_2 and NO_x emissions for the countries in Table 2.1 will increase by a factor of three, resulting in emissions of 2.6 Tg a^{-1} each for SO_2 and NO_x. Southeast Asia dominates this expansion, with Indonesia and Vietnam together accounting for 67% of the total increase. Indonesia is planning 176 new coal plants by 2030, 75 of which are already under construction, and it has relatively lax emission standards. Myanmar shows the highest relative increase in emissions by 2030, becoming the 3rd largest emitter after contributing almost no emissions

in the present day.

Table 2.1 shows almost no increase in emissions for Japan between 2011 and 2030. However, 16 GW of additional coal-fired capacity has been proposed for Japan since our emission calculations were completed (Kiko Network; http://sekitan.jp/plant-map/en/v2/table_en). This is more than twice the 6.2 GW of new capacity we assume for Japan in our analysis. This newly announced capacity will likely result in higher emissions by 2030 than is represented in our results. Conversely, the presently operating fleet of Japanese plants is significantly older than for the other countries we consider here. 26% of Japanese plants operating at the end of 2015 will have exceeded 40 years of operation by 2030 (compared to the regional average of 8%) (Platts, 2015). Up to 11 GW of Japanese fleet capacity could therefore be retired before 2030.

Various projections to 2030 are available for future coal emissions from China and India (Zhao et al., 2014; Cofala et al., 2015). The general consensus is that India emissions will increase while China emissions will decrease, the latter because of emission controls (Liu et al., 2015; Zhao et al., 2014). Emissions in both the U.S. and the European Union are projected to decrease by 70% by 2030 (USEPA, 2014; Amann et al., 2012). These reductions would result in total coal emissions of 1.5 Tg a^{-1} each for SO_2 and NO_x in the U.S. and 1 Tg a^{-1} each for SO_2 and NO_x in Europe. Our results suggest that coal emissions from Southeast Asia in 2030 could exceed the sum of emissions in the U.S. and Europe.

2.2.4 Health impact assessment

We follow the methods outlined in Anenberg et al. (2010) to estimate the premature mortality from coal-related $PM_{2.5}$ and ozone pollution. We use for this purpose the population distribution for 2010 from the Center for International Earth Sci-

ence Information Network (CIESIN) (http://beta.sedac.ciesin.columbia.edu/data/collection/gpw-v4), scaled to match the national population totals for 2011 from the 2015 Revision of the United Nations World Population Prospects (http://esa.un.org/unpd/wpp/). The adjusted CIESIN population data are regridded from 0.5 x 0.5 horizontal resolution to the GEOS-Chem resolution of 0.5 x 0.666. Coal-related pollution in 2011 is calculated as the difference between the GEOS-Chem simulation with 2011 emissions for the countries in Table 2.1 and the simulation with zero coal emissions for these countries.

Premature deaths attributable to a particular risk factor, in this case coal-related $PM_{2.5}$ and ozone, are those occurring in excess of the baseline death rate (the death rate observed in the absence of the risk factor of interest, in number of deaths per 1000 people per year). Death rates can be calculated for all causes of death (all-cause) or for individual causes (cause-specific). We use cause-specific death rates because this approach is thought to incur lower errors when applying concentration response factors (discussed below) based on cohort studies done in the U.S. (Anenberg et al., 2012). We include stroke, ischemic heart disease (IHD), other cardiovascular disease, lung and throat cancer, chronic obstructive pulmonary disease (COPD), lower respiratory infections (LRI), and other respiratory diseases as independent causes of premature death due to $PM_{2.5}$ pollution. We only include ozone-related deaths related to respiratory diseases. For our 2011 mortality calculations, we use national cause-specific baseline death rates for 2012 from the World Health Organization (WHO, 2014) (http://www.who.int/healthinfo/global_burden_disease/en/). Death rates for the 2030 health calculations are discussed in the Future health impact projections section below.

Relating a change in pollutant concentration to premature mortality requires con-

centration response factors, or CRFs, empirically derived from long-term cohort studies. Annual average $PM_{2.5}$ concentration is the standard metric for assessing health effects from chronic $PM_{2.5}$ exposure (Krewski et al., 2009; USEPA, 2010). For ozone, we use the average daily maximum 1-h ozone concentration during the seasonal 6-month window of peak ozone exposure (Jerrett et al., 2009).

To quantify the burden of disease from coal pollution in each country, we first calculate the population-weighted exposure by multiplying the population distribution from CIESIN with the annual coal-related increases in annual mean $PM_{2.5}$ or seasonal maximum 1-h ozone from GEOS-Chem, and dividing by the national population totals. We then take the cause-specific death rates by country and assume the same CRF function shape used in Anenberg et al. (2010) to calculate the change in annual premature mortality ΔM deaths per year due to coal pollution for each cause of death in each country k:

$$\Delta M_{\alpha k} = y_{0_{\alpha k}}(1 - exp^{-\beta_\alpha \Delta x_k})P_k \tag{2.3}$$

where y_0 is the cause-specific baseline death rate [% per year] in the country, Δx is the population-weighted change in pollutant concentration in μg m^{-3} (for $PM_{2.5}$) or ppb (for ozone), βis the cause-specific CRF relating a one-unit change in each pollutant to the predicted change in premature mortality (see Table A.1 for βvalues used for each cause of death), and P is the total population of the country. The uncertainty ranges reported are derived using low, central, and high estimates for each CRF value (Table A.1). We also tested the sensitivity of our calculations to imposing high (HCT) and low (LCT) $PM_{2.5}$ concentration thresholds above and below which

the relationship between mortality and pollutant concentration becomes less certain. Following Anenberg et al. (2010), we impose a HCT of 50 μg m^{-3} and a LCT of 5.8 μg m^{-3} on the gridded GEOS-Chem $PM_{2.5}$ results before calculating the national population-weighted $PM_{2.5}$ averages to estimate mortality. The combined effect of imposing both thresholds on total estimated mortality was less than 7% (not shown).

2.2.5 Future health impact projections

To estimate changes in premature mortality due to future coal pollution, we follow the approach outlined above but also account for changes between 2011 and 2030 in the population size, geographic distribution and epidemiological profile. Aside from overall population growth, many countries in Southeast Asia are experiencing rapid urbanization, resulting in higher population densities in polluted areas. The populations are also undergoing changes in age structure and lifestyle (diet, activity level, income, etc) that may influence vulnerability to disease, resulting in changes in baseline death rates. Before including these factors in our mortality estimates, we first calculate national population-weighted pollution totals for 2030 from the increase in coal pollution from GEOS-Chem, taken as the difference between the 2030 and 2011 simulations, and the geographic population distribution for 2011. These initial 2030 estimates will hereafter be referred to as the original exposure estimates. The future population projections discussed below are then used to modify the original exposure estimates to reflect the additional influences of population growth, urbanization, and epidemiological shifts on pollution exposure and associated mortality in 2030.

For changes in population numbers by 2030, we use country-level projections of population growth for 2030 from the World Bank (http://data.worldbank.org/data-catalog/population-projection-tables). We multiply the original exposure

estimates for each country by the updated population totals for 2030 to include the influence of national population growth on future coal pollution exposure.

We account for the influence of urbanization by including World Bank projections of the fraction of the population living in urban areas in 2030 (http://databank.worldbank.org/data/, Health Nutrition and Population Statistics: Population estimates and projections database). These projections are only given at the national level. Following Brauer et al. (2012), we define urban grid cells in 2011 as those in the CIESIN GPWv4 data with population density greater than 600 people per km^2. We then use the World Bank projections to scale the urban vs. rural fractions of individual countries to estimated 2030 levels.

To estimate the expected changes in baseline cause-specific death rates due to changes in epidemiological characteristics in 2030, we used the central (rather than pessimistic or optimistic) total death rate projections from the Global Burden of Disease (GBD) for 2030 updated with the 2013 Global Health Estimates (http://www.who.int/healthinfo/global_burden_disease/projections/en/)(Mathers & Loncar, 2006). The GBD projections for 2030 are not done by country but by various groupings. Here we use the World Bank Income Groups: low income, lower middle income, upper middle income, and high income. Each country is assigned to one of these income groups based on gross national income per capita (http://data.worldbank.org/news/new-country-classifications-2015). We estimate cause-specific baseline death rates for each country in 2030 by scaling the national 2012 specific baseline death rates (described above) based on the relative change of GBD death rate projections between 2012 and 2030 for the relevant income category for each country.

2.3 Results and Discussion

Figure 2.2 shows the increases (Δ) in annual mean surface $PM_{2.5}$ and 6-month averaged daily maximum 1-h ozone in 2011 due to coal emissions for the countries of Table 2.1. The resulting exposure densities, computed by multiplying by population density, are also shown. Corresponding figures showing increases from coal emissions in individual countries are in the Supporting Information (Figures A.2-A.3). Our $PM_{2.5}$ calculations assume dry conditions and do not include water vapor, resulting in conservative estimates (assuming 35% relative humidity increases inorganic $PM_{2.5}$ mass by 33% compared to dry conditions). $PM_{2.5}$ increases are localized over major urban areas and reach 3 $\mu g\ m^{-3}$ over northern Vietnam. Ozone increases are more spread out but again show peaks of 2-5 ppb over urban areas. These urban influences are magnified in the population exposure density panels, which also show large impacts on eastern China caused by transboundary transport of pollution from Southeast Asia. We discuss the influence on China in more detail below.

Figure 2.3 shows the same results for 2030. Increases in $PM_{2.5}$ exceed 11 $\mu g\ m^{-3}$ over Hanoi and reach 5 $\mu g\ m^{-3}$ over Jakarta and much of southern Sumatra. Increases in ozone are as high as 15 ppb over Indonesia and northern Vietnam. Sulfate contributes 56% of the overall regional increase in $PM_{2.5}$, followed by ammonium (18%), nitrate (15%), and primary particulate emission (11%). From an exposure perspective, sulfate is somewhat less important (38%) while nitrate is more important (29%) because most of the excess ammonia available for nitrate formation comes from croplands near populated areas.

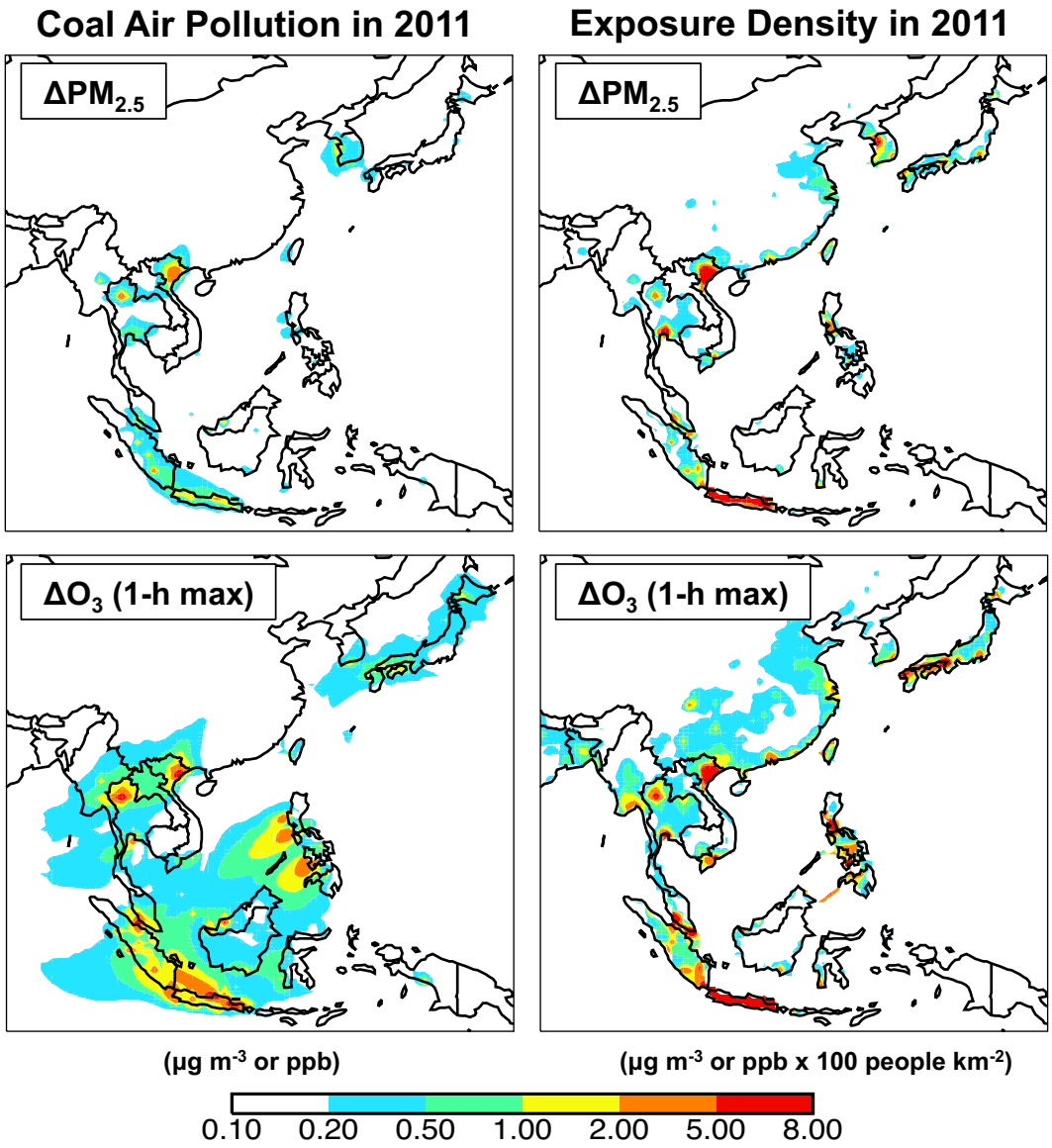


Figure 2.2: Simulated increases (Δ) in surface $PM_{2.5}$ ($\mu g\ m^{-3}$) and ozone (ppb) in Southeast Asia due to coal pollution in 2011, and associated population exposure density (multiplying the concentration increase by the population density). Coal pollution in 2011 is determined by the difference between a simulation with 2011 emissions and a simulation with zero coal emissions for the countries in Table 2.1 (emissions in other countries are unchanged). Values for $PM_{2.5}$ are annual means and values for ozone are 1-h daily maxima averaged for the locally determined 6-month high-ozone season. These metrics are used for the premature mortality calculations as described in the text.

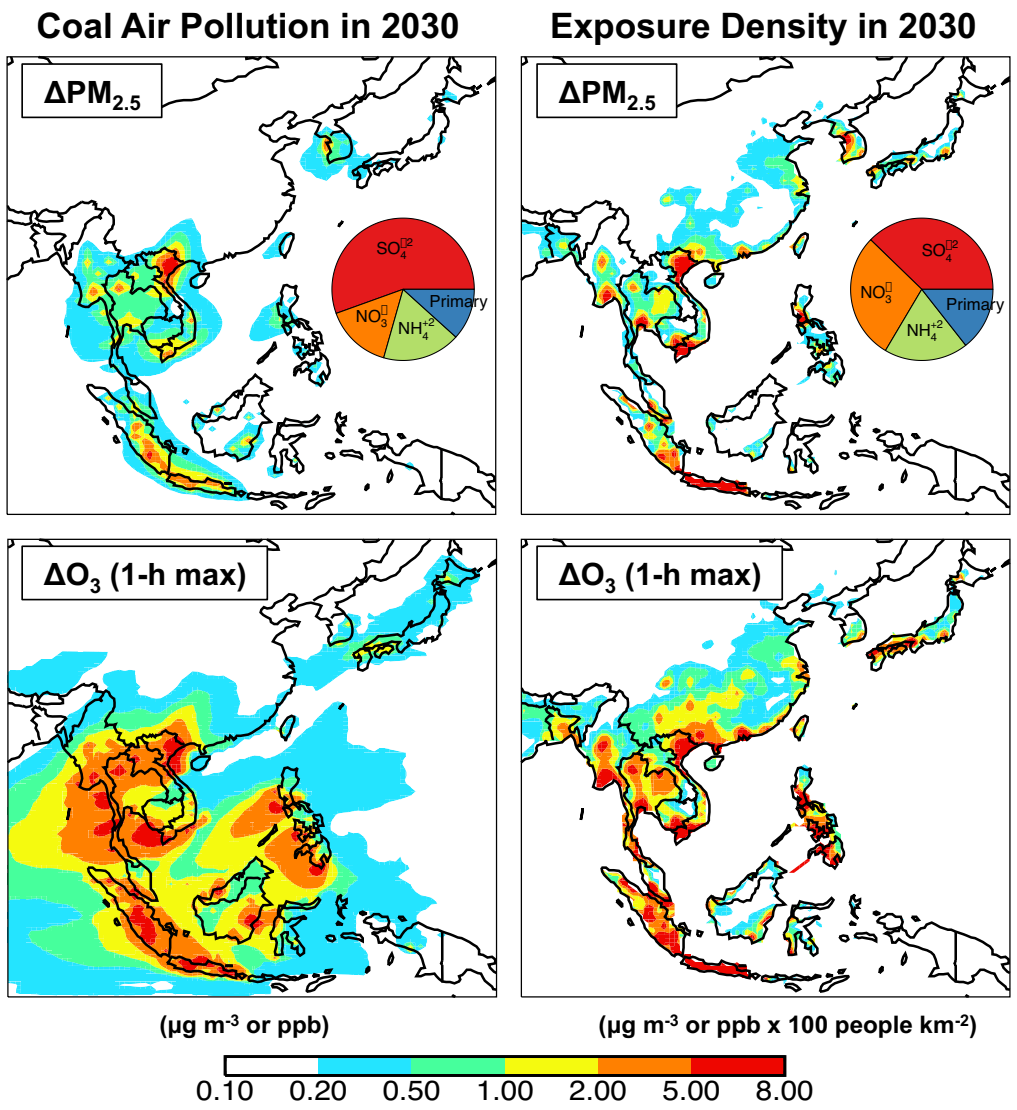


Figure 2.3: Same as Figure 2.2 but for 2030. Pie charts inset show relative contributions of different aerosol types to regional $PM_{2.5}$ coal pollution.

The population-weighted $PM_{2.5}$ and ozone increases in Figures 2.2 and 2.3, combined with equation (2.3), allow us to compute the current and future premature deaths caused by coal emissions. We estimate 19,880 (11,400-28,400) premature deaths in 2011 from coal combustion in the countries of Table 2.1, where the numbers in parentheses indicate the uncertainty bounds of the estimate derived from the high and low CRF values shown in Table A.1. Of these 17,940 are due to $PM_{2.5}$ and 1,940 due to ozone. Figure 2.4 shows the breakdown by country and by cause of death (the breakdown shown is for 2030, but percentages for 2011 are almost identical). Most premature deaths are due to ischemic heart disease (6,470) and stroke (5,970). Mortality is highest in Indonesia (7,480 excess deaths per year) followed by Vietnam (4,250 excess deaths per year). China incurs the third highest mortality after Indonesia and Vietnam with 3,150 excess deaths per year.

By 2030, we project that total regional premature mortality due to coal pollution will be 63,520 excess deaths from $PM_{2.5}$ and 6,140 from ozone, resulting in a total of 69,660 (40,080-126,710) excess deaths per year (Figure 2.4; see Figure A.4 for the relative contributions of projected population growth, urbanization, and epidemiological shifts to these estimates). The highest mortality totals again occur in Indonesia (24,400 excess deaths per year), Vietnam (19,220 excess deaths per year), and China (8,870 excess deaths per year). Myanmar experiences the 4th-highest mortality in 2030 with 4,030 excess deaths per year, reflecting the dramatic increase in emissions projected there (Table 2.1).

The right panel of Figure 2.4 shows for each country the contributions to 2030 premature mortality from domestic and foreign coal emissions. These were obtained from the national simulation results with vs. without coal emissions for individual countries. We find that more than 80% of coal-related mortality in individual countries

of Southeast Asia is due to domestic emissions. The exception is Thailand, for which transboundary pollution from nearby Vietnam is larger than the domestic source.

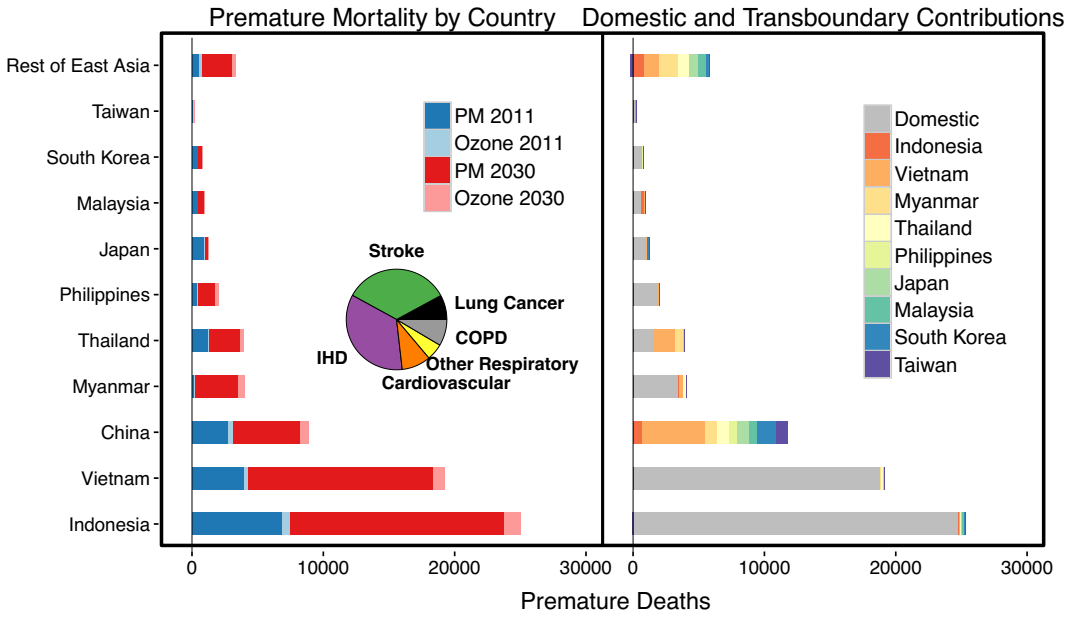


Figure 2.4: Coal-related mortality due to emissions in Southeast Asia (countries in Table 2.1). The left panel shows the premature deaths in individual countries. Premature deaths due to 2011 emissions are shown in blue, and increases from projected 2030 emissions are shown in red. Deaths due to $PM_{2.5}$ and ozone are shown separately. The fraction of $PM_{2.5}$-related mortality by cause is shown in the pie chart as an average for the whole region in 2030 (IHD $\equiv$ ischemic heart disease, COPD $\equiv$ chronic obstructive pulmonary disease). All ozone-related mortality is from respiratory diseases. The right panel shows the 2030 coal-related mortality in each country broken down by contributions from domestic and transboundary sources (see Figure A.5 for the domestic and transboundary contributions in 2011). Source countries responsible for transboundary pollution are identified in the legend. As computed here, mortality in China and Rest of East Asia (not included in Table 2.1) is solely from transboundary pollution. The mortality totals in the right panel are the sums of the contributions from the national simulations with vs. without coal emissions for the individual countries in Table 2.1; because of chemical and CRF non-linearities they may be greater than the mortality totals in the left panels.

Vietnam is the largest transboundary contributor to 2030 mortality in China, mainly influencing southern China by direct transport of coal $PM_{2.5}$. In addition, we see in Figure 2.3 significant population exposure in the densely populated East China Plain.

The increase in $PM_{2.5}$ there is mostly driven by $PM_{2.5}$ pollution transported from South Korea (Figure A.2) and by the increase in ozone, speeding up the rate at which local Chinese SO_2 and NO_x emissions are converted to sulfate and nitrate.

Leibensperger et al. (2011) previously showed that NOx emissions in the US, Europe, and China cause intercontinental $PM_{2.5}$ pollution by increasing surface ozone on a hemispheric scale, leading to faster $PM_{2.5}$ production in downwind continents from the oxidation of locally emitted SO_2 and NO_x, i.e., the same effect that we find here on a smaller scale for the East China Plain (Figure 2.3). We used the global GEOS-Chem simulation to examine the influence of Southeast Asian coal emissions on other continents but found the effects to be very small. Maximum annual average intercontinental $PM_{2.5}$ enhancements occur over polluted northern Europe but are less than 0.01 $\mu g\ m^{-3}$. Peak intercontinental increases in seasonal average daily maximum 1-h surface ozone occur over other tropical continents but are less than 0.5 ppb. Even when normalized to the magnitude of NOx emissions, intercontinental influence from Southeast Asia on surface $PM_{2.5}$ in the U.S. and Europe is small compared to that from northern mid-latitude continents (Leibensperger et al., 2011; Fiore et al., 2009) because Southeast Asia is out of the westerly mid-latitude circulation. On the other hand, seasonal southerly flow from Southeast Asia leads to stronger influence on China as shown in Figure 3. Intercontinental influence from Southeast Asia on surface pollution in other tropical continents is weak in part because of strong vertical mixing, limiting influence on ozone, and relatively low emissions of SO_2 and NO_x in these other continents, limiting oxidant-mediated influence on $PM_{2.5}$.

In contrast to the global trend towards cleaner fuel, the future of power generation in Southeast Asia presently relies on coal (IEA, 2013). Our analysis shows that the cost to human health of this coal-dominated energy trajectory is severe. We estimate

20,000 premature deaths every year due to coal pollution from currently operating power plants in Southeast Asia, with the largest effects in Indonesia and Vietnam. These numbers may increase to 70,000 excess deaths per year by 2030 if all currently approved coal plants in Southeast Asia become operational. Beyond Indonesia and Vietnam, the third greatest mortality toll from Southeast Asian coal emissions is in China, where we expect 9,000 premature deaths annually by 2030. Coal emissions from power plants in China are presently declining (Klimont et al., 2013; Shuo, 2015), so that rising transboundary pollution influence from Southeast Asia will likely become of increasing concern.

In January 2016, the Vietnam government announced plans to drastically reduce their plans for future coal expansion (King, 2016) citing both climate and air quality concerns. The air quality concerns drew from preliminary accounts of our work presented at news conferences (Greenpeace, 2015). Recognition of the public health costs of a coal-based future may guide other countries in Southeast Asia to follow Vietnams lead and choose a more sustainable pathway for meeting their energy needs.

3

Public health impacts of the severe haze in Equatorial Asia in September-October 2015: Demonstration of a new framework for informing fire management strategies to reduce downwind smoke exposure

A version of this chapter was published with Loretta J. Mickley, Miriam E. Marlier, Jonathan J. Buonocore, Patrick S. Kim, Tianjia Liu, Melissa P. Sulprizio, Ruth S. DeFries, Daniel J. Jacob, Joel Schwartz, Montira Pongsiri, and Samuel S. Myers in Environmental Research Letters, vol. 11 (0904023), 2016.

3.1 Introduction

The thick smoke that blanketed Equatorial Asia during September-October of 2015 was likely the worst haze episode since 1997, when land use fires caused billions of dollars in damage and thousands of premature deaths (Johnston et al., 2012; Marlier et al., 2013). The degraded peatlands that typically burn during such episodes contain significant combustible organic material and so release large amounts of fine particulate matter ($PM_{2.5}$), the leading cause of global pollution-related mortality (WHO, 2010; Lelieveld et al., 2015). As in previous episodes, the prevailing winds in 2015 transported the smoke to densely populated areas across Indonesia and the Malay Peninsula, including Singapore and Kuala Lumpur. In this work, we identify provinces where land use policies and management strategies could most effectively mitigate the downwind smoke exposure and consequent costs to human health during such haze events. We also compare the 2015 event to another large smoke episode in 2006 in order to determine how fire emission patterns driven by land use and land cover change may be evolving.

Across Indonesia, fires are frequently used to burn agricultural residue, clear forest, or prepare land for plantations and smallholder farms. Fires also occur from vandalism and accidental ignitions (Dennis et al., 2005; Gaveau et al., 2014a). Fire emission levels are greatest from degraded peatlands, especially in dry years (Marlier et al., 2015a,b). In 2006, burning in industrial concessions to clear land for oil palm and timber plantations accounted for 40% of total fire emissions in Sumatra and 25% in Kalimantan (Indonesian Borneo) (Marlier et al., 2015c). As on oil palm plantations, fire on timber plantations is used to clear native vegetation quickly and cheaply in order to establish commercial wood pulp species. Such species include fast growing trees

such as Acacia, whose turnover rate is about three times faster than oil palm (7 years compared to 25 years), potentially resulting in more frequent post-harvest burning (Effendy & Hardono, 2001; Feintrenie et al., 2010).

As in 1997 and again in 2006, the severe haze in September-October 2015 was enabled by a combination of El Nino and positive Indian Ocean Dipole (pIOD) conditions, both of which promote drought and greatly enhance fire activity in the region, either because fuel loads are drier allowing fires to escape and burn out of control or because farmers take advantage of the dry weather and clear more land than usual (Field & Shen, 2008; van der Werf et al., 2008, 2010; Reid et al., 2012). Though the underlying meteorological triggers are similar across these extreme haze events, the spatial distributions of land cover and fire emissions are evolving rapidly, driven largely by expanding global markets for oil palm, pulpwood and timber, and by increases in small-scale agriculture (Field et al., 2009; Miettinen et al., 2011; Gaveau et al., 2014b; Margono et al., 2014; Marlier et al., 2015a). A comparison between the 2006 and 2015 events is critical for 1) quantifying the contributions of specific fire source locations to smoke exposure in downwind population centers during extreme haze events, and 2) identifying possible trends in the magnitudes of these differentiated contributions over the last decade. We chose 2006 and not 1997 for this comparison since modern satellite technology (e.g., the multi-wavelength instruments on board Terra and Aqua that can capture burned area and AOD) was not available until 1999 (King et al., 2003). Diagnosis of the fire emission locations that result in the greatest smoke exposures downwind can guide the design of more informed strategies to prevent or minimize recurrent haze events.

In this study, we demonstrate the potential of a new analytical framework to rapidly assess in near real-time the emission sources and health impacts of an ongoing smoke

episode in Equatorial Asia. The framework, presented here all together for the first time, integrates information on 1) fire emissions related to land cover and land use (Marlier et al., 2015a,b,c), 2) meteorological drivers of smoke transport, 3) domestic and transboundary source-receptor relationships, which quantify the sensitivity of $PM_{2.5}$ concentrations in receptor areas to the specific locations of fire emissions (Kim et al., 2015a; Marlier et al., 2015a,c), and 4) health impact functions incorporating regionally-specific data on mortality rates, age structure, and population. Previous efforts to quantify health impacts from biomass burning in Equatorial Asia have proven computationally expensive(e.g. (Johnston et al., 2012; Marlier et al., 2013)). In contrast, once the source-receptor relationships have been mapped, our novel framework can readily quantify smoke exposure from any given distribution of fire emissions without the need for additional computationally expensive model simulations. In this way, stakeholders can quickly identify the key emission areas contributing to that exposure and estimate the resulting morbidity and premature mortality in downwind populations, even as an extreme smoke event unfolds.

3.2 Methods

Below we describe the fire emissions estimates and the surface and satellite observations used in this analysis. In the Supplement, we describe the GEOS-Chem adjoint used to calculate smoke exposures and the health impact calculations.

3.2.1 Fire emissions

We use near-real time fire emission estimates for the 2015 haze event from the Global Fire Assimilation System, a product that was readily available for next-day process-

ing at the time of our analysis (GFAS) http://join.iek.fz-juelich.de/macc/ (Kaiser et al., 2012). GFAS emissions are derived at 0.5 x 0.5 horizontal resolution from observations of fire radiative power (FRP) from the Moderate Resolution Imaging Spectroradiometer (MODIS) instruments on board the Terra and Aqua satellites. The emissions are based on observed relationships between FRP and combusted dry matter for eight land cover types based on those used in the Global Fire Emissions Database [GFED; (van der Werf et al., 2010), supplemented with maps of organic soil and peatlands. Here we define smoke as the sum of organic carbon (OC) and black carbon (BC) aerosol, the primary components of smoke-related $PM_{2.5}$. Based on comparisons with satellite AOD, Kaiser et al. (2012) recommended scaling GFAS OC and BC emissions by a global factor of 3.4. However, the Kaiser et al. (2012) underestimate in modeled AOD may be partly due to model treatment of carbon aerosol in the atmosphere rather than emissions (Andela et al., 2013). Somewhat arbitrarily, we instead scale the GFAS emissions up by 50%, which produces model results that better match surface observations during 2015 (Section 3.2.2). Scaling up by 50% also yields $PM_{2.5}$ emission totals for Indonesia in 2006 that match those obtained from a different emission inventory (Marlier et al., 2015c). To identify sources of fire emissions, we rely on estimates of the spatial distributions of peatlands and industrial concessions in 2010, the only year for which such data are available (Figure B.1). We overlay these estimates onto 1 x 1 km2 MODIS FRP detections to attribute fire activity to these sources (Table B.1). This finer spatial scale information is necessary given the multiple types of land use and land cover within each 0.5 x 0.5 GFAS grid cell.

3.2.2 Surface particulate matter observations

We compare the GEOS-Chem adjoint estimates for smoke exposure in Singapore during 2015 against observed $PM_{2.5}$ concentrations for five stations in Singapore operated by the National Environment Agency (NEA; http://www.nea.gov.sg/). In order to isolate enhancements in surface $PM_{2.5}$ due only to smoke aerosol, we first calculate the average observed $PM_{2.5}$ during June (13.6 g m^{-3}), the earliest available measurements before the onset of the haze event. We then subtract the June average non-smoke concentration from the full time series.

3.2.3 Satellite observations

We also compare the adjoint smoke exposures from the 2006 and 2015 haze events to two satellite products: ultraviolet aerosol index (AI) from the Ozone Monitoring Instrument (OMI; Torres et al., 2002, 2007) and aerosol optical depth (AOD) at 550 nm from MODIS aboard the Terra satellite (Levy et al., 2010). We use the Level 3 quality-assured products from both instruments, processed at 1 horizontal resolution. Both products are frequently employed to characterize smoke aerosol in Southeast Asia (Reid et al., 2013; Chang et al., 2015). By using two different aerosol products, we overcome some of the uncertainty associated with representing smoke optical properties in the retrievals (Zender et al., 2012). We also maximize the amount of usable satellite data retrieved during the time periods of interest in an environment that is challenging to observe from space due to frequent cloudiness, lengthy coastlines, and mountainous terrain (Reid et al., 2013).

3.3 Results

3.3.1 Fire emissions

Figure 3.1 shows the 1995-2015 time series of the NINO3.4 index and Dipole Mode Index (DMI), the standard indices used to represent the phases of the El Nino Southern Oscillation (ENSO) and the Indian Ocean Dipole (IOD; www.stateoftheocean.osmc.noaa.gov). Both El Nino and positive phases of the IOD result in suppressed convection over Indonesia, leading to drought and increased fire activity. September 2015 was the strongest El Nino on record since 1997 and much stronger than September 2006. September 2006, however, saw a slightly stronger positive IOD. Over the entire 20-year record, there are only three instances when both the NINO3.4 and DMI indices simultaneously exceed a value of +1: 1997, 2006, and 2015. Prior to 2015, the 1997 regional haze event was the most severe on record. However, due to a lack of available satellite data for 1997, we focus our comparison on 2006, the second most extreme haze event prior to 2015.

South Sumatra and Central Kalimantan both burned strongly during the 2006 event, contributing 30% and 31% respectively of total Indonesian OC+BC emissions released (Figure 3.2; Figure 3.3). The July-October 2015 Indonesian fire emissions were 2.1 Tg higher compared to the 2006 emissions over the same months, an increase of 110% (Figure 3). South Sumatra contributed 62% (1.3 Tg) of the emission difference between 2015 and 2006, while Central Kalimantan contributed only 18% (0.4 Tg). Jambi Province, which was responsible for less than 5% of the haze during 2006, contributed the third highest emissions of any individual province in 2015 and 12% to the emission difference between 2015 and 2006. Contributions from West Kalimantan decreased from 16% in 2006 to 6% in 2015.

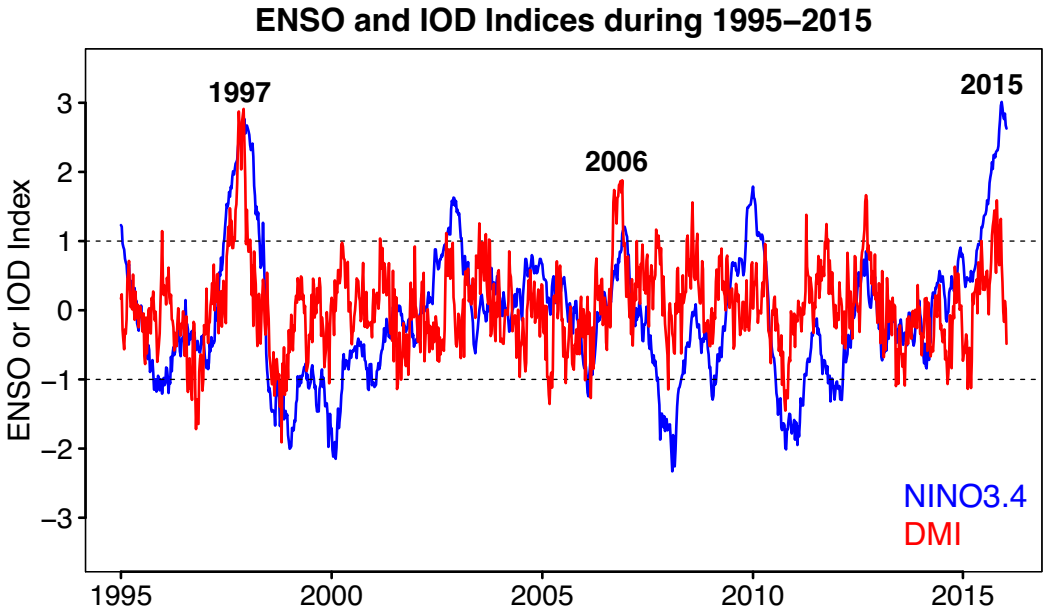


Figure 3.1: Indices of large scale circulation patterns in Equatorial Asia. The blue line shows the NINO3.4 index for the El Nino-Southern Oscillation for January 1995-December 2015. The red line shows the Dipole Mode Index (DMI) for the Indian Ocean Dipole (IOD). Dotted lines indicate the thresholds for El Nino (+1) or La Nina (-1) in the NINO3.4 series, and for strongly positive (+1) or strongly negative (-1) IOD conditions in the DMI series. Data are from the National Oceanic and Atmospheric Administration (stateoftheocean.osmc.noaa.gov).

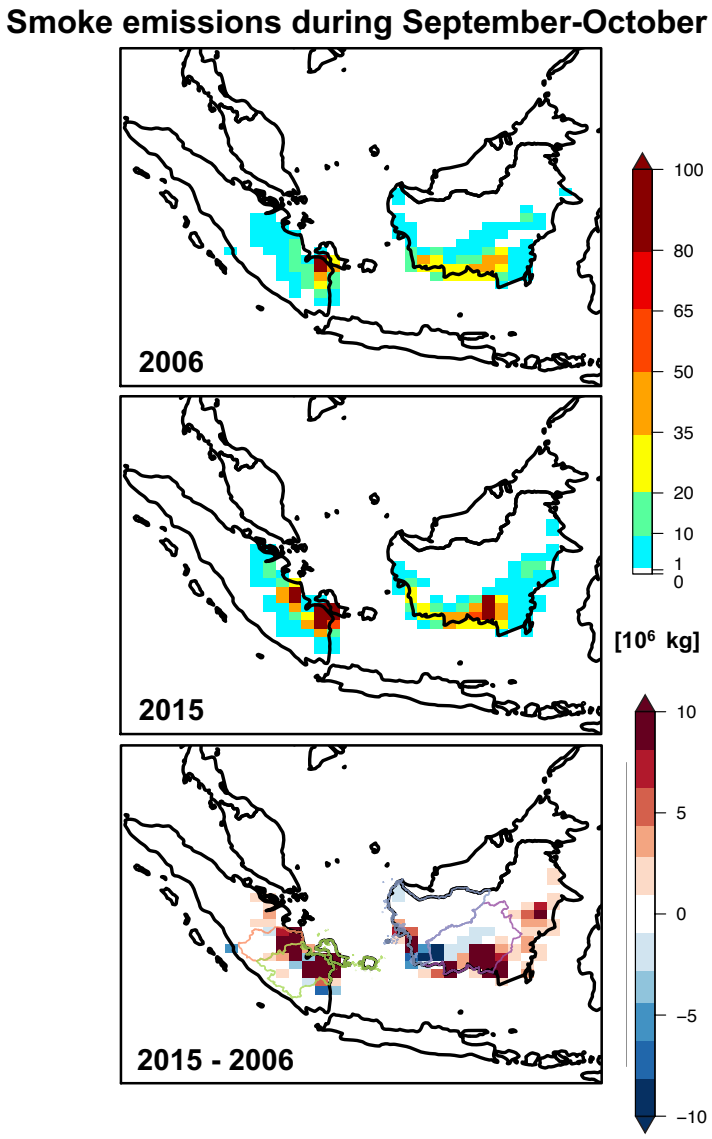


Figure 3.2: September-October total emissions of organic and black carbon (OC+BC) from GFAS during 2006 and 2015. The top panel shows 2006, the middle panel shows 2015, and the bottom panel shows the difference (2015 2006). Province boundaries are shown in the bottom panel by colored lines, corresponding to Jambi in coral, South Sumatra and Bangka-Belitung in green, West Kalimantan in blue, and Central Kalimantan in purple.

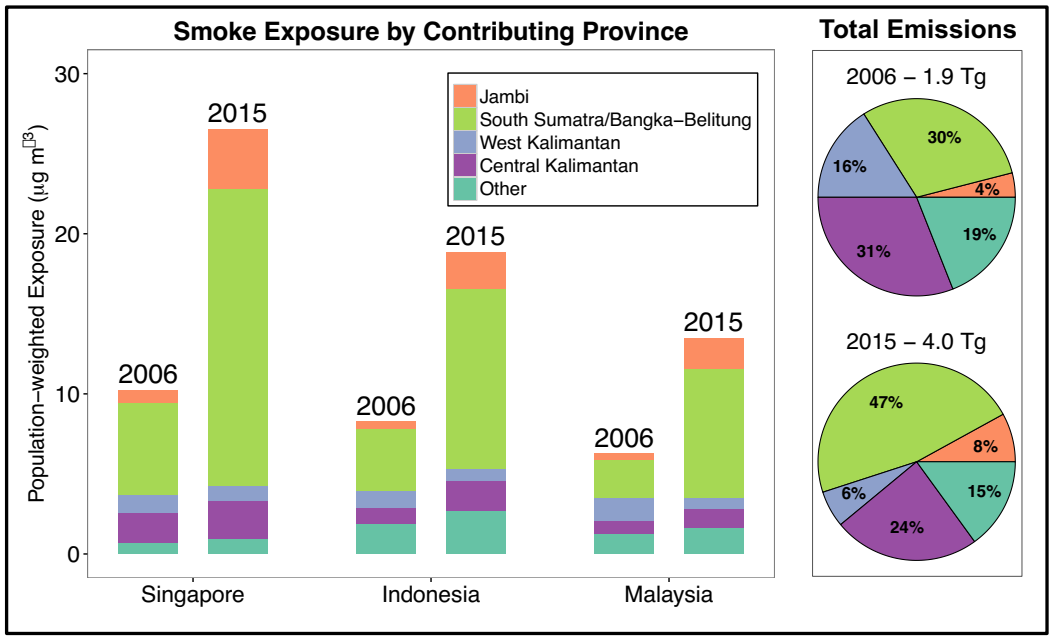


Figure 3.3: Contributions by province to average regional population-weighted smoke exposures (left) and total Indonesian fire emissions of OC+BC (right) during July-October 2006 and 2015. The island province of Bangka-Belitung is included with South Sumatra. Province boundaries are shown in Figure 3.2 and Supplement Figure B.2.

3.3.2 Smoke exposure during haze events

To estimate smoke exposure at each receptor area during the two haze events, we multiply the GFAS emissions for July-October 2006 and July-October 2015 by the adjoint sensitivities simulated for July-October 2006 (Figure B.3). Although the most intense haze occurred during September-October in both years (65% of total annual fire emissions in 2006, 80% in 2015), we extend our time horizon to include the entire burning season from July-October (83% of total annual fire emissions in 2006, 93% in 2015). As described above, we assume that the 2006 smoke transport patterns are similar to those in 2015. Smoke transport for all three receptors shows a strong

sensitivity to the prevailing southeasterly winds governed by the location of the Intertropical Convergence Zone (ITCZ) during September-October (Chang et al., 2005). To test our results using meteorology from other years we also calculated smoke exposures in Singapore due to the 2015 fire emissions with adjoint sensitivities for 2005 and 2007-2009 (Figure B.4). Seasonal mean exposures are similar across the 2005-2008 sensitivities, while 2009 is 25% greater than the 2006 average.

Figure 3.4 shows a combined time series of daily NEA $PM_{2.5}$ concentrations at Singapore for July 1 to October 31 2015. Smoke concentrations returned to normal levels in late October with the onset of monsoonal rains (Cochrane 2015). The NEA data reveal an average observed smoke exposure of 30 g m^{-3} in Singapore for July-October 2015. Our approach yields an average July-October 2015 smoke exposure at Singapore of 27 g m^{-3}, consistent with the NEA surface observations. Estimated population-weighted smoke exposures in Indonesia and Malaysia during 2015 are 19 g m^{-3} and 14 g m^{-3}, respectively. Mean July-October non-smoke $PM_{2.5}$ concentrations in these areas are 10-15 g m^{-3} (Section 3.2.2; GEOS-Chem forward model simulation, not shown), yielding total annual average $PM_{2.5}$ exposures below 50 g m^{-3} and within the range of linearity (Supplement Section B.2).

During 2006, we find that July-October exposures are lower by at least a factor of 2 at all three receptors compared to 2015, with values of 10 g m^{-3} in Singapore, 8 g m^{-3} in Indonesia, and 6 g m-3 in Malaysia. Figure 5 compares OMI AI and MODIS AOD for September-October 2006 to those quantities in September-October 2015. Also shown for 2015 is a comparison of MODIS AOD to AOD measurements at several sites in the Aerosol Robotic Network (AERONET; Holben et al., 1998); no data are available at these sites for September-October 2006. Both satellite instruments reveal an approximate doubling in aerosol levels in 2015 compared to 2006 across much

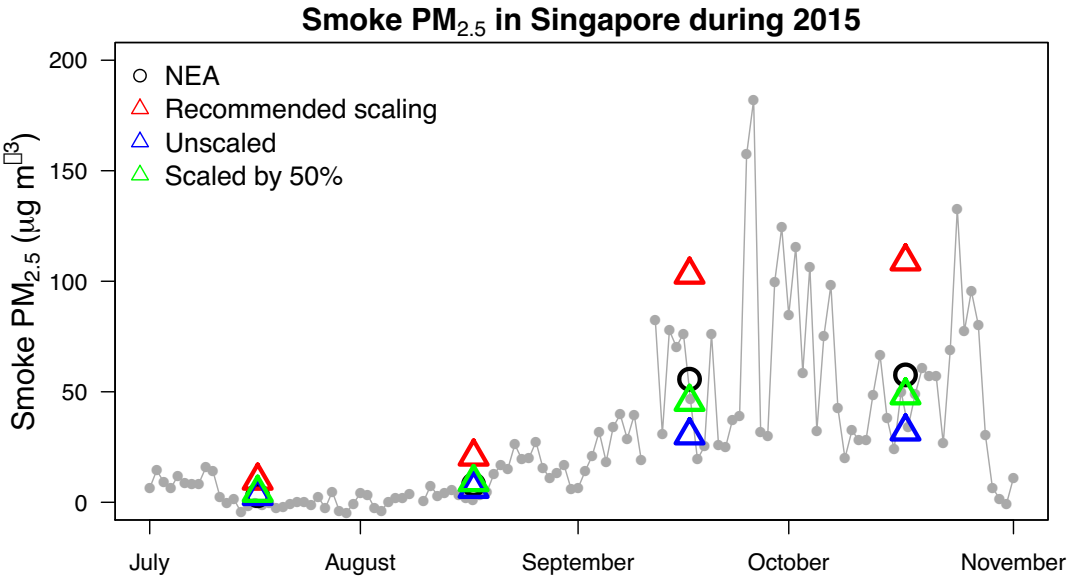


Figure 3.4: Time series of observed daily smoke $PM_{2.5}$ concentrations in Singapore from the National Environment Agency (NEA; www.nea.org) for July 1-October 31, 2015. Grey dots represent mean 24-hour concentrations averaged across five stations: Central, North, South, West, and East Singapore. Unfilled black circles at mid-month represent monthly mean observed smoke $PM_{2.5}$ from NEA averaged across all five stations. Non-smoke $PM_{2.5}$ has been removed from the time series by subtracting the average observed $PM_{2.5}$ concentrations during June, before the onset of the haze event. Triangles show monthly mean smoke exposure at Singapore estimated by this work for July-October 2015 using unscaled GFAS emissions (blue), GFAS emissions scaled by the recommended factor of 3.4 (red) and GFAS emissions scaled by 50% (green).

of the domain, consistent with the adjoint exposure results and confirming the utility of our approach.

3.3.3 Emission sources

During 2006, South Sumatra and Central Kalimantan contributed roughly equally to regional emissions (30-31%), but across all three receptor areas, South Sumatra accounted for more than three times as much smoke exposure than did Central Kalimantan (Figure 3.3). Also in 2006, West Kalimantan contributed only 16% to regional emissions, but was responsible for the second highest exposure levels in Malaysia, after South Sumatra. In 2015, the percent contributions to smoke exposure from South Sumatra increased by 10-15% in the absolute sense across all receptors, compared to South Sumatras contribution to smoke exposures across the same areas in 2006. Exposure contributions from Jambi doubled in 2015 compared to 2006, while contributions from the other regions decreased. The trends in smoke exposure from South Sumatra and Jambi in 2015 suggest significant changes in land use occurred in these regions during the intervening years as discussed below.

Emission source regions for both the 2006 and 2015 haze events differ from those contributing to a severe haze event in June 2013 that severely affected Singapore and the Malay Peninsula (Gaveau et al., 2014a). The 2013 haze has been traced to agricultural burning in Riau, a province in northern Sumatra covered extensively by peatlands and oil palm concessions (Figure B.1; Gaveau et al., 2014a). In contrast, we find that Riau did not contribute significantly to smoke exposure at any receptor during either the 2006 or 2015 haze events. This difference is partly due to the longer burning season in Riau than further south in Indonesia, with increased burning earlier in the year (Reid et al., 2013). Also, the prevailing winds over Riau shift from westerly

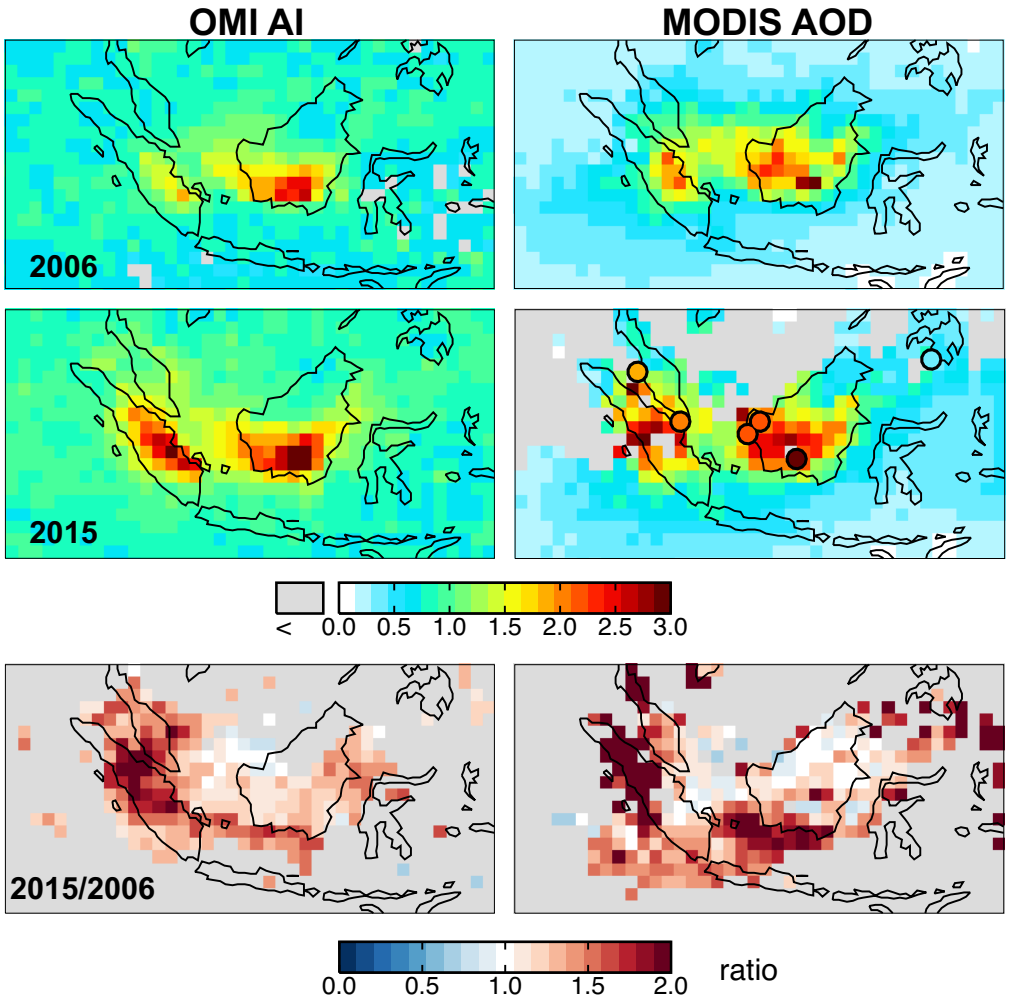


Figure 3.5: Average satellite aerosol observations for September-October during the 2006 and 2015 haze events. Observations during the 2006 event are shown in the top two panels; the 2015 event is shown in the middle panels. Values of Aerosol Index (AI) from the Ozone Monitoring Instrument (OMI) are shown at left; aerosol optical depths (AOD) at 550 nm from the Moderate Resolution Imaging Spectroradiometer (MODIS) on the Terra satellite are on the right. Grey pixels indicate missing data. Colored circles in the MODIS AOD 2015 panel indicate mean September-October AERONET observations. These data are level 1.5, which include cloud filtering but not the final calibrations of the quality-assured level 2.0 product. For consistency with the Terra MODIS morning overpass time, the AERONET data has been averaged during 9am-12pm local time. The bottom two panels compare the 2015 values to those in 2006 for the two satellite products, calculated as the ratio of 2015 / 2006. For clarity, ratios in those gridboxes with low aerosol content in both products (AOD <0.5 and AI <1.0) are not shown.

in June to southeasterly during September-October as the ITCZ moves southward across Equatorial Asia, transporting what smoke there is later in the season toward the northwest rather than towards the populated Malay Peninsula.

To estimate the contributions of different types of land use and land cover to fire activity, we used satellite FRP observations at high-resolution (1 km x 1 km) for July-October 2006 and 2015 (Table B.1). While FRP totals are not directly comparable to emissions, they are available in near real-time and can reveal the spatial distribution of fire activity and land use types affected by fires, as demonstrated by Marlier et al. (2015c). For example, although oil palm concessions have previously been implicated as a major driver of peat burning in Indonesia (Koh et al., 2011), we find that burning in oil palm concessions in 2006 accounted for only 11% of total FRP in Sumatra and 32% in Kalimantan. In 2015, these contributions declined to just 5% and 20%, respectively. In Sumatra, FRP in timber concessions increased from 27% in 2006 to 55% in 2015, while in Kalimantan the timber contribution was <10% in both years. In contrast, the percentage of total FRP occurring in peatlands increased in both Sumatra (44% to 72%) and Kalimantan (32% to 43%) from 2006 to 2015. Reasons for the apparent increase in fire activity in peatlands are not clear. Draining of peatlands to prepare for agricultural use in the intervening years may have made the peat more vulnerable to fires (Carlson et al., 2012; Turetsky et al., 2015). Further analysis of the 2015 event with updated land use maps is needed to fully understand these patterns at a spatial scale that is useful for stakeholders.

3.3.4 Health impact estimates

The U.S. Environmental Protection Agency (EPA) primary standard for unhealthy levels of annual average $PM_{2.5}$ is 12 $\mu g\ m^{-3}$. According to the World Bank, much of

Equatorial Asia is close to this standard in non-haze years e.g., annual mean values reported for 2011 are 13-14 g m^{-3} for Indonesia, Malaysia, and Singapore (http://data.worldbank.org/indicator/EN.ATM.PM25.MC.M3). Based on smoke exposures for 2006 (Section 3.3.2), we estimate the following excess deaths for that year, with 95% confidence intervals calculated as in Driscoll et al. (2015): 34,600 (9,000-60,100) in Indonesia, 2,300 (600-4,000) in Malaysia, and 700 (200-1,200) in Singapore. For 2015, we estimate these excess deaths to be: 91,600 (24,000-159,200) in Indonesia, 6,500 (1,700-11,300) in Malaysia, and 2,200 (600-3,800) in Singapore. (See Supplement Section B.2 for description of the health impact calculations and comparison to previous estimates for the 1997 event). Our results suggest that regional smoke-related mortality was 2.7 times higher in 2015 than in 2006, an increase whose causes we summarize in the Discussion and Conclusions.

3.4 Discussion and Conclusions

A combination of El Nino and positive Indian Ocean Dipole conditions in July-October 2015 led to dry conditions that exacerbated agricultural and land clearing fires in southern Sumatra and Kalimantan. The resulting dense haze persisted across much of Equatorial Asia for weeks, imposing adverse public health impacts on populations in Indonesia, Singapore, and Malaysia. Using the adjoint of the GEOS-Chem global chemistry model together with health response functions, we estimate 60 g m^{-3} of population-weighted smoke $PM_{2.5}$ exposure and 100,300 premature deaths across Indonesia, Malaysia, and Singapore due to extreme haze in 2015. These values are more than double the 25 g m^{-3} of smoke $PM_{2.5}$ and 37,600 premature deaths that we estimate for a similar haze event in the region in 2006. The approximate doubling of

regional smoke exposure in 2015 compared to 2006 is consistent with observations of haze from both OMI AI and MODIS AOD during the two events.

Smoke exposures in downwind population centers in both 2006 and 2015 stemmed mainly from burning in South Sumatra, an area that contributed more than 30% of the regional emissions and more than 50% of the regional smoke exposure during both events. We also find that Jambi Province, which did not burn significantly during 2006, contributed about 20% of the increased smoke exposure between 2006 and 2015. High resolution FRP data suggests that fire activity on Sumatra in 2015 was dominated by burning on timber concessions (55%) and peatlands (72%). An updated analysis of the sectors and land types contributing to smoke exposure would build on Marlier et al. (2015c) and test our hypothesis.

There are several limitations to the model framework we present. First, peatland emissions are difficult to quantify and thus lead to a wide range of emission estimates across fire inventories. Peat fires can smolder in the subsurface for weeks to months after ignition, often at temperatures too low to be detected accurately from space (Tansey et al., 2008). The contribution of this low temperature burning to total smoke emissions in peatlands is uncertain. The amount of peat fuel consumed during each fire event is also uncertain and currently not explicitly represented in fire emission inventories (Konecny et al., 2016). Second, the concession maps we use in our attributions correspond to 2010 rather than 2015, and a subset of the concessions recorded in 2010 may have been converted to other land use types prior to 2015. Also, since our analysis was conducted on a 0.5 x 0.67 grid, there is some uncertainty in our attributions of emissions and exposure contributions to specific provinces. Third, our method produces population-weighted average smoke exposures, which neglect the spatial variability in exposures within a receptor region. Populations liv-

ing close to fires may experience annual average $PM_{2.5}$ exposures above the 50 μg m^{-3} linearity threshold in the concentration response function we used. We also focus only on adult mortality due to lack of knowledge on the effects of air pollution on child mortality, even though impacts on children are likely significant. Additionally, the concentration response function used here is based on studies done in high-income countries with different baseline health characteristics and air pollution sources. To date, there is little evidence quantifying the relationship between $PM_{2.5}$ composition and toxicity, and so we do not consider this factor (Levy et al., 2012). Our approach also does not explicitly eliminate the potential influence of confounding health effects from conditions related to El Nino-pIOD meteorology that are independent from fire pollution, such as heat waves or excess airborne dust from the drier conditions. Ideally we would validate our results with a multi-year epidemiological study, but such an evaluation is beyond the scope of our analysis. Finally, our approach relies on the assumption that the prevailing transport patterns between 2015 and 2006 are likely similar given the background meteorological conditions (Section 3.3.1-3.3.2). Predictive real-time tools to forecast haze in Southeast Asia exist and have recently been improved upon (Hertwig et al., 2015), but these methods require substantial computational investment and do not readily provide the geographical source attribution information inherent in our adjoint approach.

These limitations in our approach are largely offset by the benefits of 1) identifying in near real-time the key fire locations contributing significantly to downwind smoke exposure during haze events in Equatorial Asia, and 2) rapidly producing estimates of the associated health impacts when the policymakers and civil society groups are seeking ways to effectively address seasonal burning in Equatorial Asia. In particular, our approach provides an early-response diagnosis of those provinces where effec-

tive fire and land use management would yield the greatest benefits to human health, even as the haze event is still unfolding. (See Supplement Section B.6 for discussion of challenges facing existing fire management strategies in Indonesia.) Applying the framework presented in this work requires only spatially explicit estimates of carbon aerosol emissions from fires, the archived GEOS-Chem adjoint sensitivities (available upon request), and a health impact model. The exposure calculations are effectively a one-step multiplication combining the sensitivities with the fire emissions, taking only seconds to perform and requiring minimal computational resources. In the immediate aftermath of large haze events, when the incentive for constructive decision-making among stakeholders is greatest, our framework supplies detailed information on the air quality consequences of agricultural fires, a common land use practice in Equatorial Asia.

Our modeling approach quantifies the public health impacts of smoke pollution, including haze crossing international borders. The capacity of our framework to quickly identify the provinces where fire emissions are most severely affecting downwind populations and to quantify the resulting $PM_{2.5}$-related health impacts can help government agencies prioritize forested and peatland areas for protection and restoration. Furthermore, our integrated modeling approach can help policymakers reduce health impacts from haze and strengthen long-term efforts like Reducing Emissions from Deforestation and Forest Degradation (REDD+) to decrease greenhouse gas emissions, maximizing the climate co-benefits of preventing the release of carbon from trees, peat, and other soil. Finally, the frameworks ability to causally link specific fire events to public health impacts in domestic and transboundary locations could support implementation of laws that hold responsible those individuals and entities involved in illegal burning of land and forests in this region.

4

Madden-Julian Oscillation during negative Indian Ocean Dipole conditions as a driver of severe haze events in the Malay Peninsula

4.1 Introduction

In June 2013, Singapore experienced one of its worst air pollution events on record, with surface particulate matter (PM) concentrations exceeding 300 g m^{-3} as mea-

A version of this chapter written with Loretta J. Mickley, Daniel J. Jacob, Miriam E. Marlier, Ruth S. DeFries, David L. A. Gaveau, Bruno Locatelli, and Sam S. Myers has been submitted to Journal of Geophysical Research: Atmospheres.

sured by the Singapore National Environment Agency (http://www.nea.gov.sg/) (Hertwig et al., 2015). This severe haze has been attributed to smoke from agricultural fires in the Riau province of Central Sumatra (Forsyth, 2014; Gaveau et al., 2014a), which is close to (100km) and upwind of the Malay Peninsula for much of the year (Figure 4.1). Extreme fire activity and haze in Equatorial Asia is typically linked to positive El Nino Southern Oscillation (ENSO) (Rasmusson & Wallace, 1983) [and references therein] and Indian Ocean Dipole (pIOD) (Saji et al., 1999) conditions, when periods of drought can last a few months to a year. Examples include the large haze events of September 1997 (Page et al., 2002), October 2006 (Field & Shen, 2008) and September-October 2015 (Koplitz et al., 2016). However, conditions during the June 2013 event were ENSO-neutral and characterized by a negative phase of the IOD (nIOD), which is associated with increased precipitation over Indonesia (Li et al., 2003). June is also several months earlier than the September-November window that is typical of the El Nino-pIOD events listed above. In addition to June 2013, there is evidence that two other recent haze events in the region not associated with El Nino-pIOD conditions occurred in Kuala Lumpur, a dense urban area northwest of Singapore, in August 2005 (Aglionby, 2005; Forsyth, 2014), and again in Singapore in October 2010 (Salinas et al., 2013), although these events have not been explored extensively in the scientific literature. In this work we use visibility data from two sites in the Malay Peninsula together with assimilated meteorology and observations of fire activity in Riau to investigate the drivers of the extreme haze during the August 2005, October 2010, and June 2013 events. In particular, we examine the influence of the phase of the Madden-Julian Oscillation (MJO) on smoke transport during these events. Better understanding of ENSO-neutral haze events in Equatorial Asia could provide a means to predict when such catastrophic events are likely to occur.

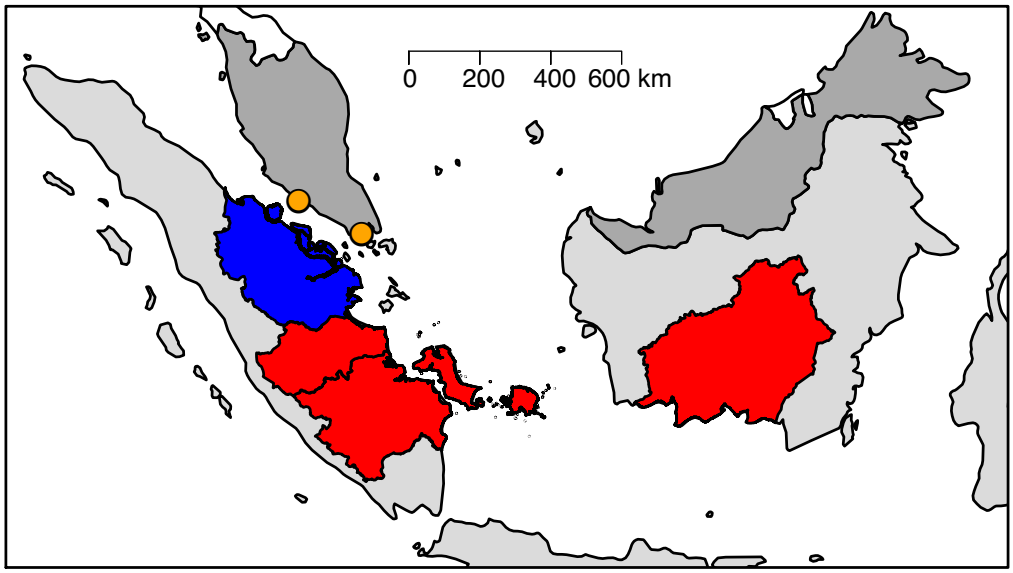


Figure 4.1: Provinces contributing to severe haze in Equatorial Asia. Riau province, location of the fires associated with haze in the Malay Peninsula during June 2013, is shown in blue. In red are provinces associated with burning during El Nino-pIOD events like 1997 and 2015 (from west to east: Jambi, South Sumatra/Bangka-Belitung, Central Kalimantan). Other Indonesian provinces are shown in light grey; Malaysia is dark grey. Singapore and Malacca are denoted by the orange circles.

Land clearing by fire for agricultural expansion has increased rapidly in Indonesia since the 1970s, particularly in coastal peat swamps (Page et al., 2009). Emissions of particulate and gaseous pollution from peat fires are estimated to be twice those emitted from other tropical forest fires (Levine, 1999). The extreme haze events that sometimes accompany agricultural fires in Indonesia exert a severe toll on human health because of the very high population density; estimates of premature mortality across Equatorial Asia from the severe smoke pollution events in 1997 and 2015 range from 13,000 to 300,000 excess deaths per event (Johnston et al., 2012; Marlier et al., 2013; Koplitz et al., 2016). These events also weaken local economies through airport closures, suspended economic activity, and reductions in tourism (Glover & Jessup, 1999). Understanding the meteorological pathways of severe haze events in this region has particular importance as the population continues to grow rapidly and land clearing for agricultural use expands. By 2030, fire emissions from crop expansion in Sumatra are expected to increase by a factor of 2.5 (Marlier et al., 2015a), while the population in Indonesia is expected to increase by 50 million people (2.5% per year) (McDonald, 2014).

Gaveau et al. (2014a) attributed the June 2013 haze episode in Singapore to high fire activity in Riau following a two-month drought there. These authors analyzed 130 fire events in Sumatra over the July 2002-August 2013 time period and diagnosed a negative relationship between two-month precipitation averages and monthly fire radiative power (FRP). Mean May-June precipitation was particularly low in 2013 (125 mm), while FRP in June 2013 reached the highest level of the 2002-2013 period (270 GW). Gaveau et al. (2014a) proposed that the June 2013 haze in Singapore can be explained by high FRP in Riau combined with monsoonal westerlies typical during June-August that carried the smoke across the Straits of Malacca to the Malay

Peninsula.

The Gaveau et al. (2014a) relationship of FRP with precipitation in Riau leaves two issues unresolved. First, two outliers in the plot revealing the negative relationship, October 2010 and August 2005, suggest that other factors play a role in driving fires in this region (Figure 3 in Gaveau et al., 2014a). In both these cases, anomalously high fire activity followed a two-month period of relatively high precipitation. As we shall see, these two fire episodes, like that in June 2013, led to intense haze in the Malay Peninsula. Second, two other high fire months identified by Gaveau et al. (2014a), June 2005 and July 2006, occurred during months characterized by seasonal westerly winds. Unlike the June 2013 fires, however, these other fires did not result in severe haze in the Malay Peninsula. In this paper, we build on the work of Gaveau et al. (2014a) to explain a) why high fire activity occurred in Riau during August 2005 and October 2010 despite relatively high precipitation in the preceding two months, and b) why these two fire episodes resulted in severe haze in the Malay Peninsula, but the large Riau fires during June 2005 and July 2006 did not. To our knowledge, our work offers the first mechanistic explanation for the extreme haze of August 2005 and October 2010.

Specifically, we demonstrate here that the August 2005, October 2010, and June 2013 smoke episodes, three of the five worst haze events on record for the 21st century in the Malay Peninsula, were likely related to the timing and strength of the Madden-Julian Oscillation (MJO). The MJO is a synoptic scale system of convection that propagates eastward across the Indian and Pacific Oceans with a period of 30-90 days and is the major driver of intraannual variability in both precipitation and winds across Equatorial Asia (Madden & Julian, 1972, 1994). Typically, the eastern side of a well-organized MJO system is associated with enhanced convection and asso-

ciated precipitation, followed by an area of suppressed convection on the western side. The patterns of low-level air flow associated with these alternating zones of enhanced and suppressed convection lead to near-surface easterly wind anomalies on the eastern edge of the MJO, while the western edge is characterized by near-surface westerly anomalies (Lin & Johnson, 1996; Zhang, 2005; Woolnough et al., 2007). As a result, later phases of the MJO frequently strengthen surface winds near Riau and the Malay Peninsula. Similarly, later MJO phases also have a greater correlation with enhanced fire activity in Riau compared to earlier phases, attributed to the drier conditions typical of these phases (Reid et al., 2012; Zhang, 2013). Xian et al. (2013) also suggested that stronger MJO activity over Equatorial Asia may increase the lifetime of smoke particles over Indonesia due to a reduction in wet scavenging during the later, drier phases. Beyond these studies, however, no research to date has directly linked the MJO to extreme haze events in Equatorial Asia.

Here we investigate the potential role of MJO-associated wind changes on smoke transport from Riau Province to the Malay Peninsula. During the three ENSO-neutral events of August 2005, October 2010, and June 2013, we observe a relationship between a well-organized MJO entering its later phase and short-term pulsing in anomalously strong westerly winds over Riau, leading to intense haze crossing the Straits of Malacca to the Malay Peninsula. Recognizing the MJO as a significant, potentially predictable mechanism leading to haze in the Malay Peninsula would be of great value to policymakers as they take steps to prepare for such catastrophic haze events in the future.

4.2 Data and Methods

To identify episodes of extreme haze in the Malay Peninsula, we use 2005-2015 hourly visibility data, averaged to daily means, from Changi Airport in Singapore and from the Malacca site in the Iowa Environmental Mesonet Automated Surface Observing System network (mesonet.agron.iastate.edu/request/download.phtml). We define visibility reduction at each site as the daily visibility value subtracted from the maximum visibility reported throughout the time series. Daily anomalies of visibility reduction are calculated by subtracting daily values from the long-term mean and normalizing by the standard deviation. We classify days with normalized anomalies greater than 2 (i.e., in the 95^{th} percentile) as extreme haze days.

To characterize the wind patterns during August 2005, October 2010, and June 2013, we rely on assimilated 800-hPa wind fields from the NASA Goddard Earth Observing System (GEOS-5, 2004-2011, 0.5 x 0.666) and from MERRA-2 (2012-2014, 0.5 x 0.625). Both sets of meteorology are from the NASA Modeling and Assimilation Office (GMAO). Wind fields at this pressure level are representative of transport patterns in the lower troposphere.

To demonstrate the spatial extent and direction of smoke plumes over Riau and the Malay Peninsula during the August 2005, October 2010, and June 2013 haze episodes, we use aerosol optical depths (AOD) from the Moderate Resolution Imaging Spectroradiometer (MODIS v6, Level 3) on both the Terra and Aqua satellites (Remer et al., 2005; Levy et al., 2013). To qualitatively assess the performance of MODIS AOD in detecting haze over Riau at the daily scale, we compare the MODIS AOD to observations of Aerosol Index (UVAI, Level 3) from the Ozone Monitoring Instrument (OMI) (Torres et al., 2002, 2007) on the Aura satellite.

The progression of the MJO across the Indian Ocean Basin can be described by an index based on a pair of empirical orthogonal functions (EOFs) that combine information on 850 hPa zonal winds, 200 hPa zonal winds, and outgoing longwave radiation (http://www.bom.gov.au/climate/mjo) (Wheeler & Hendon, 2004). The index, known as the Real-Time Multivariate MJO Index, consists of two principal components, RMM1 and RMM2, calculated by projecting daily meteorological data onto the two EOFs, resulting in eight phases tracking the MJO from the African coast (phase 1) eastward to the Pacific Ocean (phase 8) (Zhang, 2013). MJO patterns in which the absolute magnitude of either the RMM1 and RMM2 component is greater than one are considered to be organized or strong. During boreal summer (May-October), the east-west trajectory of the MJO slowly shifts toward the north, with August-September marking the time period of peak shift. The summertime MJO is sometimes called the boreal summer intraseasonal oscillation (BSISO) (Lee et al., 2013). In all seasons, fire activity and haze transport in Equatorial are most affected by phases 4-7 of the MJO, when areas of suppressed convection and enhanced westerly wind bursts are located over Indonesia (Figure 4.2).

4.3 Results

4.3.1 Extreme haze in the Malay Peninsula during 2005-2015

We first examine the MJO-related haze events in the context of other haze episodes in the Malay Peninsula over the time period available for the visibility data (2005-2015). Figure 4.3 shows daily visibility reduction anomalies greater than the 95th percentile value, a proxy for extreme haze days, in Singapore and Malacca during 2005-2015. We mainly focus our analysis on the June-October timeframe because conditions are

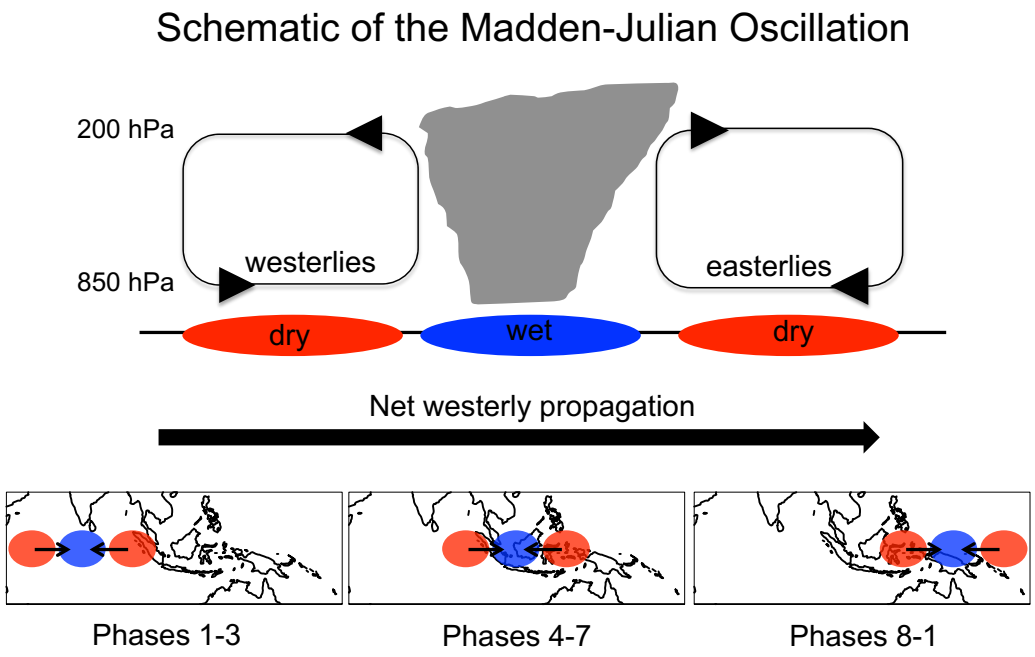


Figure 4.2: Simple schematic of the Madden Julian Oscillation (MJO). The top panel shows the general vertical structure of the MJO, where areas characterized by suppressed convection and drier conditions are shown in red and the main area of enhanced convection and increased precipitation is shown in blue. Corresponding circulation patterns, characterized by lower tropospheric easterlies on the eastern side of the convection and westerlies on the western side, are shown by the black arrows. The bottom panels show the general location of these alternating dry-wet-dry areas and associated lower level wind fields as the MJO moves through phases 1-8. Phases 4-7 are conducive to transport of haze from Riau to the Malay Peninsula. Black arrows in the bottom panels represent the predominant direction of low-level flow on the eastern and western sides of the primary convective area, as shown in the top panel.

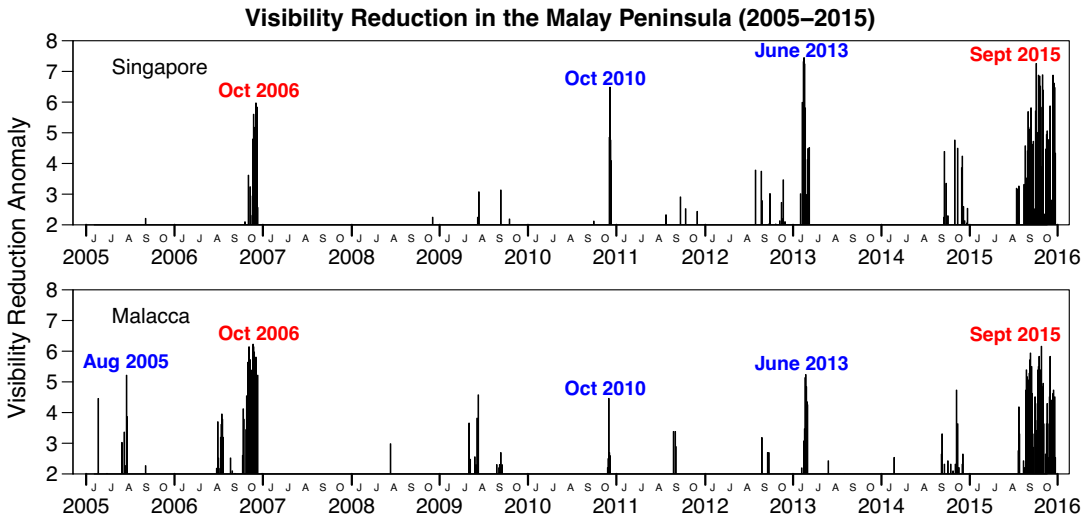


Figure 4.3: Time series of extreme anomalies in daily visibility reduction recorded in Singapore (Changi Airport) and Malacca during June-October 2005-2015. Station locations are shown in Figure 4.3. Anomalies are constructed by subtracting daily visibilities from the maximum visibility reported at each site and then normalizing the resulting timeseries. The panels show only extreme values of visibility reduction, defined as normalized anomalies greater than two (i.e., in the 95th percentile), which we use as a proxy for severe haze. Haze events driven by El Nino and positive Indian Ocean Dipole conditions are indicated by red text; those events associated with strong MJO activity are in blue. Visibility data are from the Iowa Environmental Mesonet (IEM) ASOS network.

relatively dry then and the prevailing wind flow is conducive to transport of smoke from fire regions in Indonesia to the Malay Peninsula (Okamoto et al., 2003). Based on the visibility data, we identify four major haze events in Singapore over the past decade: October 2006, October 2010, June 2013, and September-October 2015. Analysis of the Malacca time series reveals similar peaks, with the October 2010 and June 2013 events somewhat less extreme than in Singapore, and with an additional event in August 2005 that is not apparent in the Singapore timeseries.

As discussed in the introduction, the October 2006 and September-October 2015 events are well understood to be the consequence of strong El Nino-pIOD condi-

tions, which led to drought and increased fire activity across Indonesia, primarily in southern Sumatra and Kalimantan Borneo (Field & Shen, 2008; van der Werf et al., 2008; Koplitz et al., 2016). We therefore focus our analysis on the three extreme haze events in August 2005, October 2010, and June 2013 that cannot be explained by the El Nino-pIOD mechanism.

4.3.2 Fire activity in Riau

Table 4.1 lists the top ten fire months in Riau during 2002-2013 in terms of monthly FRP, as identified by Gaveau et al. (2014a). The Table also indicates the ENSO and IOD conditions associated with these fires. None of these high fire events occurred during El Nino-pIOD conditions, demonstrating a fundamental difference between the drivers of high fire activity in Riau compared to southern Sumatra and Kalimantan. Reasons for this difference remain unclear, although a longer history of anthropogenic alteration of the landscape may have left Riau more vulnerable to fires, even in ENSO-neutral conditions (Page et al., 2009; Gaveau et al., 2014a).

The relationship between FRP and precipitation from Gaveau et al. (2014a) explains the majority of the high fire months in Table 1; except for August 2005, March 2006, and October 2010, the other seven high fire months saw a normalized anomaly of less than -1 (160 mm) of mean rainfall in Riau over the previous two months. However, as the Table makes clear, high fire activity in Riau is not always associated with strong haze in the Malay Peninsula. The fires of January-March 2005 and March 2006 led to little or no haze in the Peninsula, probably because the prevailing northeasterly winds make sustained haze transport from Riau to the region unlikely at this time of year. (No doubt Riau did experience haze during these months.) However, two other major Riau fire episodes June 2005 and July 2006 also did not lead to severe haze

Table 4.1: Top ten fire months in Riau during July 2002-August 2013 from Gaveau et al. (2014a), as defined by monthly fire radiative power (FRP).[a]

High fire month[a]	Fire days during MJO4-7	nIOD[b]	El Nino[b]	Two-month mean rainfall anomaly[a]	Monthly FRP anomaly[a]	Haze (days)
June-October						
June 2004	10	Yes	No	-1.9	+2.4	>2[c]
June 2013	8	Yes	No	-1.9	+5.5	18
October 2010	7	Yes	No	+0.4	+1.2	9
August 2005	5	Yes	No	+1.2	+3.2	7
July 2006	1	No	No	-1.3	+1.2	0
June 2005	0	Yes	Yes	-1.4	+3.0	1
December-March						
February 2005	13	Yes	No	-2.0	+4.3	2
January 2005	12	Yes	Yes	-1.2	+4.2	0
March 2006	4	No	No	-0.2	+1.1	0
March 2005	0	Yes	No	-1.7	+3.4	2

[a] Fire months are grouped by season and ordered within each group by number of days with high fire activity in Riau (FRP >1 standard deviation above the 2005-2015 mean) occurring during an organized MJO phases 4-7 (MJO4-7). Prevailing winds over Riau during June-October are west-southwesterly/south-southeasterly; winds during December-March are north-easterly. Two-month mean rainfall totals for the high fire month and the preceding month are from Gaveau et al. (2014a). Rainfall and FRP anomalies are calculated as the difference from the 2002-2013 climatological mean, divided by the climatological standard deviation (i.e., the normalized anomaly). Severe haze, defined as a daily visibility reduction anomaly >2 (i.e., in the 95th percentile), is indicated by the combined number of haze days in either Singapore or Malacca. For example, in June 2013 there were 10 haze days in Singapore and 8 in Malacca, so the number of haze days is reported as 18.

[b] Columns 3 and 4 indicate whether or not the high fire months coincided with an El Nino (NINO3.4 >0.4) or negative Indian Dipole conditions (nIOD, Dipole Mode Index <-0.1). Data are from http://stateoftheocean.osmc.noaa.gov/.

[c] No visibility data are available for 2004. Satellite aerosol observations from 2004 indicate haze in the Malay Peninsula during MJO phases 4-7 (Figure C.1).

in the Malay Peninsula, even though the prevailing winds were favorable. Malacca experienced haze for one day in June 2005, but that was before the onset of peak fire activity in Riau (not shown). Importantly, neither June 2005 nor July 2006 saw sustained (>1 day) fire activity concurrent with organized MJO activity in phases 4-7 (Table 4.1). We explain the relevance of MJO phases 4-7 for smoke transport to the Malay Peninsula in the following section.

Of the other four high fire months occurring during June-October, three (August 2005, October 2010, and June 2013) resulted in extreme haze in either Singapore or Malacca as recorded in the visibility data from these sites. We investigate these three events in detail below. June 2004 also followed the pattern of these three ENSO-neutral but severe events, with negative IOD conditions and multiple high fire days concurrent with MJO phases 4-7. Satellite observations from June 2004 also show an enhanced aerosol plume over the Malay Peninsula during the dates when the MJO was in phases 4-7 (Figure C.1). However, because no visibility data are available at either Singapore or Malacca for June 2004, we do not consider this event further.

4.3.3 Wind anomalies and smoke plumes during August 2005, October 2010, and June 2013

Figure 4.4 shows monthly mean westerly wind anomalies in the lower troposphere (800 hPa) during August 2005, October 2010, and June 2013 compared to the 2004-2014 average for those months. During all three months, a significant westerly wind anomaly appeared over Riau province and most of the Malay Peninsula, ranging in speed from 2-3 m s^{-1} in August 2005 to 5 m s^{-1} in June 2013. During August 2005 and June 2013, these anomalies strengthened the west-southwesterlies prevailing in the May-September timeframe (Okamoto et al., 2003). The strong westerly winds

observed during October 2010 were particularly unusual; due to the location of the Intertropical Convergence Zone (ITCZ) at this time of year, winds are typically weak and from the south-southeast over Riau (Figure C.2). During August 2005, the spatial pattern of the wind anomalies was shifted northward compared to that it October 2010 and June 2013. This shift likely reflects the seasonal behavior of the MJO, as we explain below.

Figure 4.5 shows MODIS AOD averaged during the times of extreme haze in the Malay Peninsula, as diagnosed in the visibility record: August 2-12, 2005; October 18-22, 2010; and June 16-25, 2013. The smoke plumes during all three events clearly originated from regions of agricultural burning in Riau and traveled almost due east to the Malay Peninsula, consistent with the wind anomalies shown in Figure 4.4. The northward shift of the most intense haze from Singapore to Malacca in August 2005 is also apparent. Although the monthly mean AOD products from MODIS capture smoke plumes during all three haze events (Figure 4.5), an assessment of daily AOD compared to OMI AI and active fire counts in Riau suggests that MODIS cannot detect the onset of these events at the daily scale (Figure C.3).

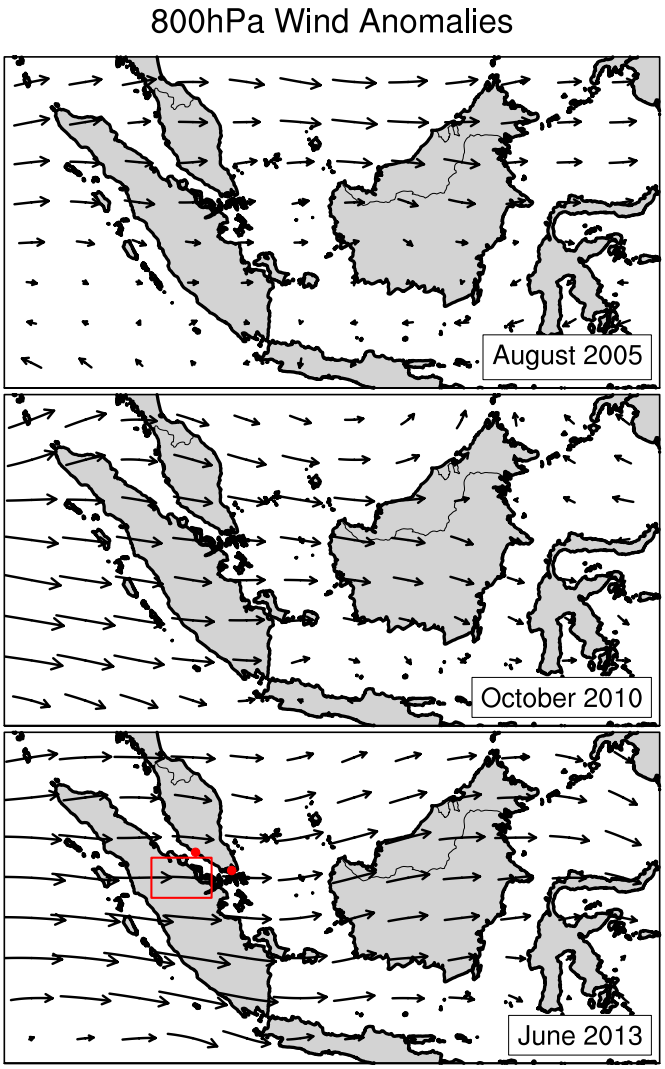


Figure 4.4: Monthly wind anomalies in the lower troposphere (800hPa) during August 2005, October 2010, and June 2013 compared to their respective 2004-2014 averages. Wind data are from the NASA Global Modeling and Assimilation Office (GMAO); data for 2004-2011 are from the GEOS5 product at the native 0.5 x 0.67 horizontal resolution, while data for 2012-2014 are from MERRA2, regridded from 0.5 x 0.625 to 0.5 x 0.67 for consistency with the GEOS5 data. Corresponding figures showing monthly climatologies for 2004-2014 are shown in the Supplemental (Figure C.2). Red circles indicate the visibility data sites for Malacca (2.3 N, 102.2 E) and Singapore (1.4 N, 104.0 E), The domain for Riau wind and fire data in Figure 4.6 is shown by the red rectangle.

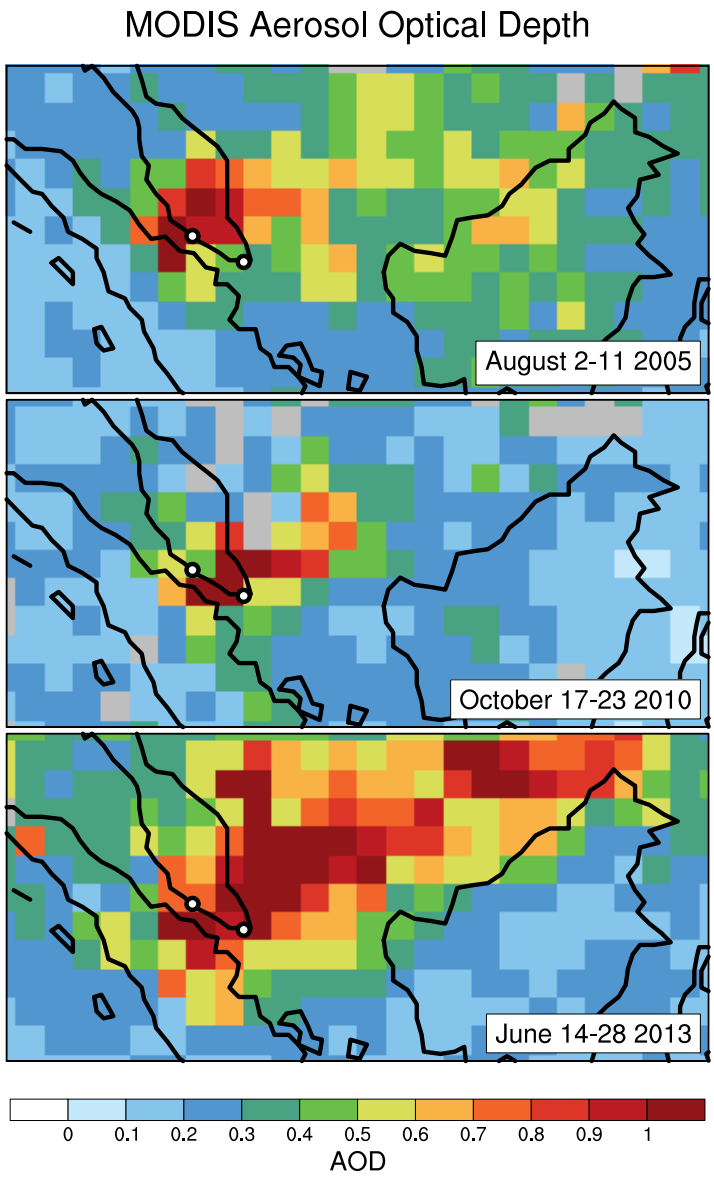


Figure 4.5: Mean aerosol optical depths (AOD) from the MODIS instrument on board the Aqua satellite during August 2-11, 2005; October 17-23, 2010; June 14-28, 2013. Locations of Malacca and Singapore are shown in the white circles.

4.3.4 The role of the Madden-Julian Oscillation

Figure 4.6 shows a time series of MJO phase, westerly wind strength, and fire activity in Riau, together with visibility reduction in the Malay Peninsula during the three severe ENSO-neutral events: June 2013 and October 2010 in Singapore and the August 2005 event which mainly affected Malacca. We begin with a description of June 2013, as the role of the MJO is most salient in this event. On June 10, immediately prior to the Singapore haze event, westerly wind speeds over Riau increased by 4 m s^{-1} above the 2004-2014 June average as the MJO entered phase 4. Fire activity in Riau began increasing around June 14, several days after the onset of the strong westerlies, peaking on June 19. As the MJO progressed through phases 5 and 6, the westerly winds remained anomalously strong, transporting smoke from the fires toward Singapore, which experienced peak pollution during June 16-23. Wind speeds, fire activity, and haze levels all dropped significantly as the MJO left phase 7 on June 23, returning to normal levels several days later when the MJO exited phase 8. This sequence of events is consistent with the diagnosis of Hertwig et al. (2015), who attributed both the strong winds and the sudden increase in precipitation near Riau on June 23 to the presence of a tropical cyclone near Indonesia at this time.

We next examine the sequence of phenomena leading to the intense haze during October 2010. Again, anomalously strong westerlies over Riau coincided with a strong MJO entering phase 4 (Figure 4.6). Severe haze began in Singapore on October 20, three days after the enhanced fire activity in Riau (October 15-17) and while westerly wind speeds over Riau were still moderately enhanced. The westerly wind anomaly in Riau remained apparent until October 22, when the MJO weakened. Unlike the June 2013 event, the haze in Singapore lagged the peak fire activity in Riau by several days

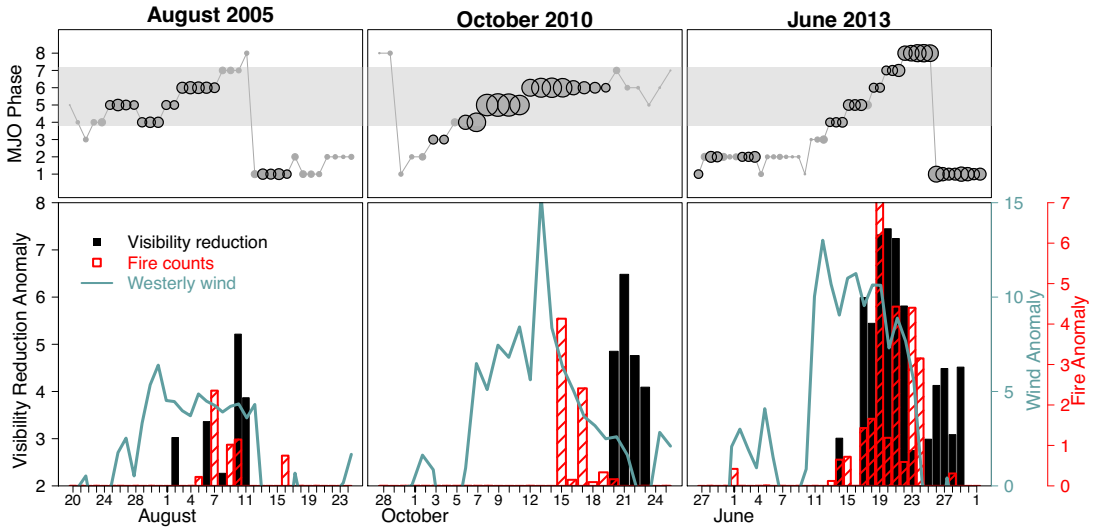


Figure 4.6: Time series of MJO phase, daily fire activity and wind speed over Riau, together with visibility reduction anomalies downwind in Malacca (August 2005) and Singapore (October 2010 and June 2013). MJO phase is shown in the top panels, with symbol size scaled by the absolute magnitude of the dominant Real-Time Multivariate (RMM) index on that day. RMM is a measure of MJO strength, and symbols denoting strong MJO occurrences are outlined in black. Grey shading indicates the MJO phases associated with strong westerlies and precipitation deficits over Riau (phases 4-7). The bottom panels show fire count anomalies (red bars), westerly wind anomalies (blue line) and visibility reduction anomalies greater than 2 (i.e., extreme haze) in the Malay Peninsula (black bars).

in October 2010. A similar lag occurred between the Riau fires and haze in Malacca (Figure C.4). The reason for these lags is not clear, but may have to do with the drop in westerly wind speeds.

The haze event in the Malacca-Kuala Lumpur region during August 2005 was again characterized by strong westerlies over Riau, which began to increase on July 27 just as the MJO entered phase 5. Similar to the June 2013 event, westerly wind speeds during August 2005 remained elevated as haze arrived in Malacca on August 2 and peaked on August 10-11. The strong westerlies dropped off abruptly after the MJO exited phase 8 on August 12. In this case, the first sign of haze in Malacca appears to have preceded fire activity in Riau, which began on August 5 and quickly ramped up. The absence of haze in Singapore may be explained by the northward shift in peak MJO westerlies at this time of year. The timing and strength of the BSISO during August 2005, as well as during two other moderate haze events in Malacca during August 2006 and August 2009, are consistent with this hypothesis (Figures C.5-C.6).

Our analysis has so far linked the MJO-driven westerlies to transport of haze to the Malay Peninsula. But the coincidence in timing of elevated windspeeds with fire counts in Riau for all three events (Figure 4.4) suggests that the strong winds that characterize the MJO may also exacerbate existing fire activity in Riau. Such winds could increase the oxygen supply needed for combustion and promote the spread of fires (Huang et al., 2016). In addition, MJO phases 5-8, which are conducive to westerly haze transport, are also associated with a brief period of dry weather over Riau (Reid et al., 2012; Zhang, 2013). It is possible that high winds concurrent with relatively dry weather amplified fire activity in Riau during October 2010 and August 2005, counteracting the relatively moist conditions preceding the fires shown by Gaveau et al. (2014a).

Westerly transport of smoke during all three events may have also been strengthened by the nIOD conditions, which were particularly strong in October 2010 and June 2013. A negative IOD phase is characterized by warm sea surface temperature (SST) anomalies around Sumatra, which enhance near-surface westerlies (Saji et al., 1999; Wilson et al., 2013). Although mechanisms governing the formation, strength, and propagation of the MJO are uncertain, one hypothesis is that the MJO is driven by moisture availability (Genio et al., 2015; Wang et al., 2015). Under this hypothesis, the warmer SSTs in the eastern Indian Ocean characteristic of nIOD provide a source of energy that strengthens the MJO (Wilson et al., 2013). Such a relationship between the nIOD and strong MJO activity compared to positive or neutral IOD conditions has been observed during August-November (Wilson et al., 2013).

4.4 Discussion and Conclusions

The conventional view has been that extreme haze events in Equatorial Asia are associated with strong El Nino-pIOD conditions, when smoke from drought-exacerbated burning in southern Sumatra and Borneo is gradually transported up to the Malay Peninsula by weak southeasterly winds. Here we identified a previously unrecognized pathway for extreme haze in the Malay Peninsula where nIOD conditions combined with an organized MJO moving across Indonesia (i.e. MJO phases 4-7) intensifies westerly wind strength over nearby Riau province in northern Sumatra. Riau experiences frequent agricultural fire activity (Gaveau et al., 2014a), and the anomalous westerly winds transport the smoke to Singapore and other densely populated areas of the Malay Peninsula. Our results suggest that this MJO-nIOD pathway is a recurring mechanism of severe smoke exposure for the Malay Peninsula, of which June 2013 is

just one example. While the duration of these MJO-related haze events is relatively short, on the order of several days compared to the multi-week time frames typical of the El Nino-pIOD events, the magnitude of the haze increase in the Malay Peninsula is just as severe and the occurrence may be more frequent.

The MJO has been of long-standing interest as a driver of many features of the regional climate of Equatorial Asia as well as the global climate and weather system including temperature and rainfall anomalies, severe flooding, tropical cyclones, and tornadoes (Zhang, 2013). Our results bring to attention an additional effect of the MJO as driver of extreme air quality degradation in the Malay Peninsula.

Despite the broad environmental impacts of the MJO, accurately forecasting individual MJO events and projecting the effect of climate change on MJO frequency remains a challenge. The fundamental mechanisms governing the formation and propagation of the MJO are still a matter of debate (Crueger & Stevens, 2015), limiting the accuracy to which the MJO can be represented in climate models (Kim et al., 2011). The response of MJO strength and organization to mountainous terrain, such as that along the coast of Sumatra just to the west of Riau, is also uncertain (Peatman et al., 2014; Kim et al., 2016), complicating the forecast of individual MJO events passing over Riau. Improving scientific understanding of these and other aspects of MJO dynamics is a top research priority in the tropical meteorology community and is a major focus of an upcoming international field campaign, Years of the Maritime Continent (YMC), planned for 2017-2019 (`http://www.bmkg.go.id/ymc/`).

Future trajectories of land use change in Riau may result in increased fire emissions due to continued crop expansion (Marlier et al., 2015a,b,c). Recent work also suggests an increased frequency of MJO events in a warmer, more moist climate (Arnold et al., 2015), which would make extreme haze occurrences over the Malay Peninsula increas-

ingly likely. The MJO, in turn, may also influence both the IOD and ENSO systems (Zhang, 2013). For example, strong MJO activity in boreal spring is often followed by an El Nino event within six months to a year (Hendon et al., 2007). March 2015 saw record-breaking MJO activity, which may have amplified the development of the strong El Nino during September-October 2015 (Marshall et al., 2016). Better representation of the MJO in models might therefore improve our ability to forecast not only future MJO-related haze events as discussed in this work, but also El Nino-pIOD haze events such as those of 1997, 2006, and 2015.

A

A.1 Concentration response factors

Table A.1: Concentration response factors (β) by cause of death. See references given in the Methods section.

Cause of death	Low	Central	High
COPD	1.077	1.128	1.182
Stroke	1.077	1.128	1.182
IHD	1.177	1.287	1.407
Lung cancer	1.057	1.142	1.234
Other cardiovascular	1.077	1.128	1.182
Lower respiratory infection	1.03	1.12	1.3
Other respiratory	1.077	1.128	1.182
Respiratory disease (ozone only)	1.01	1.04	1.067

A.2 Coal plant locations

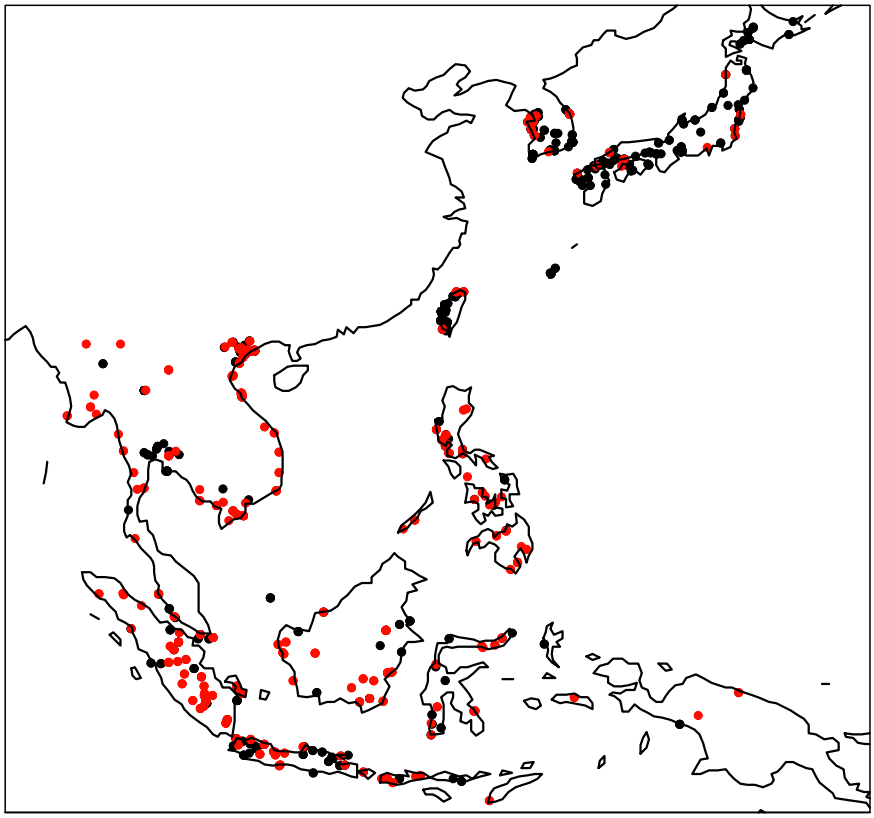


Figure A.1: Power plant locations in 2011 and projected for 2030 in Southeast Asia outside of China and India. Plants operating in 2011 are shown in black. Plants planned for development by 2030 are shown in red.

A.3 National simulations

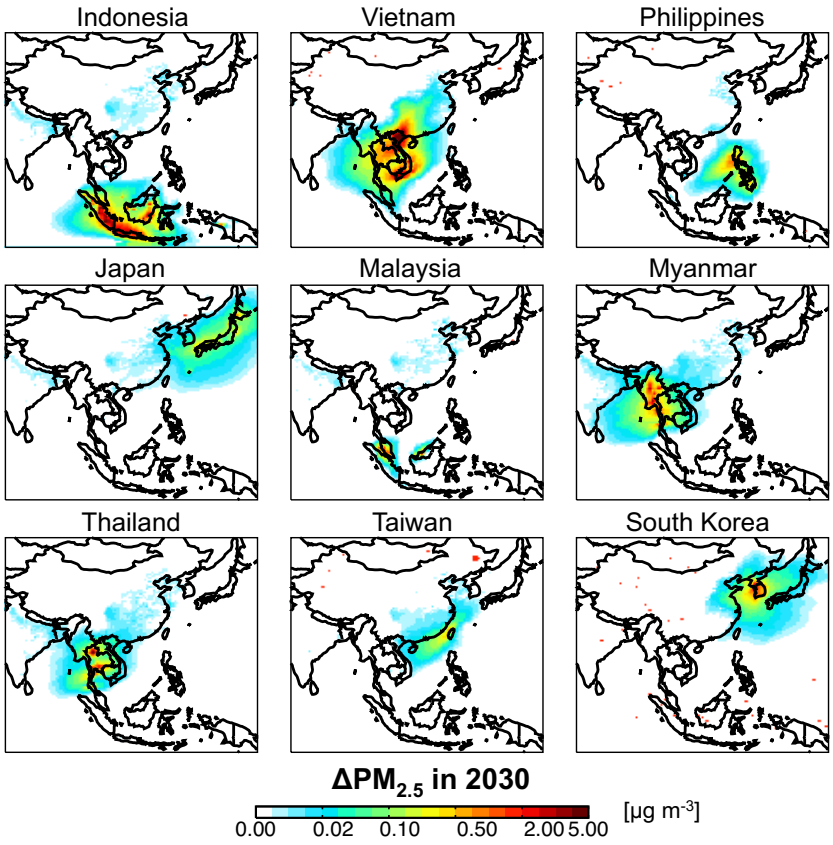


Figure A.2: Projected increases (Δ) in surface $PM_{2.5}$ in Southeast Asia due to coal in 2030, as determined by difference between the regional simulation with 2030 emissions and a simulation with zero coal emissions in each country in Table 1.1 (emissions in other countries are unchanged).

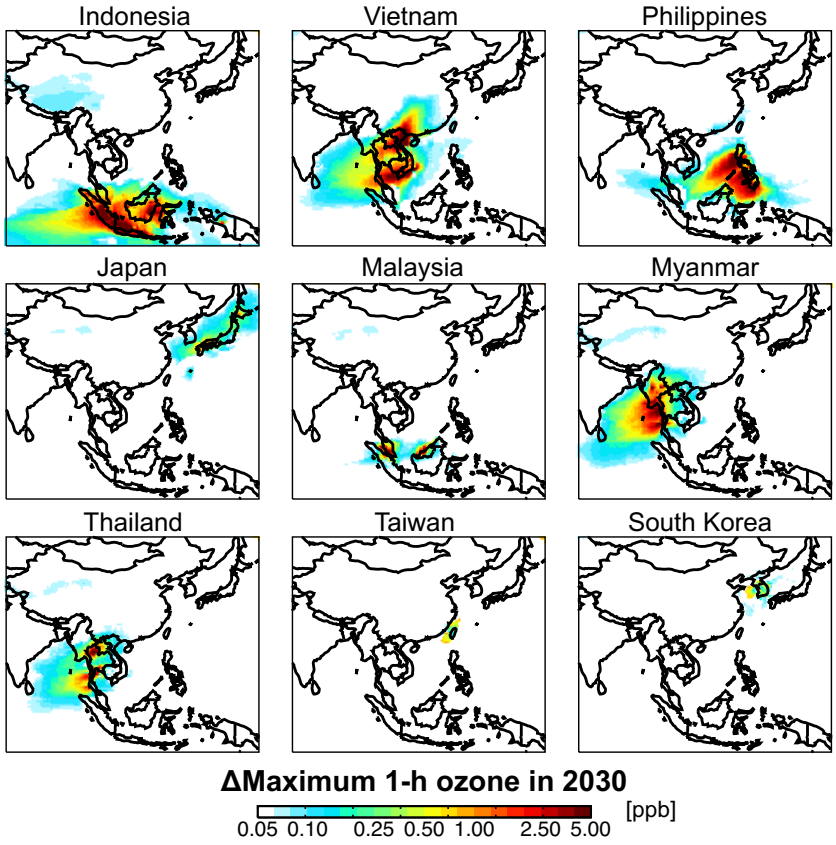


Figure A.3: Same as Figure A.2 but for 6-month averaged maximum 1-h ozone.

A.4 Contributions to mortality from population projections

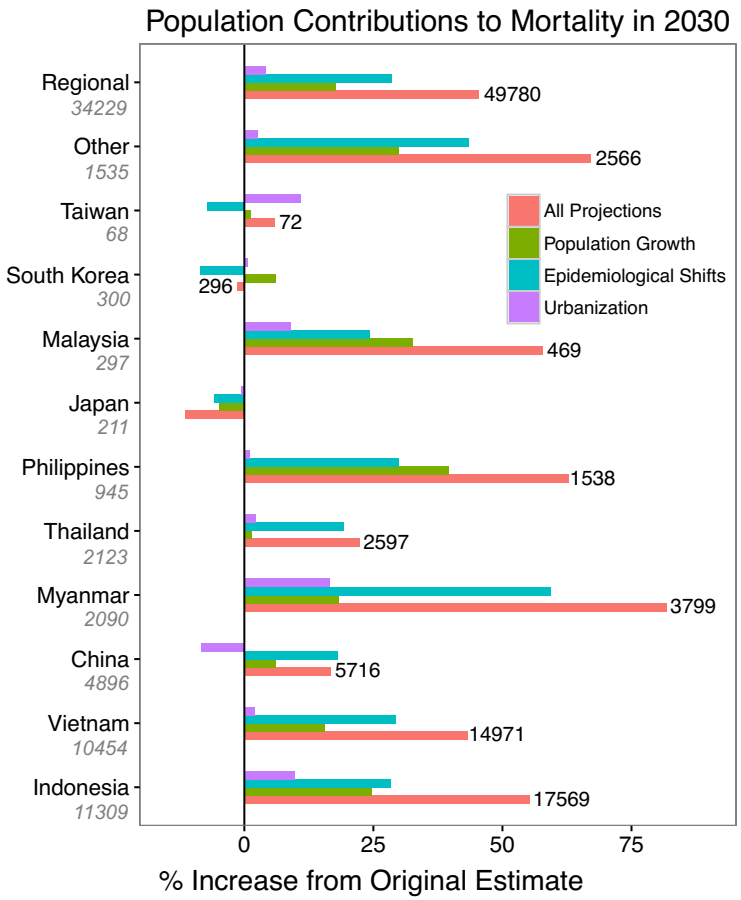


Figure A.4: Percent contributions of population changes to coal-related premature mortality increases between 2011 and 2030 by country. Values shown by the colored bars represent the percent change in mortality due to including each population factor relative to the baseline mortality estimate using the 2030 pollution change (2030 simulation 2011 simulation) and the original 2011 population estimates. The combined contribution from all factors for each country is shown in pink. Contributions from population number growth are shown in green, shifts in epidemiological factors (age structure, incidence of disease, obesity, etc) are shown in blue, and spatial changes driven by urbanization are shown in purple. See Future health impact projections section for descriptions of datasets used for each factor. The original estimates for the increase in mortality between 2011 and 2030 in each country before including the population projections are shown in grey under the corresponding country label. The final estimates after including all population factors (i.e. the values used in the estimates reported in the main text) are shown at the end of the pink bars.

A.5 Domestic and transboundary contributions to mortality in 2011

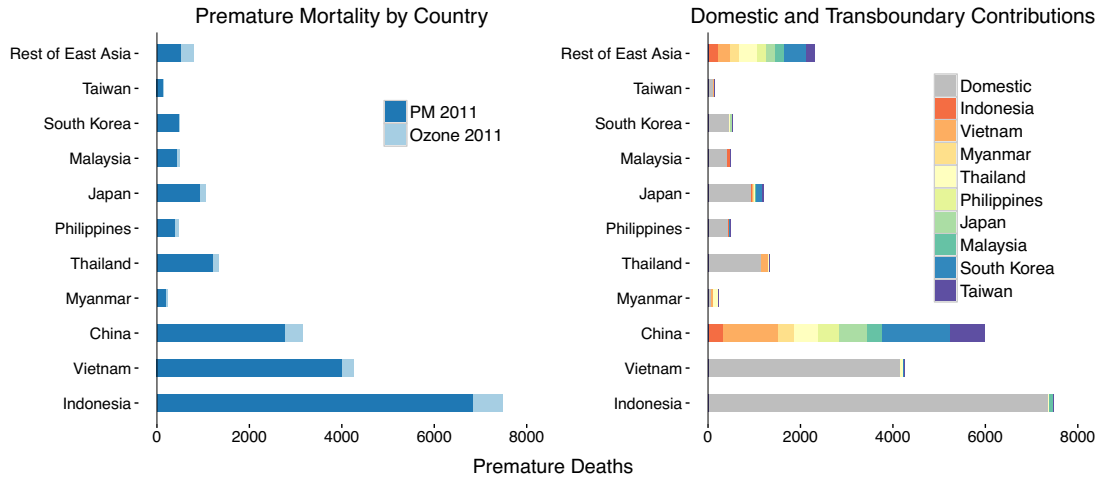


Figure A.5: Coal-related mortality in 2011 due to emissions in Southeast Asia (countries in Table 2.1). The left panel shows the premature deaths in individual countries. Deaths due to $PM_{2.5}$ and ozone are shown separately. The right panel shows the 2011 coal-related mortality in each country broken down by contributions from domestic and transboundary sources. As computed here, mortality in China and Rest of East Asia (not included in Table 2.1) is solely from transboundary pollution. The mortality totals in the right panel are the sums of the contributions from simulations with vs. without coal emissions for the individual countries in Table 1; because of chemical and CRF non-linearities, they may be greater than the mortality totals in the left panels.

B

B.1 The GEOS-Chem adjoint

We use version 8-02-01 of the GEOS-Chem chemical transport model and its adjoint (Henze et al., 2007; Kopacz et al., 2011; Kim et al., 2015b) to quantify the source-receptor relationships relevant for smoke exposure in Equatorial Asia during large haze events. GEOS-Chem is driven by Goddard Earth Observing System (GEOS-5) assimilated meteorological data from the NASA Modeling and Assimilation Office (GMAO) at 0.5 x 0.67 native horizontal resolution with 72 vertical levels. Following Kim et al. (2015b), we use the GEOS-Chem adjoint (v34) to calculate the potential influence of smoke emissions in each 0.5 x 0.67 grid cell for the whole Equatorial Asia model domain [70-150 E, 11 S-55 N] on population-weighted $PM_{2.5}$ concentrations in three receptor regions (Indonesia: 250 million people in 2015, Malaysia: 30 million people, and Singapore: 4 million people) for each month during July-October based on meteorology for 2006. Population weighting of the mean receptor concentrations was carried out by first weighting the smoke concentration of each grid cell by its fractional population within the receptor area, then taking the average concentration across those grid cells. The resulting sensitivities i.e., the fractional contribution of each grid cell to smoke exposure at each receptor downwind are applied to the fire emission inventory, yielding a gridded estimate of the monthly mean smoke-related $PM_{2.5}$ exposure that results from those emissions. We scale the resulting OC-related $PM_{2.5}$ by a factor of 2.1 to account for additional organic matter acquired through atmospheric processing (Turpin & Lim, 2001). The fractional contributions to exposure from each grid cell are then summed together to estimate the total population-weighted exposure at each receptor. For this study, we apply the 2006 sensitivities to both the 2006 and 2015 emissions. This approach assumes that the smoke transport

patterns for these two haze events are similar, which is likely given that they both occurred during similar phases of the ENSO and the IOD, the two major drivers of interannual meteorological variability in Equatorial Asia (Li et al., 2003). Calculation of new adjoint sensitivities would require processing of 2015 GMAO meteorological fields and considerable computational expense, while our streamlined approach allows for near real-time assessment of smoke exposure and attribution to emission sources.

B.2 Health impact calculations

We estimate health impacts from smoke pollution using an approach similar to that in Anenberg et al. (2012) and two studies quantifying the Global Burden of Disease (Lim et al., 2012; Burnett et al., 2014). We derive a concentration response relationship (CRF) between relative mortality and $PM_{2.5}$ from the epidemiological literature, modeling health impacts as a 1% increase in annual baseline all-cause mortality per 1 μg m-3 increase in annual average $PM_{2.5}$ levels when annual average $PM_{2.5}$ concentrations are less than 50 g m^{-3} (Schwartz et al., 2008; Anenberg et al., 2012; Lepeule et al., 2012). Using annual average $PM_{2.5}$ exposure increases the likelihood of capturing the effects of both acute and chronic pollution exposure. In our calculations there were no locations where annual average concentrations exceeded this 50 g m^{-3} threshold, likely because our estimates reflect population-weighted exposures rather than actual smoke concentrations. Using gridded population data from the Center for International Earth Science Information Network (CIESIN; Center for International Earth Science Information Network, 2005) and country-level data on baseline mortality rates and population age structure from the Global Burden of Disease for 2013 (the most recently available year; Lim et al., 2012; GBD, 2015), we estimate the ex-

cess deaths attributable to smoke $PM_{2.5}$ as follows. We first calculate a July-October population-weighted average $PM_{2.5}$ exposure for each receptor country during both 2006 and 2015 (Section B.1 above). We next convert these July-October average population-weighted smoke $PM_{2.5}$ exposures to annual average values. We then calculate the total population in each receptor country using the CIESEN population distributions, and apply the baseline mortality rate and age structure information for each country to calculate population over 25 years of age. Finally, we calculate the total mortality attributed to $PM_{2.5}$ from fires in each receptor country i using:

[Equation B.1]

Attributable Mortality[i] = Baseline Mortality[i] x Population[i] x β x Population-weighted x $\Delta PM_{2.5}[i]$

where β is the CRF from epidemiological studies, corresponding to the slope of the relationship (1%) between pollutant concentration and mortality, and $\Delta PM_{2.5}$ is the estimated change in $PM_{2.5}$ from smoke pollution.

Previous estimates of excess deaths from smoke $PM_{2.5}$ pollution for the 1997 event range widely, e.g., 296,000 in Johnston et al. (2012) and 13,200 in Marlier et al. (2013). Our estimate of 100 thousand in 2015 falls between these two extremes. Johnston et al. (2012) included health impacts on the whole population, including children, and considered all causes of premature mortality, capping exposure above 50 g m^{-3} in each model grid cell. In contrast, Marlier et al. (2013) restricted their analysis to cardiovascular mortality in adults and used a different CRF form. In sensitivity analyses Marlier et al. (2013) found that applying differently shaped CRFs to the same smoke concentrations yielded mortality increases up to four times higher than their reported

estimate. Due to the lack of consistent emissions datasets, we cannot directly compare our estimate of excess mortality for 2015 to those reported for 1997. Nonetheless the fine spatial resolution of our approach likely better captures smoke exposure to peak pollution concentrations in populated areas. We also use more recent information about baseline mortality rates and population age structure.

B.3 High resolution FRP observations in concessions

Table B.1: Average percent contributions of fire radiative power (FRP) on concessions and peatlands to total FRP observed by MODIS on the Aqua and Terra satellites during July-October in 2006 and 2015 over Sumatra and Kalimantan. The term mixed indicates regions in which boundaries of oil palm, timber, and/or logging concessions overlap. Estimates of percent contributions for peat take into account peatland areas both within and outside of concessions. All values are calculated using FRP Collection 6, and so differ slightly from those reported by Marlier et al. (2015c), who relied on Collection 5.

	Year	Timber %	Oil Palm %	Logging %	Mixed %	Peat %	Total FRP (MW)
Sumatra	2006	26.55	11.33	2.01	0.51	44.47	4.57E+06
	2015	55.07	4.72	1.32	0.44	71.76	6.46E+06
Kalimantan	2006	7.81	32.01	6.57	5.66	32.39	6.59E+06
	2015	9.62	20.06	8.97	3.99	42.85	5.67E+06

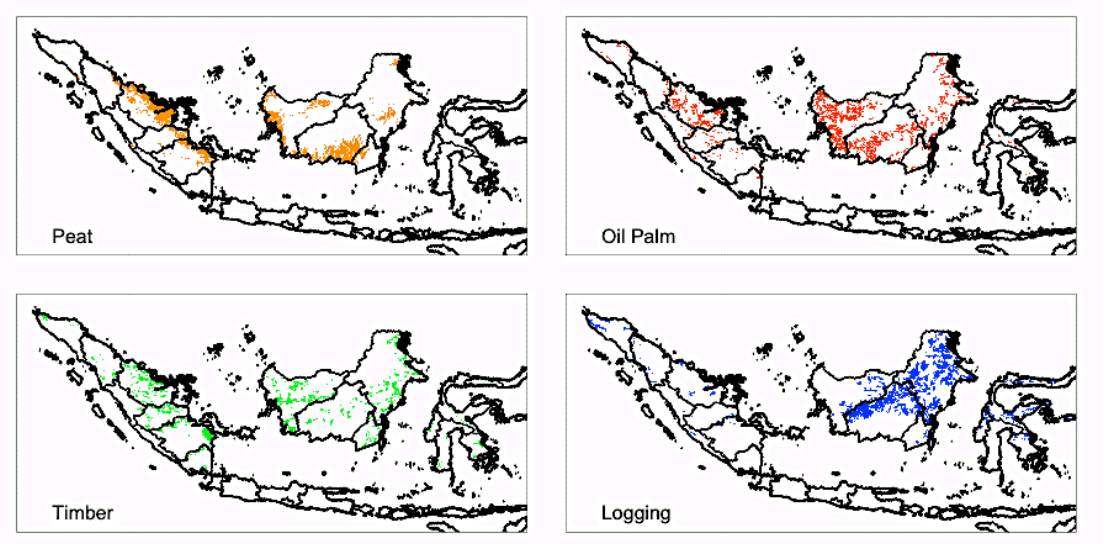


Figure B.1: Distribution of peatlands and current or planned concession types in Indonesia as of 2010. The top left panel shows the peatland distribution in orange (Wahyunto & Subagjo, 2003, 2004). The other three panels show land use distributions from the Global Forest Watch (Institute, 2015a,b,c); estimates are based on data provided by the Indonesian Ministry of Forestry. Oil palm concessions are shown in the top right in red, timber in the bottom left in green, and logging in bottom right in blue. Spatial resolution in all panels is 5 x 5 km^2.

B.4 Province masks

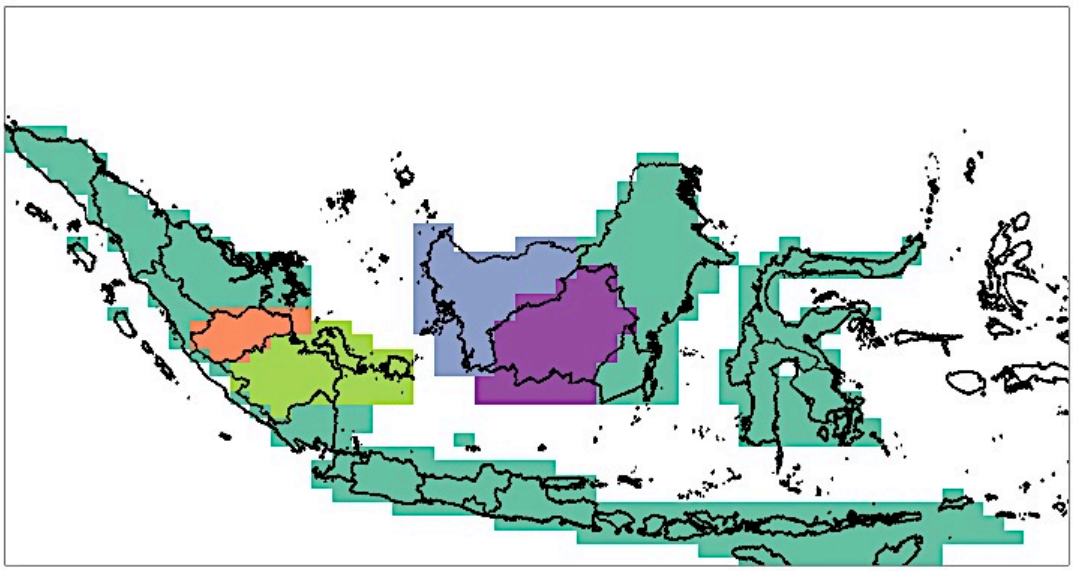


Figure B.2: Province masks at 0.5 x 0.67 resolution used in this analysis. Jambi is shown in coral, West Kalimantan in blue, and Central Kalimantan in purple. South Sumatra and Bangka-Belitung are combined and shown in green. Other provinces are shown in teal.

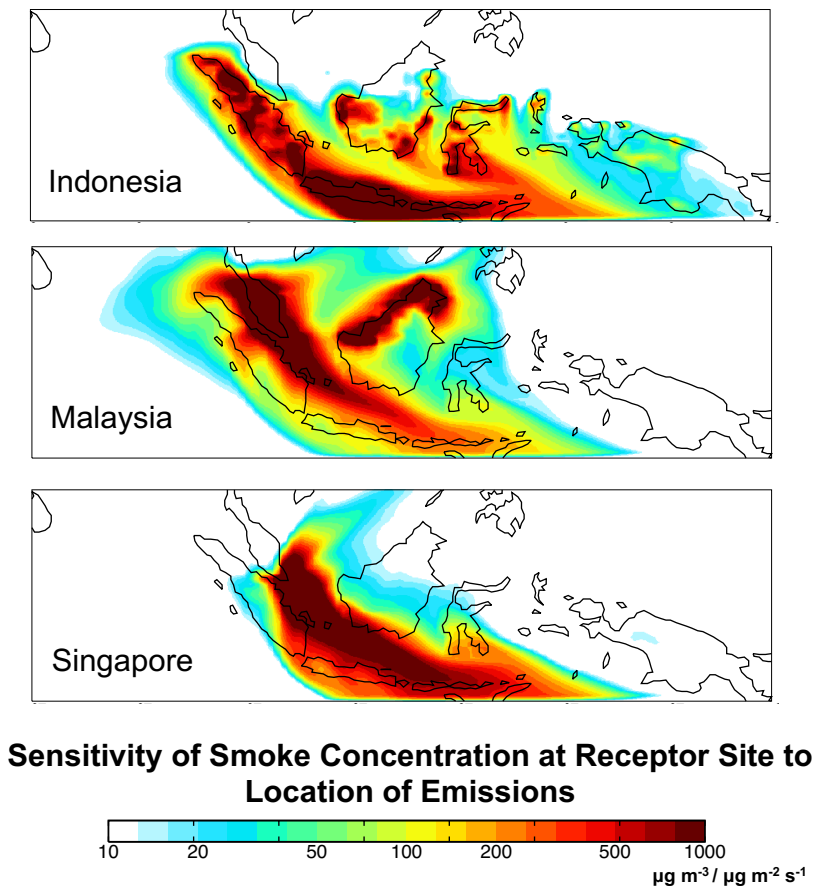


Figure B.3: GEOS-Chem adjoint sensitivities simulated for September-October 2006 of population-weighted $PM_{2.5}$ in each receptor region to smoke emissions in gridboxes across the domain. The top panel shows the sensitivities for Indonesia; the middle panel, Malaysia; and the bottom panel, Singapore. These sensitivities are for hydrophobic organic carbon (OC) specifically, but spatial patterns are similar for hydrophilic OC as well as for BC.

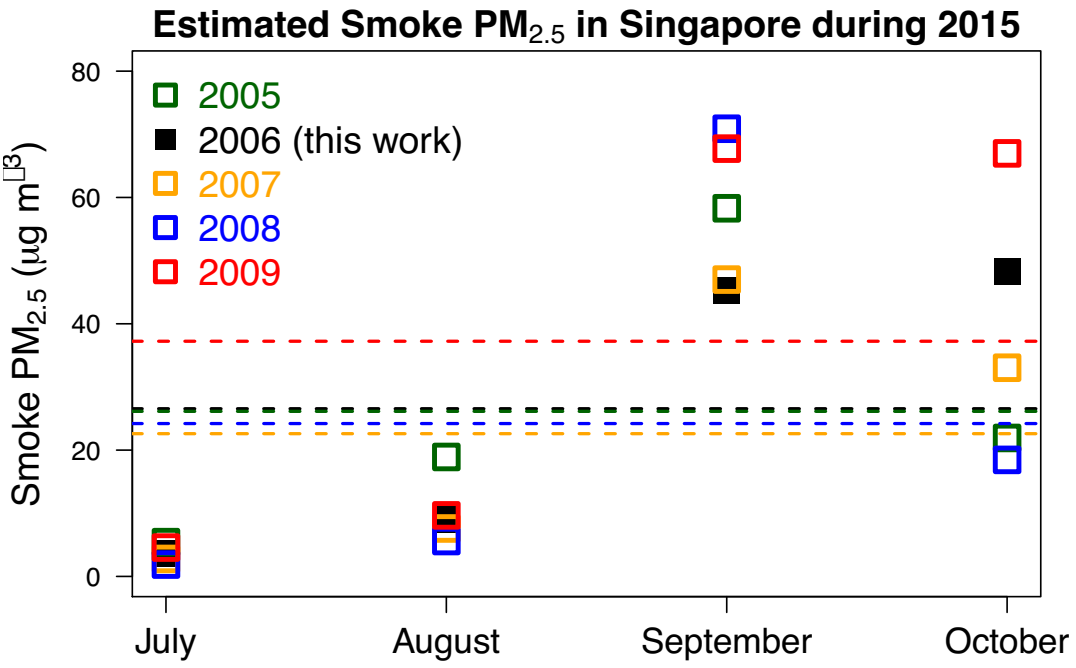


Figure B.4: Monthly mean smoke exposure at Singapore estimated using 2015 GFAS emissions scaled by 50% and a suite of adjoint sensitivities for 2005-2009. The exposures used in this work, estimated with the 2006 sensitivities, are shown in black filled squares. Estimates produced using sensitivities from 2005 are shown in green, 2007 in orange, 2008 in blue, and 2009 in red. Dashed lines show corresponding July-October averages for each year. The plot shows the impact that application of different meteorological fields has on estimates of smoke exposure in Singapore. Of the five years, only 2006 is characterized by the simultaneous El Nio and positive Indian Ocean Dipole conditions similar to those in 2015.

B.6 Fire management strategies in Indonesia

The rapid assessment framework demonstrated in this work would allow policy makers in Indonesia to quickly identify the burning areas that are leading to the most severe air pollution in populated areas downwind during extreme haze events. This information can then be used to prioritize fire management efforts including land use management strategies to help mitigate the domestic and transboundary smoke pollution resulting from these fires. However, implementing effective fire management strategies on the ground in Indonesia is challenging. We summarize here some of the difficulties currently facing effective fire management practices in Indonesia, and, when relevant, how our adjoint approach may be implemented to help address some of these issues.

B.6.1 Regulating fires in smallholder farms vs. industrial plantations

One major hurdle to effectively regulating fire activity in Indonesia is the heterogeneity of the human activity landscape. For example, it is common for local communities and small farmlands to be located immediately alongside, or even within, large scale industrial concessions such as those for oil palm or timber, making the attribution of fire ignitions difficult (Cattau et al., 2016; Gaveau et al., 2016). Conflicting land tenure claims can even be a source of fire ignitions to reclaim land, independent of any agricultural benefit (Dennis et al., 2005). Additionally, while the use of fire as a land management tool can perhaps be replaced by other alternative approaches to slash-and-burn techniques on the large plantations, fire is often the only affordable mechanism of land maintenance for small scale farmers (Tomich et al., 1998; Palm

et al., 2004). Certain land management practices outside of the burning season have been shown to help reduce smoke emissions and the likelihood of escaped fires from small farms (Saharjo & Munoz, 2005), but would require widespread efforts to incentivize the use of these practices amongst local communities in order to matter for regional haze. Using the GEOS-Chem adjoint to identify the burning areas contributing most severely to downwind pollution during extreme haze events would help identify priority areas where developing economically feasible alternative land clearing practices in small scale farms and settlements would most benefit local and regional human health.

B.6.2 Extinguishing fires in peatlands

Another challenge to firefighting efforts in Indonesia is the difficulty involved with actually extinguishing fires in peat, even with adequate resources. Because peat fires tend to burn at low temperatures, they can smolder for many days to weeks or even months, undetected within the subsurface peat layers (Turetsky et al., 2015). Due to this smoldering tendency and to the variability in peat layer depth, which can range from inches to tens of meters in some places, it is difficult for firefighters to know if the peat fires have been completely extinguished. Subsurface peat fires can even migrate through the subsurface away from their ignition source, reigniting weeks later in a completely different location (Rein, 2013). Identifying the areas contributing most to smoke downwind in near real time could help fire management officials decide quickly where best to allocate their front line fire-fighting efforts (e.g., trained personnel or helicopters for emergency water application) to better ensure that peat fires in these areas have been fully extinguished. It would also guide the development of new approaches for extinguishing peat fires when these traditional methods are ineffective

(Byron & Shepherd, 1998).

A better approach to reducing fires in peatlands would be to counteract the effects of human degradation through peatland restoration (Jaenicke et al., 2010). Peatland areas are naturally resistant to fire due to their characteristically high moisture content (Turetsky et al., 2015). Though human activity has degraded much of the peatlands in Indonesia, making these lands more fire-prone, efforts to restore peatlands to their natural fire-resistant state are ongoing (Indriatmoko et al., 2014). However, these restoration efforts face many of the challenges common amongst conservation groups, such as a lack of funding and resources, and limited participation from the public. Conservation efforts also rarely provide an obvious economic benefit to the local communities, limiting their incentive to participate (Nicolas & Beebe, 1999; Chokkalingam et al., 2007). Identifying the areas most important for regional haze events would allow for more targeted efforts to restore degraded peatland and develop sustainable partnerships with local communities in these high priority burning areas.

B.6.3 Enforcing existing policies

Lastly, effectively enforcing existing regulations related to illegal burning in Indonesia has proven difficult (Jones, 2006; Evers et al., 2016). Insufficient enforcement of these regulations during past extreme haze events has been attributed in part to inadequate planning and resource availability arising from inefficient organization within the Indonesian government (Dennis et al., 2005; Jones, 2006). In addition, many of the companies or individuals accused of burning illegally escape with minimal punishment, providing no deterrent for getting caught (Jones, 2006). Complicating the issue further is the jurisdictional ambiguity surrounding the enforcement of fire regulations; in many areas, fire use is regulated by both traditional community laws and national

regulations from the Indonesian government, which can be contradictory (Byron & Shepherd, 1998; Dennis et al., 2005; Gaveau et al., 2016). The adjoint method presented in this work would allow both state and local governments to prioritize the allocation of police resources to those areas where enforcing the bans against illegal burning would most effectively reduce damage to human health. Identifying the provinces where burning is most important for regional air quality degradation would also highlight areas where the need for cooperation between national and local governments on issues of fire regulation and enforcement is paramount. Additionally, many large companies have pledged not to use fire for land management to obtain certification from the Roundtable on Sustainable Palm Oil (RSPO; http://www.rspo.org/), though policing such pledges is a challenge. The adjoint approach could be used to both estimate the benefits to regional human health of no-burn pledges from companies in particular provinces, as well as provide a means of accountability for companies burning in the high priority areas most influencing regional air quality. Coupled with improved spatial maps to reduce inconsistencies in land tenure claims (http://blog.cifor.org/22534/new-tech-better-map-on-tap-to-protect-indonesian-forests?fnl=en), the adjoint would be a powerful tool for no-burning enforcement.

Extreme haze in Indonesia will likely continue to be an issue until the challenges mentioned above are more fully addressed. However, the capability to pinpoint the areas most affecting regional human health during extreme haze with our adjoint approach would help stakeholders and policymakers prioritize the areas where fire management is most important for domestic and regional air quality, increasing the precision and therefore the effectiveness with which all these fire management strategies can be implemented.

C

C.1 Satellite aerosol observations during June 2004

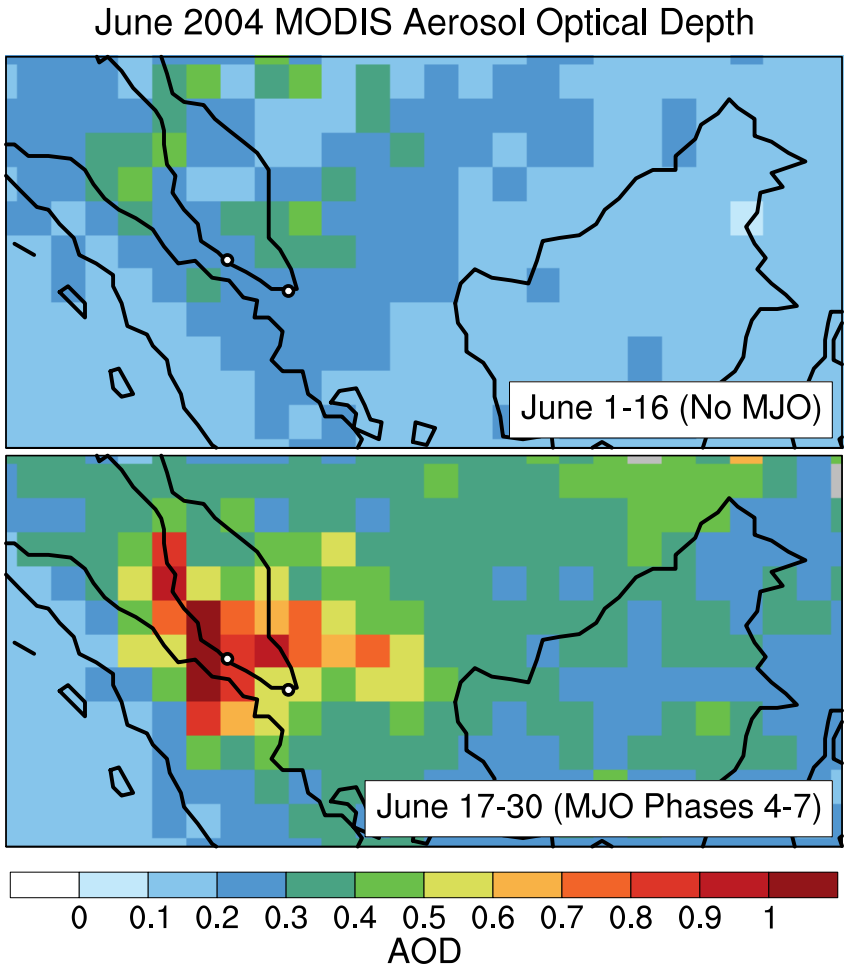


Figure C.1: Mean aerosol optical depths (AOD) from the MODIS instrument on board the Aqua satellite during June 2004. The top panel shows the mean AOD during June 1-16. There was no organized MJO signal in any phase during this time. The bottom panel shows mean AOD during June 17-30, when there was strong MJO activity in phases 4-7 (phase 6 during June 17-21 and phase 7 during June 22-30). Locations of Malacca and Singapore are shown in the white circles.

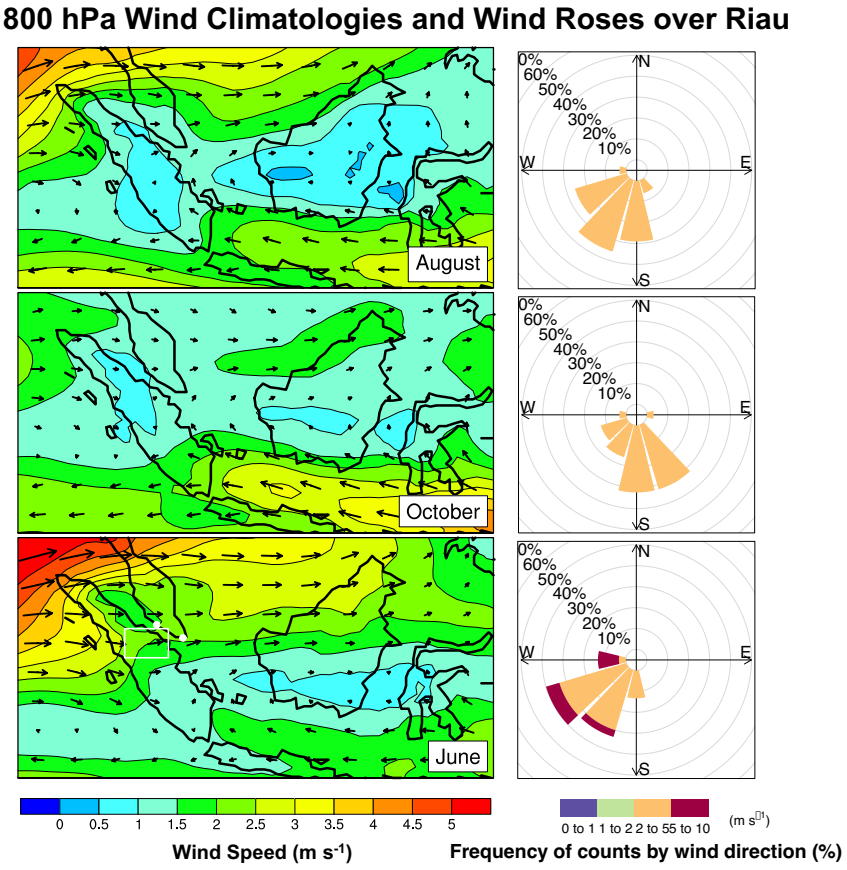


Figure C.2: Climatological wind fields at 800 hPa and associated wind roses over Riau (white rectangle in bottom panel) for June, August, and October during 2004-2014. Percentages in wind rose plots indicate the percent days that winds emanate from a particular direction for that month; colors in these plots denote different ranges in wind speed.

C.3 Daily satellite observations of haze events

Figure C.3 shows daily time series of MODIS Aerosol Optical Depth (AOD), OMI Aerosol Index (AI), and active fire counts over Riau for the three haze events. In 2013, peak fire activity occurred on June 20, coincident in time with an enhancement in OMI AI. Neither MODIS AOD product, however, increased significantly at that time. Similarly, in 2005, OMI AI responded readily to fire activity on August 7, with no clear corresponding increase in either MODIS AOD product until 2-3 days later. Satellite data are limited over Riau for much of October, although OMI AI clearly increased on October 16 just after the onset of burning. MODIS AOD again showed no obvious enhancement until several days after fire activity begins in Riau.

The apparent discrepancies between daily OMI AI and MODIS AOD during haze events may be due to multiple factors, including 1) the representation of the optical properties of organic carbon, the dominant component of biomass burning aerosol, in AOD retrievals (Jethva & Torres, 2011; Sayer et al., 2014) and 2) retrieval challenges associated with clouds (Reid et al., 2013). The significant changes in cloud cover, humidity, and wind-driven ocean aerosol fluxes associated with passage of the MJO could make monitoring the MJO-driven haze events discussed in this work especially challenging for the two MODIS instruments (Tian et al., 2008). Although the twice-daily overpass schedule of the MODIS instruments currently offers the highest frequency in temporal coverage of any aerosol remote sensing product over Equatorial Asia, it is unclear how accurately MODIS AOD can monitor haze at the daily scale, at least in this region during MJO-influenced events.

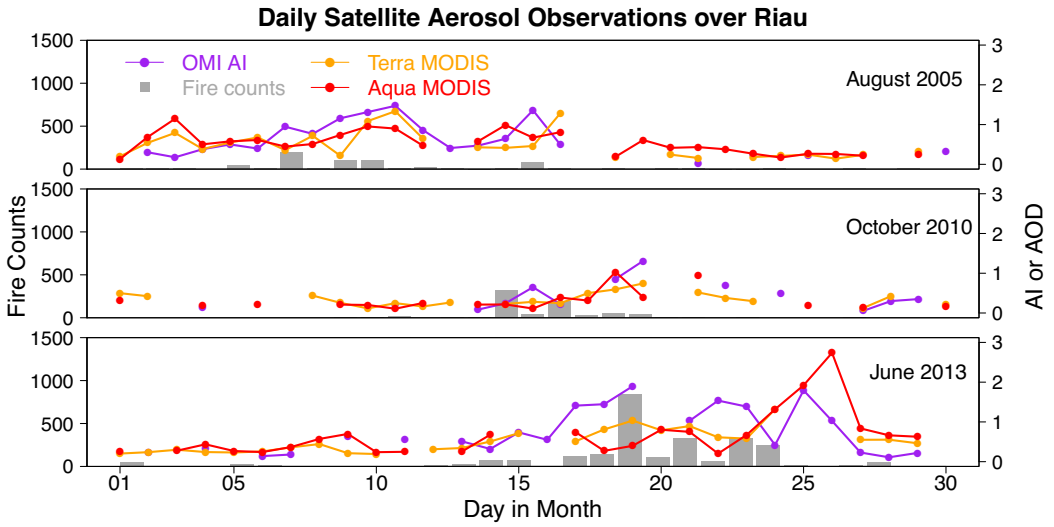


Figure C.3: Daily observations of MODIS AOD over Riau (shown by red rectangle in Figure 4.4) from the Terra (red) and Aqua (orange) satellites compared with observations of OMI AI (purple) and MODIS active fire counts (grey bars) during the June 2013, October 2010, and August 2005 haze events. The threshold for AI detection by OMI is 0.5. To ease comparison among the different satellite products, 0.5 has been subtracted from all OMI AI values.

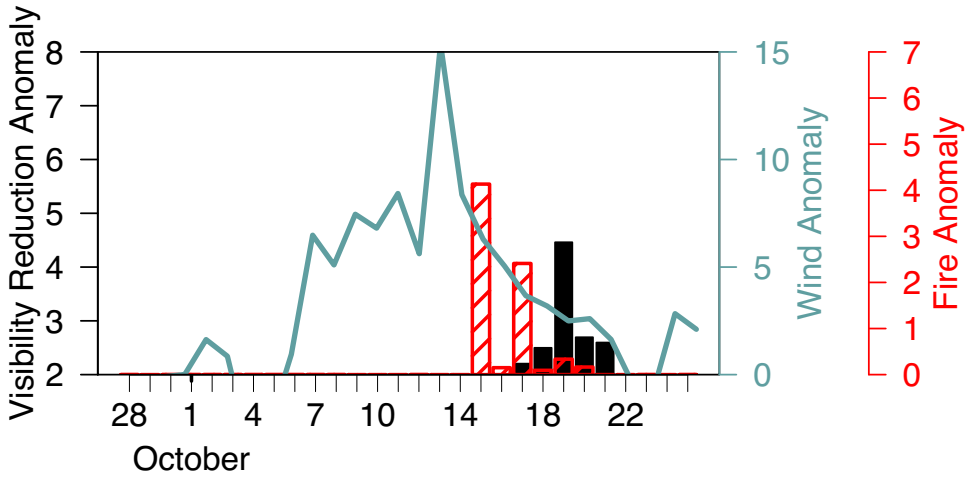


Figure C.4: Time series of daily fire counts and mean wind speed over Riau, and haze downwind in Malacca during October 2010. Fire count anomalies are shown by the red bars, westerly wind anomalies by the blue line, and visibility reduction anomalies in Malacca greater than 2 (extreme haze) by the black bars.

C.4 BSISO TIMESERIES

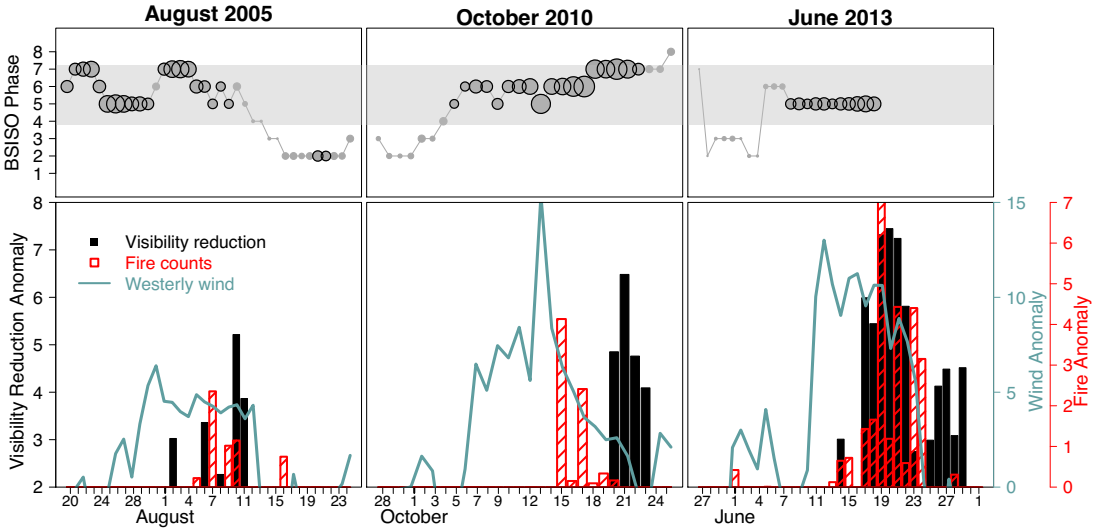


Figure C.5: Same as Figure 4.6 but with the Bi-Seasonal IntraSeasonal Oscillation (BSISO) index instead of the MJO index. BSISO data (from http://iprc.soest.hawaii.edu/users/jylee/bsiso/) are available only through June 18, 2013.

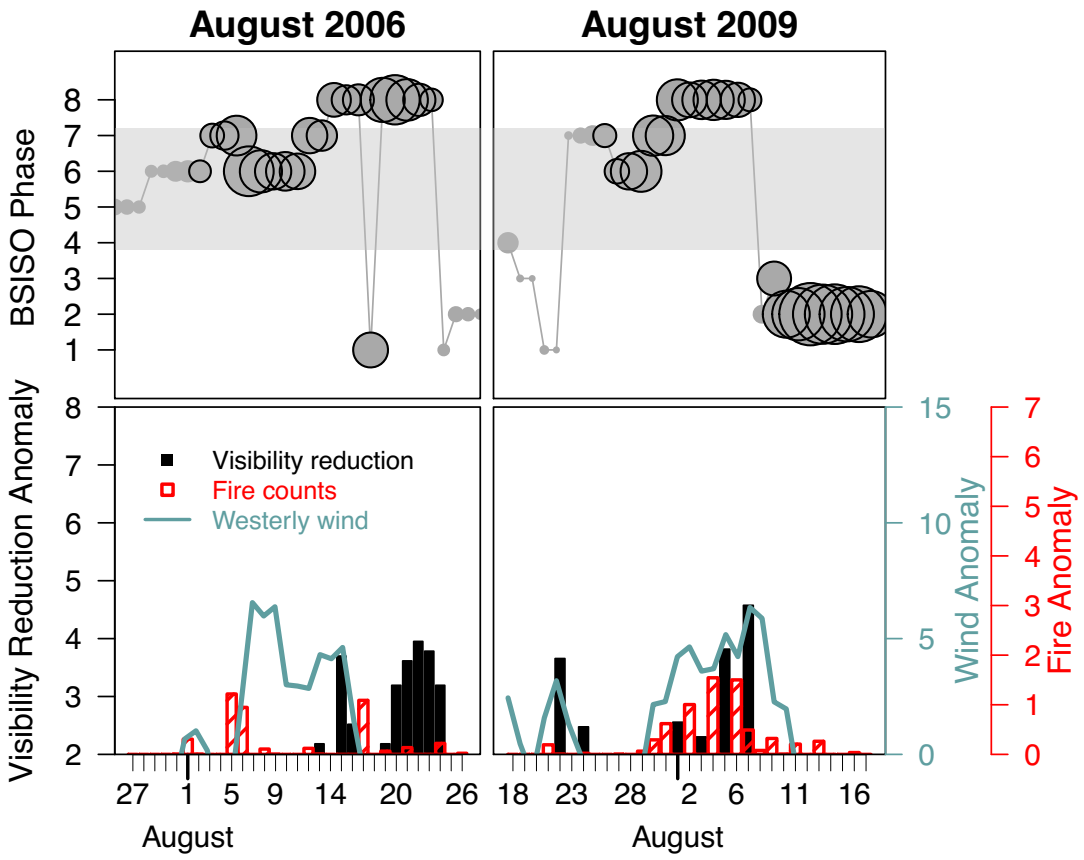


Figure C.6: Same as Figure C.5 but for August 2006 and August 2009, two moderate haze events in Malacca.

References

(2015). Institute for heath metrics and evaluation. Online: http://ghdx.healthdata.org/global-burden-disease-study-2013-gbd-2013-data-downloads.

Aglionby, J. (2005). Malaysia declares haze emergency.

Ainsworth, E. A. (2008). Rice production in a changing climate: a meta-analysis of responses to elevated carbon dioxide and elevated ozone concentration. *Global Change Biol*, 14(7), 1642–1650.

Amann, M., Borken?Kleefeld, J., Cofala, J., Heyes, C., Klimont, Z., Rafaj, P., Purohit, P., Schpp, W., & Winiwarter, W. (2012). *Future emissions of air pollutants in Europe ? Current legislation baseline and the scope for further reductions*. Technical Report TSAP Report 1, International Institute for Applied Systems Analysis.

Amann, M., Klimont, Z., & Wagner, F. (2013). Regional and global emissions of air pollutants: Recent trends and future scenarios. *Annual Review of Environment and Resources*, 38(1), 31–55.

Andela, N., Kaiser, J. W., Heil, A., van Leeuwen, T. T., van der Werf, G. R., Wooster, M. J., Remy, S., & Schultz, M. G. (2013). *Assessment of the Global Fire Assimilation System (GFASv1)*. Technical report, Monitoring Atmospheric Composition and Climate-II).

Anenberg, S. C., Horowitz, L. W., Tong, D. Q., & West, J. J. (2010). An estimate of the global burden of anthropogenic ozone and fine particulate matter on premature human mortality using atmospheric modeling. *Environ Health Perspect*, 118(9), 1189–1195.

Anenberg, S. C., Schwartz, J., Shindell, D., Amann, M., Faluvegi, G., Klimont, Z., Janssens-Maenhout, G., Pozzoli, L., Dingenen, R. V., Vignati, E., Emberson, L., Muller, N. Z., West, J. J., Williams, M., Demkine, V., Hicks, W. K., Kuylenstierna, J., Raes, F., & Ramanathan, V. (2012). Global air quality and health co-benefits of mitigating near-term climate change through methane and black carbon emission controls. *Environ Health Perspect*, 120(6), 831–839.

Ansolabehere, P. S. (2007). *The Future of Coal*. MIT.

Arnold, N. P., Branson, M., Kuang, Z., Randall, D. A., & Tziperman, E. (2015). MJO intensification with warming in the superparameterized CESM. *Journal of Climate*, 28(7), 2706–2724.

Brauer, M., Amann, M., Burnett, R. T., Cohen, A., Dentener, F., Ezzati, M., Henderson, S. B., Krzyzanowski, M., Martin, R. V., Dingenen, R. V., van Donkelaar, A., & Thurston, G. D. (2012). Exposure assessment for estimation of the global burden of disease attributable to outdoor air pollution. *Environmental Science & Technology*, 46(2), 652–660.

Burnett, R. T., C. Arden, I. P., Ezzati, M., Olives, C., Lim, S. S., Mehta, S., Shin, H. H., Singh, G., Hubbell, B., Brauer, M., Anderson, H. R., Smith, K. R., Balmes, J. R., Bruce, N. G., Kan, H., Laden, F., Prüss-Ustün, A., Turner, M. C., Gapstur, S. M., Diver, W. R., & Cohen, A. (2014). An integrated risk function for estimating the global burden of disease attributable to ambient fine particulate matter exposure. *Environ Health Perspect*.

Byron, R. N. & Shepherd, G. (1998). *Indonesia and the 1997-98 El Nino: fire problems require long-term solutions*. Center for International Forestry Research (CIFOR).

Carlson, K. M., Curran, L. M., Ratnasari, D., Pittman, A. M., Soares-Filho, B. S., Asner, G. P., Trigg, S. N., Gaveau, D. A., Lawrence, D., & Rodrigues, H. O. (2012). Committed carbon emissions, deforestation, and community land conversion from oil palm plantation expansion in west kalimantan, indonesia. *Proceedings of the National Academy of Sciences*, 109(19), 7559–7564.

Cattau, M. E., Harrison, M. E., Shinyo, I., Tungau, S., Uriarte, M., & DeFries, R. (2016). Sources of anthropogenic fire ignitions on the peat-swamp landscape in kalimantan, indonesia. *Global Environmental Change*, 39, 205–219.

Center for International Earth Science Information Network, C. U. (2005). Gridded population of the world version 3 (gpwv3): Population grids.

Chang, C.-H., Hsiao, Y.-L., & Hwang, C. (2015). Evaluating spatial and temporal variations of aerosol optical depth and biomass burning over southeast asia based on satellite data products. *Aerosol and Air Quality Research*, 15(7).

Chang, C.-P., Wang, Z., McBride, J., & Liu, C.-H. (2005). Annual cycle of southeast asia—maritime continent rainfall and the asymmetric monsoon transition. *Journal of Climate*, 18(2), 287–301.

Chen, D., Wang, Y., McElroy, M. B., He, K., Yantosca, R. M., & Sager, P. L. (2009). Regional CO pollution and export in china simulated by the high-resolution nested-grid GEOS-chem model. *Atmospheric Chemistry and Physics*, 9(11), 3825–3839.

Chen, W. & Xu, R. (2010). Clean coal technology development in china. *Energy Policy*, 38(5), 2123–2130.

Chokkalingam, U., Suyanto, Permana, R. P., Kurniawan, I., Mannes, J., Darmawan, A., Khususyiah, N., & Susanto, R. H. (2007). Community fire use, resource change, and livelihood impacts: The downward spiral in the wetlands of southern sumatra. *Mitig Adapt Strat Glob Change*, 12(1), 75–100.

Cofala, J., Bertok, I., Borken-Kleefeld, J., Heyes, C., Kiesewetter, G., Klimont, Z., Purohit, P., Rafaj, P., Sander, R., Schpp, W., & Amann, M. (2015). *Implications of energy trajectories from the World Energy Outlook 2015 for India's air pollution.* Technical report, International Institute for Applied Systems Analysis, Laxenburg, Austria.

Crueger, T. & Stevens, B. (2015). The effect of atmospheric radiative heating by clouds on the madden-julian oscillation. *J. Adv. Model. Earth Syst.*, 7(2), 854–864.

Dennis, R. A., Mayer, J., Applegate, G., Chokkalingam, U., Colfer, C. J. P., Kurniawan, I., Lachowski, H., Maus, P., Permana, R. P., Ruchiat, Y., Stolle, F., Suyanto, & Tomich, T. P. (2005). Fire, people and pixels: Linking social science and remote sensing to understand underlying causes and impacts of fires in indonesia. *Hum Ecol*, 33(4), 465–504.

Driscoll, C. T., Buonocore, J. J., Levy, J. I., Lambert, K. F., Burtraw, D., Reid, S. B., Fakhraei, H., & Schwartz, J. (2015). US power plant carbon standards and clean air and health co-benefits. *Nature Climate Change*, 5(6), 535–540.

EEA (2008). *Air pollution from electricity-generating large combustion plants An assessment of the theoretical emission reduction of SO2 and NOX through implementation of BAT as set in the BREFs.* Technical Report 4, European Environment Agency, Copenhagen, Denmark.

Effendy, A. & Hardono, D. S. (2001). *The large scale private investment of timber plantation development in Indonesia Proceedings of the International Conference on Timber Plantation De Online:.* Technical report, Food and Agriculture Organization of the United Nations.

Evers, S., Yule, C. M., Padfield, R., OReilly, P., & Varkkey, H. (2016). Keep wetlands wet: the myth of sustainable development of tropical peatlands - implications for policies and management. *Glob Change Biol*.

Fairlie, T. D., Jacob, D. J., Dibb, J. E., Alexander, B., Avery, M. A., van Donkelaar, A., & Zhang, L. (2010). Impact of mineral dust on nitrate, sulfate, and ozone in transpacific asian pollution plumes. *Atmospheric Chemistry and Physics*, 10(8), 3999–4012.

Feintrenie, L., Chong, W. K., & Levang, P. (2010). Why do farmers prefer oil palm? lessons learnt from bungo district, indonesia. *Small-scale Forestry*, 9(3), 379–396.

Field, R. D. & Shen, S. S. P. (2008). Predictability of carbon emissions from biomass burning in indonesia from 1997 to 2006. *J. Geophys. Res.*, 113(G4).

Field, R. D., van der Werf, G. R., & Shen, S. S. P. (2009). Human amplification of drought-induced biomass burning in indonesia since 1960. *Nature Geoscience*, 2(3), 185–188.

Fiore, A. M., Dentener, F. J., Wild, O., Cuvelier, C., Schultz, M. G., Hess, P., Textor, C., Schulz, M., Doherty, R. M., Horowitz, L. W., MacKenzie, I. A., Sanderson, M. G., Shindell, D. T., Stevenson, D. S., Szopa, S., Dingenen, R. V., Zeng, G., Atherton, C., Bergmann, D., Bey, I., Carmichael, G., Collins, W. J., Duncan, B. N., Faluvegi, G., Folberth, G., Gauss, M., Gong, S., Hauglustaine, D., Holloway, T., Isaksen, I. S. A., Jacob, D. J., Jonson, J. E., Kaminski, J. W., Keating, T. J., Lupu, A., Marmer, E., Montanaro, V., Park, R. J., Pitari, G., Pringle, K. J., Pyle, J. A., Schroeder, S., Vivanco, M. G., Wind, P., Wojcik, G., Wu, S., & Zuber, A. (2009). Multimodel estimates of intercontinental source-receptor relationships for ozone pollution. *J. Geophys. Res.*, 114(D4).

Forsyth, T. (2014). Public concerns about transboundary haze: A comparison of indonesia, singapore, and malaysia. *Global Environmental Change*, 25, 76–86.

Fu, T.-M., Cao, J. J., Zhang, X. Y., Lee, S. C., Zhang, Q., Han, Y. M., Qu, W. J., Han, Z., Zhang, R., Wang, Y. X., Chen, D., & Henze, D. K. (2012). Carbonaceous aerosols in china: top-down constraints on primary sources and estimation of secondary contribution. *Atmospheric Chemistry and Physics*, 12(5), 2725–2746.

Gaveau, D. L., Pirard, R., Salim, M. A., Tonoto, P., Husnayaen, Parks, S. A., & Carmenta, R. (2016). Overlapping land claims limit the use of satellites to monitorNo-deforestationcommitments andNo-burningcompliance. *Conservation Letters*.

Gaveau, D. L. A., Salim, M. A., Hergoualch, K., Locatelli, B., Sloan, S., Wooster, M., Marlier, M. E., Molidena, E., Yaen, H., DeFries, R., Verchot, L., Murdiyarso, D., Nasi, R., Holmgren, P., & Sheil, D. (2014a). Major atmospheric emissions from peat fires in southeast asia during non-drought years: evidence from the 2013 sumatran fires. *Sci. Rep.*, 4, 6112.

Gaveau, D. L. A., Sloan, S., Molidena, E., Yaen, H., Sheil, D., Abram, N. K., Ancrenaz, M., Nasi, R., Quinones, M., Wielaard, N., & Meijaard, E. (2014b). Four decades of forest persistence, clearance and logging on borneo. *PLoS ONE*, 9(7), e101654.

Genio, A. D. D., Wu, J., Wolf, A. B., Chen, Y., Yao, M.-S., & Kim, D. (2015). Constraints on cumulus parameterization from simulations of observed MJO events. *Journal of Climate*, 28(16), 6419–6442.

Glover, D. & Jessup, T. (1999). *Indonesia's Fires and Haze: The Cost of Catastrophe*. IDRC Books.

Greenpeace (2015). Coal expansion in vietnam could claim 25,000 lives per year: It?s time to transition to renewable energy.

Guttikunda, S. K. & Jawahar, P. (2014). Atmospheric emissions and pollution from the coal-fired thermal power plants in india. *Atmospheric Environment*, 92, 449–460.

Hendon, H. H., Wheeler, M. C., & Zhang, C. (2007). Seasonal dependence of the MJO–ENSO relationship. *Journal of Climate*, 20(3), 531–543.

Henze, D. K., Hakami, A., & Seinfeld, J. H. (2007). Development of the adjoint of GEOS-chem. *Atmospheric Chemistry and Physics*, 7(9), 2413–2433.

Hertwig, D., Burgin, L., Gan, C., Hort, M., Jones, A., Shaw, F., Witham, C., & Zhang, K. (2015). Development and demonstration of a lagrangian dispersion modeling system for real-time prediction of smoke haze pollution from biomass burning in southeast asia. *Journal of Geophysical Research: Atmospheres*, 120(24), 12605–12630.

Holben, B., Eck, T., Slutsker, I., Tanré, D., Buis, J., Setzer, A., Vermote, E., Reagan, J., Kaufman, Y., Nakajima, T., Lavenu, F., Jankowiak, I., & Smirnov, A. (1998). AERONET—a federated instrument network and data archive for aerosol characterization. *Remote Sensing of Environment*, 66(1), 1–16.

Huang, X., Restuccia, F., Gramola, M., & Rein, G. (2016). Experimental study of the formation and collapse of an overhang in the lateral spread of smouldering peat fires. *Combustion and Flame*, 168, 393–402.

HV, V., Thompson, F., & Tonby, O. (2014). Understanding asean: Seven things you need to know.

IEA (2013). *Southeast Asia Energy Outlook: World Energy Outlook Special Report*. Technical report, International Energy Agency, Paris, France.

IEA (2015). *Southeast Asia Energy Outlook: World Energy Outlook Special Report*. Technical report, International Energy Agency, Paris, France.

Indriatmoko, Y., Atmadja, S., Utomo, N. A., Ekaputri, A. D., & Komalasari, M. (2014). *REDD+ on the ground: A case book of subnational initiatives across the globe*, chapter Katingan Peatland Restoration and Conservation Project, Central Kalimantan, Indonesia. Center for International Forestry Research (CIFOR): Bogor, Indonesia.

Institute, W. R. (2015a). Logging. Global Forest Watch: http://www.globalforestwatch.org.

Institute, W. R. (2015b). Oil palm. Global Forest Watch: http://www.globalforestwatch.org.

Institute, W. R. (2015c). Wood fiber. Global Forest Watch: http://www.globalforestwatch.org.

Jaenicke, J., Wösten, H., Budiman, A., & Siegert, F. (2010). Planning hydrological restoration of peatlands in indonesia to mitigate carbon dioxide emissions. *Mitig Adapt Strateg Glob Change*, 15(3), 223–239.

Jerrett, M., Burnett, R. T., Pope, C. A., Ito, K., Thurston, G., Krewski, D., Shi, Y., Calle, E., & Thun, M. (2009). Long-term ozone exposure and mortality. *New England Journal of Medicine*, 360(11), 1085–1095.

Jethva, H. & Torres, O. (2011). Satellite-based evidence of wavelength-dependent aerosol absorption in biomass burning smoke inferred from ozone monitoring instrument. *Atmospheric Chemistry and Physics*, 11(20), 10541–10551.

Johnston, F. H., Henderson, S. B., Chen, Y., Randerson, J. T., Marlier, M., DeFries, R. S., Kinney, P., Bowman, D. M., & Brauer, M. (2012). Estimated global mortality attributable to smoke from landscape fires. *Environ Health Perspect*, 120(5), 695–701.

Jones, D. S. (2006). ASEAN and transboundary haze pollution in southeast asia. *Asia Europe Journal*, 4(3), 431–446.

Jones, G. (2013). *The Population of Southeast Asia*. Technical Report Working Paper Series No. 196, Asia Research Institute.

Kaiser, J. W., Heil, A., Andreae, M. O., Benedetti, A., Chubarova, N., Jones, L., Morcrette, J.-J., Razinger, M., Schultz, M. G., Suttie, M., & van der Werf, G. R. (2012). Biomass burning emissions estimated with a global fire assimilation system based on observed fire radiative power. *Biogeosciences*, 9(1), 527–554.

Kemm, J. (2001). Health impact assessment: a tool for healthy public policy. *Health Promotion International*, 16(1), 79–85.

Kim, D., Sobel, A. H., & Kang, I.-S. (2011). A mechanism denial study on the madden-julian oscillation. *J. Adv. Model. Earth Syst.*, 3(4), n/a–n/a.

Kim, H.-M., Kim, D., Vitart, F., Toma, V. E., Kug, J.-S., & Webster, P. J. (2016). MJO propagation across the maritime continent in the ECMWF ensemble prediction system. *Journal of Climate*, 29(11), 3973–3988.

Kim, P. S., Jacob, D. J., Fisher, J. A., Travis, K., Yu, K., Zhu, L., Yantosca, R. M., Sulprizio, M. P., Jimenez, J. L., Campuzano-Jost, P., Froyd, K. D., Liao, J., Hair, J. W., Fenn, M. A., Butler, C. F., Wagner, N. L., Gordon, T. D., Welti, A., Wennberg, P. O., Crounse, J. D., Clair, J. M. S., Teng, A. P., Millet, D. B., Schwarz, J. P., Markovic, M. Z., & Perring, A. E. (2015a). Sources, seasonality, and trends of southeast US aerosol: an integrated analysis of surface, aircraft, and satellite observations with the GEOS-chem chemical transport model. *Atmospheric Chemistry and Physics*, 15(18), 10411–10433.

Kim, P. S., Jacob, D. J., Mickley, L. J., Koplitz, S. N., Marlier, M. E., DeFries, R. S., Myers, S. S., Chew, B. N., & Mao, Y. H. (2015b). Sensitivity of population smoke exposure to fire locations in equatorial asia. *Atmospheric Environment*, 102, 11–17.

King, E. (2016). Vietnam to phase out coal, invest in gas and renewables.

King, M., Menzel, W., Kaufman, Y., Tanre, D., Gao, B.-C., Platnick, S., Ackerman, S., Remer, L., Pincus, R., & Hubanks, P. (2003). Cloud and aerosol properties, precipitable water, and profiles of temperature and water vapor from MODIS. *IEEE Trans. Geosci. Remote Sensing*, 41(2), 442–458.

Klimont, Z., Smith, S. J., & Cofala, J. (2013). The last decade of global anthropogenic sulfur dioxide: 2000–2011 emissions. *Environ. Res. Lett.*, 8(1), 014003.

Koh, L. P., Miettinen, J., Liew, S. C., & Ghazoul, J. (2011). Remotely sensed evidence of tropical peatland conversion to oil palm. *Proceedings of the National Academy of Sciences*, 108(12), 5127–5132.

Konecny, K., Ballhorn, U., Navratil, P., Jubanski, J., Page, S. E., Tansey, K., Hooijer, A., Vernimmen, R., & Siegert, F. (2016). Variable carbon losses from recurrent fires in drained tropical peatlands. *Glob Change Biol*, 22(4), 1469–1480.

Kopacz, M., Mauzerall, D. L., Wang, J., Leibensperger, E. M., Henze, D. K., & Singh, K. (2011). Origin and radiative forcing of black carbon transported to the himalayas and tibetan plateau. *Atmospheric Chemistry and Physics*, 11(6), 2837–2852.

Koplitz, S. N., Mickley, L. J., Marlier, M. E., Buonocore, J. J., Kim, P. S., Liu, T., Sulprizio, M. P., DeFries, R. S., Jacob, D. J., Schwartz, J., , Pongsiri, M., & Myers, S. S. (2016). Public health impacts of the severe haze in equatorial asia in september-october 2015: Demonstration of a new framework for informing fire management strategies to reduce downwind smoke exposure. *Environ. Res. Lett.*, 11(094023).

Krewski, D., Jerrett, M., Burnett, R. T., Hughes, R. M. E., Shi, Y., Turner, M. C., III, C. A. P., Thurston, G., Calle, E. E., Thun, M. J., & et al. (2009). *Extended follow-up and spatial analysis of the American Cancer Society study linking particulate air pollution and mortality.* Technical Report 140, Health Effects Institute.

Kurokawa, J., Ohara, T., Morikawa, T., Hanayama, S., Janssens-Maenhout, G., Fukui, T., Kawashima, K., & Akimoto, H. (2013). Emissions of air pollutants and greenhouse gases over asian regions during 2000–2008: Regional emission inventory in ASia (REAS) version 2. *Atmospheric Chemistry and Physics*, 13(21), 11019–11058.

Lee, J.-Y., Wang, B., Wheeler, M. C., Fu, X., Waliser, D. E., & Kang, I.-S. (2013). Real-time multivariate indices for the boreal summer intraseasonal oscillation over the asian summer monsoon region. *Clim Dyn*, 40(1-2), 493–509.

Leibensperger, E. M., Mickley, L. J., Jacob, D. J., & Barrett, S. R. (2011). Intercontinental influence of NOx and CO emissions on particulate matter air quality. *Atmospheric Environment*, 45(19), 3318–3324.

Lelieveld, J., Evans, J. S., Fnais, M., Giannadaki, D., & Pozzer, A. (2015). The contribution of outdoor air pollution sources to premature mortality on a global scale. *Nature*, 525(7569), 367–371.

Lepeule, J., Laden, F., Dockery, D., & Schwartz, J. (2012). Chronic exposure to fine particles and mortality: An extended follow-up of the harvard six cities study from 1974 to 2009. *Environ Health Perspect*, 120(7), 965–970.

Levine, J. S. (1999). The 1997 fires in kalimantan and sumatra, indonesia: Gaseous and particulate emissions. *Geophys. Res. Lett.*, 26(7), 815–818.

Levy, J. I., Diez, D., Dou, Y., Barr, C. D., & Dominici, F. (2012). A meta-analysis and multisite time-series analysis of the differential toxicity of major fine particulate matter constituents. *American Journal of Epidemiology*, 175(11), 1091–1099.

Levy, R. C., Mattoo, S., Munchak, L. A., Remer, L. A., Sayer, A. M., Patadia, F., & Hsu, N. C. (2013). The collection 6 MODIS aerosol products over land and ocean. *Atmos. Meas. Tech.*, 6(11), 2989–3034.

Levy, R. C., Remer, L. A., Kleidman, R. G., Mattoo, S., Ichoku, C., Kahn, R., & Eck, T. F. (2010). Global evaluation of the collection 5 MODIS dark-target aerosol products over land. *Atmospheric Chemistry and Physics*, 10(21), 10399–10420.

Li, T., Wang, B., Chang, C.-P., & Zhang, Y. (2003). A theory for the indian ocean dipole–zonal mode∗. *J.Atmos.Sci.*, 60(17), 2119 − −2135.

Lim, S. S., Vos, T., Flaxman, A. D., Danaei, G., Shibuya, K., & et al (2012). A comparative risk assessment of burden of disease and injury attributable to 67 risk factors and risk factor clusters in 21 regions, 1990–2010: a systematic analysis for the global burden of disease study 2010. *The Lancet*, 380(9859), 2224–2260.

Lin, X. & Johnson, R. H. (1996). Heating, moistening, and rainfall over the western pacific warm pool during TOGA COARE. *J. Atmos. Sci.*, 53(22), 3367–3383.

Liu, F., Zhang, Q., Tong, D., Zheng, B., Li, M., Huo, H., & He, K. B. (2015). High-resolution inventory of technologies, activities, and emissions of coal-fired power plants in china from 1990 to 2010. *Atmospheric Chemistry and Physics*, 15(23), 13299–13317.

Lu, Z. & Streets, D. G. (2012). Increase in NO x emissions from indian thermal power plants during 1996–2010: Unit-based inventories and multisatellite observations. *Environmental Science & Technology*, 46(14), 7463–7470.

Lu, Z., Streets, D. G., de Foy, B., & Krotkov, N. A. (2013). Ozone monitoring instrument observations of interannual increases in SO 2 emissions from indian coal-fired power plants during 2005–2012. *Environmental Science & Technology*, 47(24), 13993–14000.

Lu, Z., Zhang, Q., & Streets, D. G. (2011). Sulfur dioxide and primary carbonaceous aerosol emissions in china and india, 1996–2010. *Atmospheric Chemistry and Physics*, 11(18), 9839–9864.

Madden, R. A. & Julian, P. R. (1972). Description of global-scale circulation cells in the tropics with a 40–50 day period. *J. Atmos. Sci.*, 29(6), 1109–1123.

Madden, R. A. & Julian, P. R. (1994). Observations of the 40–50-day tropical oscillation—a review. *Mon. Wea. Rev.*, 122(5), 814–837.

Margono, B. A., Potapov, P. V., Turubanova, S., Stolle, F., & Hansen, M. C. (2014). Primary forest cover loss in indonesia over 2000–2012. *Nature Climate Change*, 4(8), 730–735.

Marlier, M. E., DeFries, R., Pennington, D., Nelson, E., Ordway, E. M., Lewis, J., Koplitz, S. N., & Mickley, L. J. (2015a). Future fire emissions associated with projected land use change in sumatra. *Glob Change Biol*, 21(1), 345–362.

Marlier, M. E., DeFries, R. S., Kim, P. S., Gaveau, D. L. A., Koplitz, S. N., Jacob, D. J., Mickley, L. J., Margono, B. A., & Myers, S. S. (2015b). Regional air quality impacts of future fire emissions in sumatra and kalimantan. *Environ. Res. Lett.*, 10(5), 054010.

Marlier, M. E., DeFries, R. S., Kim, P. S., Koplitz, S. N., Jacob, D. J., Mickley, L. J., & Myers, S. S. (2015c). Fire emissions and regional air quality impacts from fires in oil palm, timber, and logging concessions in indonesia. *Environ. Res. Lett.*, 10(8), 085005.

Marlier, M. E., DeFries, R. S., Voulgarakis, A., Kinney, P. L., Randerson, J. T., Shindell, D. T., Chen, Y., & Faluvegi, G. (2013). El niño and health risks from landscape fire emissions in southeast asia. *Nature Climate Change*, 3(2), 131–136.

Marshall, A. G., Hendon, H. H., & Wang, G. (2016). On the role of anomalous ocean surface temperatures for promoting the record madden-julian oscillation in march 2015. *Geophys. Res. Lett.*, 43(1), 472–481.

Mathers, C. D. & Loncar, D. (2006). Projections of global mortality and burden of disease from 2002 to 2030. *PLoS Med*, 3(11), e442.

McDonald, P. (2014). A population projection for indonesia, 2010–2035. *Bulletin of Indonesian Economic Studies*, 50(1), 123–129.

Miettinen, J., Shi, C., & Liew, S. C. (2011). Deforestation rates in insular southeast asia between 2000 and 2010. *Global Change Biology*, 17(7), 2261–2270.

Miller, M. J. (1986). Retrofit SO2 and NOx control technologies for coal-fired power plants. *Environ. Prog.*, 5(3), 171–177.

Mouillot, F. & Field, C. B. (2005). Fire history and the global carbon budget: a 1ox 1o fire history reconstruction for the 20th century. *Global Change Biol*, 11(3), 398–420.

Nicolas, M. V. J. & Beebe, G. S. (1999). *Fire Management in the Logging Concessions and Plantation Forests of Indonesia*. Technical report, Forest Fire Prevention and Control Project (South Sumatra) and Integrated Forest Fire Management Project (East Kalimantan).

Okamoto, N., Yamanaka, M. D., Ogino, S.-Y., Hashigushi, H., Nishi, N., Sribimawati, T., & Numaguti, A. (2003). Seasonal variations of tropospheric wind over indonesia: Comparison between collected operational rawinsonde data and NCEP reanalysis for 1992-99. *Journal of the Meteorological Society of Japan*, 81(4), 829–850.

Page, S., Hoscilo, A., Langner, A., Tansey, K., Siegert, F., Limin, S., & Rieley, J. (2009). Tropical peatland fires in southeast asia. In *Tropical Fire Ecology* (pp. 263–287). Springer Science Business Media.

Page, S. E., Siegert, F., Rieley, J. O., Boehm, H.-D. V., Jaya, A., & Limin, S. (2002). The amount of carbon released from peat and forest fires in indonesia during 1997. *Nature*, 420(6911), 61–65.

Palm, C. A., Tomich, T., van Noordwijk, M., Vosti, S., Alegre, J., Gockowski, J., & Verchot, L. (2004). Mitigating ghg emissions in the humid tropics: Case studies from the alternatives to slash-and-burn program (asb). *Environment, Development and Sustainability*, (6), 145?162.

Park, R. J. (2004). Natural and transboundary pollution influences on sulfate-nitrate-ammonium aerosols in the united states: Implications for policy. *J. Geophys. Res.*, 109(D15).

Peatman, S. C., Matthews, A. J., & Stevens, D. P. (2014). Propagation of the madden-julian oscillation through the maritime continent and scale interaction with the diurnal cycle of precipitation. *Quarterly Journal of the Royal Meteorological Society*, 140(680), 814–825.

Platts (2014). World electric power plants database.

Platts (2015). World electric power plants database.

Proops, J. L., Gay, P. W., Speck, S., & Schröder, T. (1996). The lifetime pollution implications of various types of electricity generation. an input-output analysis. *Energy Policy*, 24(3), 229–237.

Rasmusson, E. M. & Wallace, J. M. (1983). Meteorological aspects of the el nino/southern oscillation. *Science*, 222(4629), 1195–1202.

Reid, J. S., Hyer, E. J., Johnson, R. S., Holben, B. N., Yokelson, R. J., Zhang, J., Campbell, J. R., Christopher, S. A., Girolamo, L. D., Giglio, L., Holz, R. E., Kearney, C., Miettinen, J., Reid, E. A., Turk, F. J., Wang, J., Xian, P., Zhao, G., Balasubramanian, R., Chew, B. N., Janjai, S., Lagrosas, N., Lestari, P., Lin, N.-H., Mahmud, M., Nguyen, A. X., Norris, B., Oanh, N. T., Oo, M., Salinas, S. V., Welton, E. J., & Liew, S. C. (2013). Observing and understanding the southeast asian aerosol system by remote sensing: An initial review and analysis for the seven southeast asian studies (7seas) program. *Atmospheric Research*, 122, 403–468.

Reid, J. S., Xian, P., Hyer, E. J., Flatau, M. K., Ramirez, E. M., Turk, F. J., Sampson, C. R., Zhang, C., Fukada, E. M., & Maloney, E. D. (2012). Multi-scale meteorological conceptual analysis of observed active fire hotspot activity and smoke optical

depth in the maritime continent. *Atmospheric Chemistry and Physics*, 12(4), 2117–2147.

Rein, G. (2013). Smouldering fires and natural fuels. In *Fire Phenomena and the Earth System* (pp. 15–33). Wiley-Blackwell.

Remer, L. A., Kaufman, Y. J., Tanré, D., Mattoo, S., Chu, D. A., Martins, J. V., Li, R.-R., Ichoku, C., Levy, R. C., Kleidman, R. G., Eck, T. F., Vermote, E., & Holben, B. N. (2005). The MODIS aerosol algorithm, products, and validation. *J. Atmos. Sci.*, 62(4), 947–973.

Saharjo, B. H. & Munoz, C. P. (2005). Controlled burning in peat lands owned by small farmers: a case study in land preparation. *Wetlands Ecology and Management*, 13(1), 105–110.

Saji, N. H., Goswami, B. N., Vinayachandran, P. N., & Yamagata, T. (1999). A dipole mode in the tropical indian ocean. *Nature*, 401(6751), 360–363.

Salinas, S. V., Chew, B. N., Miettinen, J., Campbell, J. R., Welton, E. J., Reid, J. S., Yu, L. E., & Liew, S. C. (2013). Physical and optical characteristics of the october 2010 haze event over singapore: A photometric and lidar analysis. *Atmospheric Research*, 122, 555–570.

Sayer, A. M., Hsu, N. C., Eck, T. F., Smirnov, A., & Holben, B. N. (2014). AERONET-based models of smoke-dominated aerosol near source regions and transported over oceans, and implications for satellite retrievals of aerosol optical depth. *Atmospheric Chemistry and Physics*, 14(20), 11493–11523.

Schwartz, J., Coull, B., Laden, F., & Ryan, L. (2008). The effect of dose and timing of dose on the association between airborne particles and survival. *Environ Health Perspect*, 116(1), 64–69.

Shearer, C., Ghio, N., Myllyvirta, L., & Nace, T. (2015). *Boom and Bust: Tracking the global coal plant pipeline*. Technical report, CoalSwarm and Sierra Club.

Shuo, L. (2015). Comment: China's energy transition is happening even faster than you think.

Tansey, K., Beston, J., Hoscilo, A., Page, S. E., & Hernández, C. U. P. (2008). Relationship between MODIS fire hot spot count and burned area in a degraded tropical peat swamp forest in central kalimantan, indonesia. *J. Geophys. Res.*, 113(D23).

Tian, B., Waliser, D. E., Kahn, R. A., Li, Q., Yung, Y. L., Tyranowski, T., Geogdzhayev, I. V., Mishchenko, M. I., Torres, O., & Smirnov, A. (2008). Does the madden-julian oscillation influence aerosol variability? *J. Geophys. Res.*, 113(D12).

Tomich, T. P., van Noordwijk, M., Vosti, S. A., & Witcover, J. (1998). Agricultural development with rainforest conservation: methods for seeking best bet alternatives to slash-and-bum, with applications to brazil and indonesia. *Agricultural Economics*, (19), 159–174.

Torres, O., Decae, R., P, V., & de Leeuw, G. (2002). *OMI algorithm theoretical basis document: Volume 3, pages 47-71*. Technical report, OMI Science Team.

Torres, O., Tanskanen, A., Veihelmann, B., Ahn, C., Braak, R., Bhartia, P. K., Veefkind, P., & Levelt, P. (2007). Aerosols and surface UV products from ozone monitoring instrument observations: An overview. *J. Geophys. Res.*, 112(D24).

Trivitayanurak, W., Palmer, P. I., Barkley, M. P., Robinson, N. H., Coe, H., & Oram, D. E. (2012). The composition and variability of atmospheric aerosol over southeast asia during 2008. *Atmospheric Chemistry and Physics*, 12(2), 1083–1100.

Turetsky, M. R., Benscoter, B., Page, S., Rein, G., van der Werf, G. R., & Watts, A. (2015). Global vulnerability of peatlands to fire and carbon loss. *Nature Geoscience*, 8(1), 11–14.

Turpin, B. J. & Lim, H.-J. (2001). Species contributions to PM2.5 mass concentrations: Revisiting common assumptions for estimating organic mass. *Aerosol Science and Technology*, 35(1), 602–610.

USEIA (2011). *Electric Power Annual 2010*. Technical report, United States Department of Energy.

USEPA (1995). *Compilation of Air Pollutant Emission Factors*. Technical Report AP-42, United States Environmental Protection Agency, Research Triangle Park, NC.

USEPA (2010). *Quantitative Health Risk Assessment for Particulate Matter*. Technical Report EPA-452/R-10-005, United States Environmental Protection Agency.

USEPA (2014). *Regulatory Impact Analysis for the Proposed Carbon Pollution Guidelines for Existing Power Plants and Emission Standards for Modified and Reconstructed Power Plants*. Technical Report EPA-452/R-14-002, United States Environmental Protection Agency, Research Triangle Park, NC.

van der Werf, G. R., Dempewolf, J., Trigg, S. N., Randerson, J. T., Kasibhatla, P. S., Giglio, L., Murdiyarso, D., Peters, W., Morton, D. C., Collatz, G. J., Dolman, A. J., & DeFries, R. S. (2008). Climate regulation of fire emissions and deforestation in equatorial asia. *Proceedings of the National Academy of Sciences*, 105(51), 20350–20355.

van der Werf, G. R., Randerson, J. T., Giglio, L., Collatz, G. J., Mu, M., Kasibhatla, P. S., Morton, D. C., DeFries, R. S., Jin, Y., & van Leeuwen, T. T. (2010). Global fire emissions and the contribution of deforestation, savanna, forest, agricultural, and peat fires (1997–2009). *Atmospheric Chemistry and Physics*, 10(23), 11707–11735.

van Donkelaar, A., Martin, R. V., Leaitch, W. R., Macdonald, A. M., Walker, T. W., Streets, D. G., Zhang, Q., Dunlea, E. J., Jimenez, J. L., Dibb, J. E., Huey, L. G., Weber, R., & Andreae, M. O. (2008). Analysis of aircraft and satellite measurements from the intercontinental chemical transport experiment (INTEX-b) to quantify long-range transport of east asian sulfur to canada. *Atmospheric Chemistry and Physics*, 8(11), 2999–3014.

Wahyunto, R. S. & Subagjo, H. (2003). Maps of area of peatland distribution 339 and carbon content in sumatera, 1990?2002. Wetlands Int-Indonesia Programm and Wildl Habitat Canada, Bogor, Indonesia.

Wahyunto, R. S. & Subagjo, H. (2004). Peta sebaran lahan gambut, luas dan kandungan karbon di kalimantan/map of peatland distribution area and carbon content in kalimantan, 2000?2002. Wetlands Int-Indonesia Programm and Wildl Habitat Canada, Bogor, Indonesia.

Wang, S., Sobel, A. H., Zhang, F., Sun, Y. Q., Yue, Y., & Zhou, L. (2015). Regional simulation of the october and november MJO events observed during the CINDY/DYNAMO field campaign at gray zone resolution. *Journal of Climate*, 28(6), 2097–2119.

Wang, S., Streets, D. G., Zhang, Q., He, K., Chen, D., Kang, S., Lu, Z., & Wang, Y. (2010). Satellite detection and model verification of NO x emissions from power plants in northern china. *Environ. Res. Lett.*, 5(4), 044007.

Wang, Y., Hao, J., McElroy, M. B., Munger, J. W., Ma, H., Chen, D., & Nielsen, C. P. (2009). Ozone air quality during the 2008 beijing olympics: effectiveness of emission restrictions. *Atmospheric Chemistry and Physics*, 9(14), 5237–5251.

Wang, Y., Zhang, Q. Q., He, K., Zhang, Q., & Chai, L. (2013). Sulfate-nitrate-ammonium aerosols over china: response to 2000–2015 emission changes of sulfur dioxide, nitrogen oxides, and ammonia. *Atmospheric Chemistry and Physics*, 13(5), 2635–2652.

Wang, Y., Zhang, Y., Hao, J., & Luo, M. (2011). Seasonal and spatial variability of surface ozone over china: contributions from background and domestic pollution. *Atmospheric Chemistry and Physics*, 11(7), 3511–3525.

Wheeler, D. & Ummel, K. (2008). Calculating carma: Global estimation of co2 emissions from the power sector. *SSRN Electronic Journal*.

Wheeler, M. C. & Hendon, H. H. (2004). An all-season real-time multivariate MJO index: Development of an index for monitoring and prediction. *Mon. Wea. Rev.*, 132(8), 1917–1932.

WHO (2010). *Global Health Risks: Mortality and Burden of Disease Attributable to Selected Major Risks*. World Health Organization.

WHO (2014). *World Health Statistics 2014*. Technical report, World Health Organization.

Wilson, E. A., Gordon, A. L., & Kim, D. (2013). Observations of the madden julian oscillation during indian ocean dipole events. *Journal of Geophysical Research: Atmospheres*, 118(6), 2588–2599.

Woolnough, S. J., Vitart, F., & Balmaseda, M. A. (2007). The role of the ocean in the madden–julian oscillation: Implications for MJO prediction. *Quarterly Journal of the Royal Meteorological Society*, 133(622), 117–128.

Worden, J., Jones, D. B. A., Liu, J., Parrington, M., Bowman, K., Stajner, I., Beer, R., Jiang, J., Thouret, V., Kulawik, S., Li, J.-L. F., Verma, S., & Worden, H. (2009). Observed vertical distribution of tropospheric ozone during the asian summertime monsoon. *J. Geophys. Res.*, 114(D13).

Xian, P., Reid, J. S., Atwood, S. A., Johnson, R. S., Hyer, E. J., Westphal, D. L., & Sessions, W. (2013). Smoke aerosol transport patterns over the maritime continent. *Atmospheric Research*, 122, 469–485.

Xu, X., Wang, J., Henze, D. K., Qu, W., & Kopacz, M. (2013). Constraints on aerosol sources using GEOS-chem adjoint and MODIS radiances, and evaluation with multisensor (OMI, MISR) data. *Journal of Geophysical Research: Atmospheres*, 118(12), 6396–6413.

Zender, C. S., Krolewski, A. G., Tosca, M. G., & Randerson, J. T. (2012). Tropical biomass burning smoke plume size, shape, reflectance, and age based on 2001–2009 MISR imagery of borneo. *Atmospheric Chemistry and Physics*, 12(7), 3437–3454.

Zhang, C. (2005). Madden-julian oscillation. *Rev. Geophys.*, 43(2).

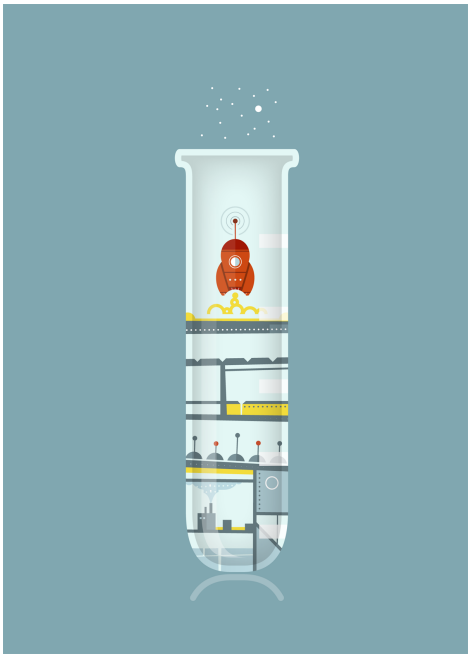
Zhang, C. (2013). Madden–julian oscillation: Bridging weather and climate. *Bull. Amer. Meteor. Soc.*, 94(12), 1849–1870.

Zhang, L., Jacob, D. J., Boersma, K. F., Jaffe, D. A., Olson, J. R., Bowman, K. W., Worden, J. R., Thompson, A. M., Avery, M. A., Cohen, R. C., Dibb, J. E., Flock, F. M., Fuelberg, H. E., Huey, L. G., McMillan, W. W., Singh, H. B., & Weinheimer, A. J. (2008). Transpacific transport of ozone pollution and the effect of recent asian emission increases on air quality in north america: an integrated analysis using satellite, aircraft, ozonesonde, and surface observations. *Atmospheric Chemistry and Physics*, 8(20), 6117–6136.

Zhao, Y., Wang, S., Nielsen, C. P., Li, X., & Hao, J. (2010). Establishment of a database of emission factors for atmospheric pollutants from chinese coal-fired power plants. *Atmospheric Environment*, 44(12), 1515–1523.

Zhao, Y., Zhang, J., & Nielsen, C. P. (2014). The effects of energy paths and emission controls and standards on future trends in chinas emissions of primary air pollutants. *Atmospheric Chemistry and Physics*, 14(17), 8849–8868.

Zhu, W. (2013). Coal to surpass gas in southeast asia power boom, iea says.



This thesis was typeset using LaTeX, originally developed by Leslie Lamport and based on Donald Knuth's TeX. The body text is set in 11 point Egenolff-Berner Garamond, a revival of Claude Garamont's humanist typeface. The above illustration, *Science Experiment 02*, was created by Ben Schlitter and released under CC BY-NC-ND 3.0. A template that can be used to format a PhD dissertation with this look & feel has been released under the permissive AGPL license, and can be found online at github.com/suchow/Dissertate or from its lead author, Jordan Suchow, at suchow@post.harvard.edu.